1-1-2010

Using Bayesian Inference in Design Applications

Chung Yong Chan
University of Mississippi

To the Graduate Council:

I am submitting herewith a dissertation written by Chung Yong Chan entitled "Using Bayesian Inference in Design Applications." I have examined the final copy of the dissertation for form and content and recommend that it be accepted in partial fulfillment of the requirements for the degree of Doctor of Philosophy in Engineering Science with emphasis in Electrical Engineering.

Paul M. Goggans
Associate Professor of Electrical Engineering
(Dissertation Advisor)

We have read this dissertation
and recommend its acceptance:

Allen W. Glisson
Professor of Electrical Engineering

Richard Raspet
Professor of Physics and Astronomy

Lei Cao
Associate Professor of Electrical Engineering

Accepted for the Council:

Dean of The Graduate School

USING BAYESIAN INFERENCE IN DESIGN APPLICATIONS

A Dissertation

presented in partial fulfillment of requirements

for the degree of Doctor of Philosophy

Chung Yong Chan

Department of Electrical Engineering

The University of Mississippi

December 5, 2010

ABSTRACT

This dissertation presents a new approach for solving scientific and engineering design problems such as the design of antenna arrays and finite impulse response (FIR) filters. In this approach, a design problem is cast as an inverse problem. Bayesian inference has been used extensively to solve inverse problems in various fields, and thus, the tools and methods previously developed for Bayesian inference are adapted and utilized to solve design problems in the present approach. Given a desired design output specified by upper and lower envelopes, the Bayesian inference framework for design is applied to achieve designs that meet the prescribed design specifications and practical design requirements. To obtain a design, Bayesian parameter estimation and model comparison are employed to determine the values of all design parameters. In the design of antenna arrays, the objective is to produce antenna arrays that realize the desired far-field radiation pattern while satisfying all prescribed practical design requirements. In the context of computation, the task is to determine the required number of antenna array elements and the values for the element parameters which include the position, current amplitude and phase. As for digital filter design, the aim is to design linear phase FIR filters that realize the desired frequency magnitude response and satisfy all prescribed practical design requirements. The computational task in this case is to determine the number of filter taps required, the tap positions and the filter coefficients.

In the Bayesian inference framework for design, the solution to a design problem is the posterior probability distribution which is a function of the design parameters. The posterior — which comes from Bayes' theorem — is proportional to the product of the likelihood and priors. The likelihood is obtained via the assignment of a probability distribution function to the error between the desired and achieved design output. The assignment of an error distribution incorporates the desired design

output into a design process. The priors are assigned probability distribution functions which express the constraints on the design parameters. In addition to the constraints on the design parameters, a design problem may have other practical design requirements which are implemented through the modifications of the likelihood. With the likelihood and priors obtained, the posterior — which cannot be determined analytically — is approximated by a Monte Carlo method. In the approximation, a reasonable number of samples are drawn from the posterior using an appropriate sampling technique such as a Markov chain Monte Carlo method. The sampling of the posterior produces an approximate solution to a design problem and concludes the inference portion of the Bayesian inference framework for design. In the context of design, each posterior sample drawn in the Monte Carlo approximation represents a design candidate. As a result, the solution to a design problem consists of a number of potential designs rather than a single final design. To obtain the final design, an additional decision step is required. This final step requires a designer to select a single design candidate as the final design based on additional design criteria.

The Bayesian inference framework for design has been applied to the design of both antenna arrays and linear phase FIR filters. The antenna array design examples presented in this dissertation use different types of antenna array such as symmetric linear array with real-valued currents, asymmetric linear array with complex currents, reconfigurable linear array and planar array to realize various desired radiation patterns while satisfying certain prescribed practical design requirements. The radiation patterns that are desired include two broadside patterns, an end-fire pattern, a shaped beam pattern which is the sector beam pattern, and a three-dimensional radiation pattern. Various practical design requirements have been incorporated into the design examples presented in this dissertation. These practical design requirements include a minimum spacing between two adjacent array elements, limitations in the dynamic range and accuracy of the current amplitudes and phases, the ability to maintain a desired radiation pattern over a frequency band, and the ability to maintain a desired radiation pattern when one or more array elements are defective or failing. For the digital filter design application, four design examples are presented. All four examples employ a linear

phase FIR filter that has symmetric impulse response and odd filter length to produce various desired frequency responses. In practice, the filter coefficients of a linear phase FIR filter are limited in dynamic range and accuracy. This practical design requirement has been incorporated into two of the design examples where the filter coefficient values are represented by a sum of signed power-of-two terms.

ACKNOWLEDGEMENTS

I would like to offer my sincere appreciation to a number of people, without whose inspiration, motivation and support, this dissertation would never have materialized. First and foremost, I would like to express my greatest gratitude to my dissertation advisor, Dr. Paul M. Goggans, for his knowledge, advice and patience. He has provided invaluable insights and precious guidance throughout my dissertation research and Ph.D. study. In addition, I am thankful to my committee members, Dr. Allen W. Glisson, Dr. Richard Raspet and Dr. Lei Cao for their inputs, feedbacks and suggestions. Finally, I would like to express my profound appreciation to my father, mother and my girlfriend, Podjanee Inthasaro, for their endless support and encouragement.

TABLE OF CONTENTS

LIST OF TABLES

LIST OF FIGURES

CHAPTER 1

INTRODUCTION

Inverse problems typically refer to problems where the results or outcomes are known while the causes are not. The solution of an inverse problem, according to the Russian proponent of Inverse Methods, Oleg Alifanov [1], entails determining unknown causes based on observation of their effects. In science and engineering, inverse problems generally involve the use of actual measurements or observations to infer the model characterizing the physical system under investigation [2, 3]. The existence and uniqueness of solutions for an inverse problem are not certain. An inverse problem may have more than one solution when different models give rise to the same observations. An inverse problem may also have no solution at all when the inferred model does not agree with the measurements. A simple example of an inverse problem is medical diagnosis which entails the determination of a disease identified by its symptoms and the results of various diagnostic tests. In this inverse problem, the known observations or outcomes are the symptoms and test results while the unknown cause is the disease. Given that different diseases can result in the same symptoms and test results, the outcome of a medical diagnosis may point to more than one disease as the cause. A medical diagnosis report may also conclude that not a single disease can be associated with the symptoms and test results due to the possibility that the actual disease has not been discovered before.

In scientific and engineering design problems, the ultimate goal is to produce a design that realizes the desired output. The solution of a design problem entails determining the values of

the design parameters based on the prescribed design specifications and requirements. A design problem may have more than one solution when different designs are capable of meeting the same design specifications and requirements. A design problem may also have no solution at all when no design can be produced to meet the specified standard. By comparing the nature of both inverse and design problems, one can draw a parallel between observations and design output as well as causes and designs. Moreover, the solutions for both inverse and design problems have the same characteristics as well in that the existence and uniqueness of solutions are not guaranteed. Because of the similarities, the process of contriving a design to meet certain prescribed design specifications and requirements can be treated as an inverse problem.

Inverse problems, which generally arise as a result of incomplete information, are commonly encountered in many scientific and engineering fields. There are many types of inverse problems such as signal detection, identification and parameter estimation. These problems have been solved using Bayesian inference tools which include model comparison and parameter estimation. An example of signal identification problem is the landmine detection problem presented in [4] and [5]. In both [4] and [5], landmine detection is cast as a model comparison problem. Two parametric models, which are the background and landmine models, are constructed to represent the physical systems in which a landmine is absent and present respectively. Given a set of measurements obtained from an electromagnetic induction sensor, Bayesian model selection is used to determine which model is the most credible model and thus, identify whether a landmine is present. The articles in [6] and [7] present a parameter estimation problem in room acoustics. In this study, a parametric model, which is Schroeder decay function, is constructed to model the sound energy decay in coupled spaces. Given a set of room impulse response measurements, Bayesian parameter estimation is used to solve the problem of estimating multiple sound energy decay times in an acoustically coupled space. In addition to the two examples mentioned above, Bayesian model comparison and parameter estimation have been successfully applied to solve many inverse problems in various fields such as radar [8], geophysics [9, 10], astronomy [11, 12] and medical

imaging [13, 14]. The examples above showcase the success and wide application of Bayesian inference in inverse problems. Since a scientific or engineering design problem can also be cast as an inverse problem, the tools and methods developed for Bayesian inference can be adapted and used to solve design problems.

1.1 The Bayesian Inference Framework for Design

This dissertation presents the Bayesian inference framework for design which utilizes Bayesian parameter estimation and model comparison to determine the values of the design parameters that meet the prescribed design specifications and requirements. Similar to solving an inverse problem, employing the Bayesian inference framework to solve a design problem requires the computation of the posterior probability distribution which is a function of the design parameters. Bayes' theorem states that the posterior is proportional to the product of the priors and the likelihood. The priors are the probability distribution functions for the design parameters. All prior probability distribution functions are assigned by the designer based on the background information at hand such as the acceptable range of the design parameters. The likelihood is obtained through the assignment of a probability distribution function, which can be the Gaussian or Laplacian distribution, to the error. In an inverse problem, the error is defined as the difference between the parametric model and measured data. The absence of data or measurements in a design problem necessitates modifications of the error definition. Using the parallelism between inverse and design problems, the error in a design problem can be identified as the difference between the desired and achieved design output. A design problem consists of other practical design requirements apart from the desired output. These additional design requirements can be included in the assignment of probability distribution functions to the priors or through modifications of the likelihood. With the likelihood and priors determined, the posterior probability distribution is approximated by a Monte Carlo method since a closed-form solution cannot be obtained. In the approximation, a reasonable number of samples are drawn from the posterior using an appropriate sampling technique such as a Markov chain

Monte Carlo method. The sampling of the posterior concludes the inference portion of the Bayesian inference framework for design. In the context of design, each of the samples drawn from the posterior represents a design candidate. This notion indicates that the solution to a design problem consists of a number of potential designs rather than a single final design. To obtain the final design, a designer has to select a design candidate among all the design candidates as the final design based on additional design criteria.

The Bayesian inference framework for design is applied to two design applications: antenna arrays and linear phase finite impulse response (FIR) filters. The design problems in these two design applications are commonly cast as optimization problems. The optimization framework has a critical drawback in that the design process requires physical systems with prescribed design complexity. This drawback typically results in designs that have higher design complexity than required. On the contrary, the Bayesian inference framework for design has the ability to design physical systems that have design complexity appropriate to the desired output and design requirements. In addition, the Bayesian inference framework for design is also robust and facilitates the incorporation of various practical design requirements into a design problem. The following sections provide a comparison between the Bayesian inference framework for design and other developed methods that have been used to solve antenna array and linear phase FIR filter design problems.

1.2 Design of Antenna Array

When analytic or textbook methods are inadequate to solve a design problem, the design of an antenna array is commonly formulated as an optimization problem. In the design of an antenna array, the goal of the optimization approach is to minimize the error between the desired and achieved far-field radiation pattern. The error is defined by a fitness function that measures the difference between the desired and obtained array factor. While many optimization techniques such as Taguchi's method [15], particle swarm optimization (PSO) [16–22], genetic algorithm [23–25], simulated annealing [26], differential evolution algorithm [27] and Schelkunoff polynomial method [28]

have achieved notable success, the optimization approach has a significant drawback in that the array synthesis is performed with a fixed number of antenna elements. Prior to the optimization process, the designer must prescribe the number of antenna elements via some ad hoc methods of his own devising. In the absence of a systematic procedure, the designer has to rely on his intuition, experience or personal judgement for determining the number of array elements required to realize the desired radiation pattern. Driven by the urge to design an antenna array that can produce the desired radiation pattern, a designer usually ends up having an antenna array design that has more antenna elements than needed. This is because the design objectives can always be achieved by using more array elements than required. In applications such as satellite communication where minimizing the number of antenna elements is critical, having an antenna array that can meet design requirements with as few antenna elements as possible is very desirable. In all applications, having fewer array elements simplifies an antenna system and reduces the cost of production. Although designers typically specify more antenna elements than necessary, there still exists the possibility of designers proposing fewer antenna elements than required. In this case, the achieved radiation pattern will miss the design pattern specifications considerably because the number of array elements used is insufficient. Therefore, it is very desirable to have the number of antenna elements determined automatically.

A recent article [29] presents a method that can reduce the number of antenna elements used in a designed linear antenna array. Given a far-field radiation pattern that is produced by a designed linear antenna array, the method can be utilized to reconstruct the original radiation pattern to within a specified accuracy using a reduced number of antenna elements. However, as mentioned in [29], the method may fail in shaped beam pattern design problems. For these problems, the authors have suggested varying the number of antenna elements between the minimum number determined by Eq. (10) in [29] and the original number. Even if the proposed idea works, it is not computationally efficient. Moreover, reconstruction of a produced radiation pattern is not the same as designing a linear antenna array to meet certain design pattern specifications and requirements.

It is not known if the method can be employed to design a linear antenna array to meet certain common design pattern specifications such as a maximum allowed sidelobe level or beamwidth, as evident by Example 3 in [29].

The sidelobe level is a very critical factor in the design of an antenna array. Many research works [16, 19, 20, 27, 30] focus on minimizing or lowering the sidelobe level. Using a prescribed number of antenna elements, the methods presented in these research works determine the parameter values of either the position, current amplitude or phase, or a combination of two or more element parameters that minimize the sidelobe level. However, it is more practical and desirable to specify a desired maximum sidelobe level in advance, and have the ability to design a linear antenna array that meets the specification. The techniques in [15, 21, 22] have the desired ability but are limited to the design of linear antenna arrays that have fixed number of antenna elements. In addition, these methods use uniformly spaced linear antenna arrays which are inferior to unequally spaced linear antenna arrays in many aspects. The synthesis of unequally spaced linear antenna arrays has been studied in many research works [19], [20], [26], [27], [30], [31]. The reason for the extensive study is that unequally spaced linear antenna arrays can produce lower sidelobe level using fewer number of antenna elements. Apart from the sidelobe level, the beamwidth, particularly the width of the main beam, is also an important factor. Generally, the main beamwidth and sidelobe level cannot be reduced at the same time. If a design problem uses a fixed number of antenna elements and has two design goals which are a desired maximum sidelobe level and main beamwidth, a compromise between the two design goals is required. This scenario is depicted in [19] which attempts to seek the best strategy for trading-off the two design goals in what is referred to as a multi-objective design problem.

Multi-objective design problems are very common in practice. An example is the design of a reconfigurable linear antenna array to achieve multiple desired radiation patterns. The article [18] presents the design of a reconfigurable linear antenna array that has common current amplitudes and varying current phases to produce two desired radiation patterns, which are a sector beam

pattern and a broadside pattern. The authors of [32–35] have extended the work presented in [18] to include an additional design requirement, which is limitations in the dynamic range and accuracy of the current amplitudes and phases. Another example of multi-objective design problem is the design of an antenna array that can maintain the desired radiation pattern over a frequency band. The articles [36–38] discuss the design of wideband antenna arrays that are widely used in radio communication, radar and acoustics. A much more challenging multi-objective design problem is the design of an antenna array that can maintain the desired radiation pattern when one or more array elements are defective or failing. The article [39] presents the design of self-healing antenna arrays that have the ability to recover reasonable antenna performance when as many as 30% of the array elements are inoperable. The recovery technique used in [39] is to reconfigure the complex currents of the remaining array elements so that the degraded antenna performance is minimized. All of the above design problems showcase the wide range of practical design requirements that are desired to be fulfilled. Therefore, it is very desirable to have a design technique that can incorporate various design requirements in a design problem.

The proposed Bayesian inference framework for design has all the desired abilities mentioned above. Given design pattern specifications such as a maximum allowed sidelobe level, main beamwidth and a minimum allowed half-power beamwidth, the Bayesian inference framework has the ability to design an antenna array that meets all prescribed design pattern specifications and has design complexity appropriate to the desired radiation pattern. In addition, unlike the method in [29], the Bayesian inference framework can be applied to solve shaped beam pattern design problems as well. Even though the Bayesian inference framework does not enforce the use of unequally spaced antenna arrays, it is very unlikely, if not impossible, for a designed antenna array to have a uniform element spacing. This is because both the number of antenna elements and element positions are not fixed and more importantly, the number of antenna elements used in a designed linear antenna array is minimal. In addition to the automatic determination of design complexity, the Bayesian inference framework allows various design requirements to be incorporated into a design problem.

Practical design requirements such as a minimum spacing between two adjacent array elements, a maximum width of the antenna aperture, limitations in the dynamic range and accuracy of the current amplitudes and phases, the ability to generate multiple desired radiation patterns, the ability to maintain a desired radiation pattern over a frequency band, and the ability to maintain a desired radiation pattern when one or more array elements are defective or failing have all been successfully incorporated into a design problem.

1.3 Design of Linear Phase FIR Filter

A fundamental approach to the design of linear phase FIR filter is the window method [40, Ch. 7]. FIR filters designed using the window method exhibit oscillatory behavior around the discontinuity of the ideal frequency response. In addition, this method does not allow individual control over the magnitude of the passband and stopband errors. In the 1970's, Parks and McClellan developed a classical algorithm which is based on optimization. The design objective in the Parks and McClellan algorithm is to minimize the maximum weighted error between the achieved and desired frequency response which is typically the frequency response of an ideal filter. FIR filters designed by the Parks and McClellan algorithm have equal ripples in both the passband and stopband and are optimum in the sense of minimax error. In recent years, more methods have been developed to design FIR filters such as the multiple exchange algorithm [41], genetic algorithms [42] and particle swarm optimization (PSO) [43]. These algorithms including the Parks and McClellan have a drawback in that the length of the designed filter has to be specified in advance. In addition, the designed filter uses every tap which means that none of the filter coefficients is zero. As a result, filters designed using these techniques can easily be greater in length than necessary and easily use more taps than required. The studies in [44], [45] and [46] prove that a linear phase FIR sparse filter, which has more filter taps but uses fewer multiplications due to zero-valued filter coefficients, matches the performance of or even outperforms a traditional non-sparse FIR filter. Since fewer multiplications are required, it follows that the computation cost in the implemented filter is reduced

as well. For these reasons, it is desirable for a linear phase FIR filter to use only the specific taps that are required and to have these taps along with the filter length determined automatically.

In practice, the filter coefficients of a linear phase FIR filter are limited in dynamic range and accuracy. This is because the filter coefficients have to be represented using finite word length in the practical implementation of a designed linear phase FIR filter. Because of the truncation or quantization of the filter coefficients, the implemented linear phase FIR filter cannot retain the frequency response of the original filter designed using continuous valued coefficients. Consequently, the frequency response of the implemented filter may not meet the prescribed design specifications. The practical issue of having limited dynamic range and accuracy in the filter coefficients has been studied extensively over the past 10 years. Many methods such as those presented in [47–51] have been developed to design finite word length or discrete coefficient FIR filters.

All of the above methods require multipliers in the practical implementation of a designed linear phase FIR filter. The use of multipliers requires high implementation cost and results in high power dissipation. To reduce the design complexity, cost and power dissipation, the filter coefficients are represented by a sum of one or more signed power-of-two (SPoT) terms, so that the multipliers can be replaced by a number of shifters and adders. The design of linear phase FIR filter using SPoT terms has been studied extensively in recent years. Many methods such as [52–57] have been developed to design linear phase FIR filters that use SPoT terms. In all these methods, a linear phase FIR filter that meets the specified frequency response using continuous filter coefficients is required to be designed first. The continuous filter coefficients are then quantized and represented by a sum of one or more SPoT terms. FIR filters designed using these methods may have filter coefficients which are zero-valued. However, since the filter length is fixed in advance, the number of non-zero discrete filter coefficients used is likely to be more than required.

The Bayesian inference framework for design has the ability to design a linear phase FIR sparse filter that has computation complexity appropriate to the design specifications [58]. Given design

specifications such as the passband and stopband edge frequencies, the maximum passband ripple and the minimum stopband attenuation, the proposed method automatically determines the specific taps and their corresponding non-zero valued coefficients required to meet the prescribed design specifications. Since the taps to be used are automatically determined, it follows that the length of the filter is also automatically determined as the filter length corresponds to the order of the last tap used. As in the antenna array design, the limitations in the dynamic range and accuracy of the filter coefficients have also been incorporated into a design problem. Unlike the methods in [52–57], the Bayesian inference framework for design can be applied directly to design a linear phase FIR filter design that uses SPoT terms without having to determine a set of continuous filter coefficients that meet the desired frequency response.

1.4 Preview

This dissertation is organized as follows. Chapter 2 details the mathematical theory behind the Bayesian inference framework for design. This chapter begins with the descriptions of the parametric models, design requirements and design goals of the two design applications: antenna arrays and linear phase FIR filters. The descriptions are followed by explanations of the Bayesian inference portion of the design process. The chapter then proceeds with an in-depth discussion on how to select a final design from all the design candidates. To explain the reason behind the ability of the Bayesian inference framework to design physical systems that have design complexity appropriate to the design specifications and requirements, an intuitive description of the Ockham's Razor principle in the context of design is presented. Chapter 3 provides an overview of the sampling program that is used here, namely BayeSys [59]. This chapter describes the basic ideas, structures, and underlying theory of the program. Chapter 4 and 5 presents several antenna array and linear phase FIR filter design problems respectively. These chapters demonstrate how various design requirements are implemented in the design process. Comparison of results with the optimization approach and other methods is made to illustrate the advantages that the Bayesian

inference framework possesses. Chapter 6 summarizes and concludes this dissertation. Discussions pertaining to some design issues and suggestions for future work are presented.

CHAPTER 2

THE THEORY

The approach presented in this dissertation treats a design problem as an inverse problem. Since both design and inference problems are generalized inverse problems, the tools and methods developed for Bayesian inference can be adapted and used to solve design problems. Here, Bayesian parameter estimation and model comparison are applied to solve antenna array and linear phase FIR filter design problems.

Bayesian inference uses probability theory as extended logic for conducting scientific inference [60–64]. The use of Bayesian probability theory provides a systematic and logically consistent mean for making scientific inference. In Bayesian inference, the ultimate goal is to determine the posterior probability distribution function. From Bayes' theorem, the posterior is proportional to the product of the likelihood and prior probability distribution functions. The likelihood is obtained via the assignment of a probability distribution function to the difference between the model and data. The priors are assigned probability distribution functions based on the background information with regard to the model parameters. The posterior cannot be determined analytically; however, it can be approximated by a Monte Carlo method. In the approximation, an appropriate sampling method such as a Markov chain Monte Carlo method is used to draw a reasonable number of samples from the posterior.

The inference framework for design is analogous to Bayesian inference and its computation process is similar to the procedure described above. The mathematical theory behind the Bayesian

inference framework for design is presented in this chapter. It begins with the descriptions of the parametric model used in a design problem, the design requirements and design goals. These topics are followed by the explanation of Bayes' theorem, the assignment of probability distribution functions, the sampling of the posterior that produces a number of design candidates and the final decision for obtaining a final design.

2.1 The Models, Design Requirements and Design Goals

The two design applications of interest in this dissertation are antenna array and linear phase FIR filter designs. These two design applications have analogous parametric models, design requirements and goals. The parametric models used in both design applications are atomic models which can be expressed as

$$g(\theta) = \sum_{n=1}^{N} G_n(\mathbf{X}_n, \theta), \tag{2.1}$$

where N is the number of atoms, G_n is a mathematical function of an atom, $\mathbf{X}_n$ denotes the parameters of an atom and θ is the independent variable of interest. In an atomic model, every atom is required to have the same functional form for G_n and hence, the same number of unknown parameters. In the context of both antenna array and FIR filter designs, N and $\mathbf{X}_n$ represent the design parameters of a design problem, and the design goals are to determine the values for all design parameters. The following discussions detail the descriptions of all of the above design aspects for each design application.

2.1.1 Design of Antenna Array

In the application of designing antenna arrays, the parametric model is of the form

$$g(\theta, \phi) = 10 \log_{10} |AF(\theta, \phi)|^2 \quad \text{for} \quad 0 \leq \theta \leq \pi, \quad 0 \leq \phi \leq 2\pi, \tag{2.2}$$

where θ and ϕ denote the far-field observation angle defined in Figure 2.1 and $AF(\theta, \phi)$ is the array factor. Antenna elements can be arranged to form a one, two or three dimensional antenna array.

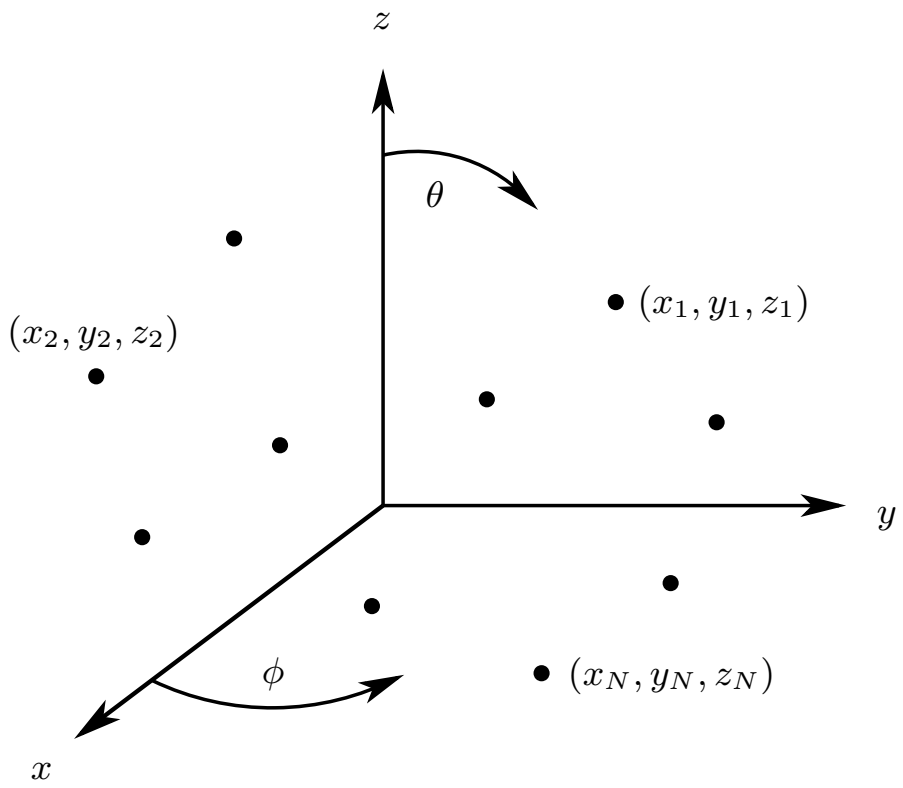

Figure 2.1: 3D antenna array of N antenna elements.

For a three dimensional antenna array with N isotropic radiators in an arbitrary geometry as shown in Figure 2.1, the array factor is expressed as

$$AF(\theta,\phi) = \sum_{n=1}^{N} |I_n| \exp(j\psi_n) \exp\left[j\frac{2\pi}{\lambda}\left(x_n \cos\phi \sin\theta + y_n \sin\phi \sin\theta + z_n \cos\theta\right)\right], \qquad (2.3)$$

where $j = \sqrt{-1}$ and λ is the free space wavelength at the time-harmonic operating frequency. The element parameters I_n, ψ_n, x_n, y_n and z_n, denote the current amplitude, phase, x, y and z positions of the nth antenna element respectively. For a planar antenna array that has N isotropic radiators positioned on the xy plane as shown in Figure 2.2, the array factor in Eq. (2.3) can be rewritten as

$$AF(\theta,\phi) = \sum_{n=1}^{N} |I_n| \exp(j\psi_n) \exp\left[j\frac{2\pi}{\lambda}\left(x_n \cos\phi \sin\theta + y_n \sin\phi \sin\theta\right)\right]. \qquad (2.4)$$

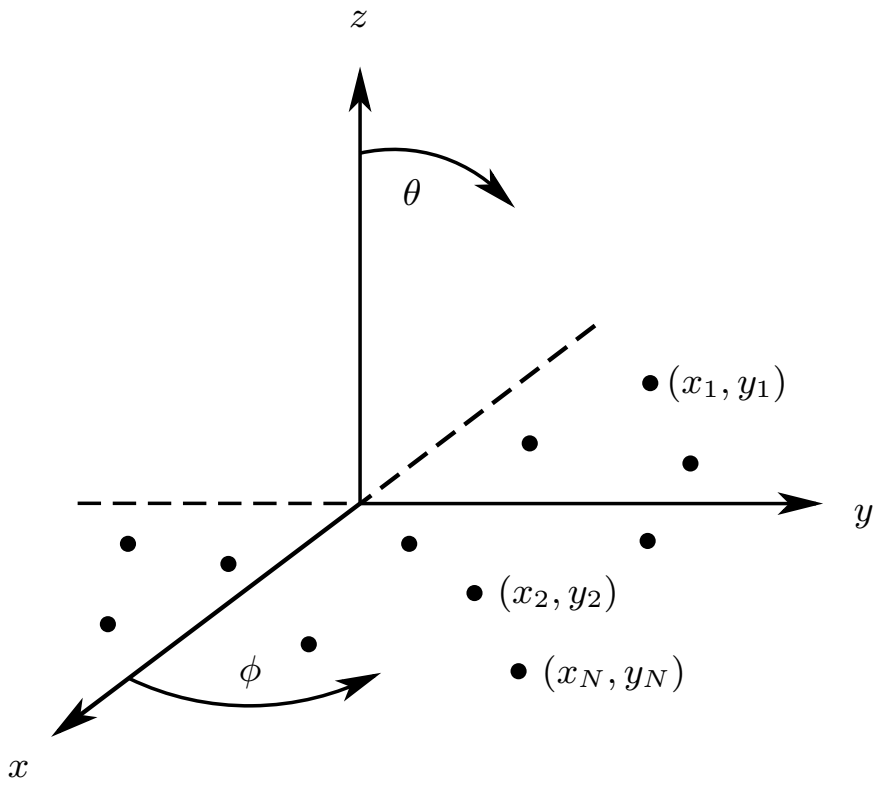

Figure 2.2: Planar antenna array of N antenna elements.

Figure 2.3 illustrates the geometry of a linear antenna array that has N isotropic radiators positioned on the z-axis. For this antenna array, the array factor is

$$AF(\theta) = \sum_{n=1}^{N} |I_n| \exp(j\psi_n) \exp\left[j2\pi \frac{z_n}{\lambda} \cos\theta\right]. \tag{2.5}$$

The array factor in Eq. (2.5) can be rewritten as

$$AF(\theta) = 2\sum_{n=1}^{N} |I_n| \exp(j\psi_n) \cos\left[2\pi \frac{z_n}{\lambda} \cos\theta\right] \tag{2.6}$$

for a symmetrical linear antenna array where N in this case denotes the number of element pairs. If all the excitation currents in a symmetric linear antenna array have only real values, the array factor can be further simplified to

$$AF(\theta) = 2\sum_{n=1}^{N} I_n \cos\left[2\pi \frac{z_n}{\lambda} \cos\theta\right]. \tag{2.7}$$

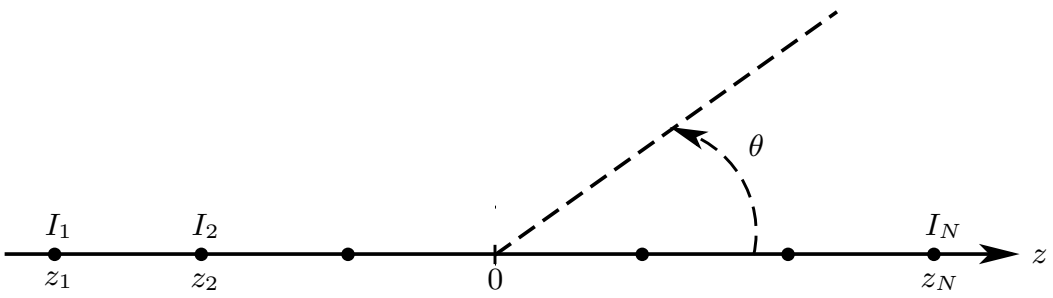

Figure 2.3: Linear antenna array of N antenna elements.

There are a number of ways to specify the desired radiation pattern. In the work presented here, upper and lower bounds in decibels at a finite set of designated angles denoted respectively by $\mathbf{B}_U = \{B_U(\theta_1, \phi_1), B_U(\theta_2, \phi_2), B_U(\theta_3, \phi_3), \cdots, B_U(\theta_M, \phi_M)\}$ and $\mathbf{B}_L = \{B_L(\theta_1, \phi_1), B_L(\theta_2, \phi_2), B_L(\theta_3, \phi_3), \cdots, B_L(\theta_M, \phi_M)\}$ are used, where M is the total number of designated angles. The use of upper and lower envelopes allows important design pattern specifications such as a maximum sidelobe level, main beamwidth, a minimum half-power beamwidth, a desired maximum radiation direction, and a maximum ripple value to be incorporated. In addition to the desired radiation pattern, there are other design requirements that have to be taken into consideration. These design requirements may include a minimum spacing between two adjacent elements, a maximum width of the antenna aperture and a specified operating frequency bandwidth. As explained in Chapter 3, these additional design requirements can be included through the assignment of prior probability distribution functions or modifications of the likelihood. Given specific design requirements, the ultimate goal is to come up with a final design. In this context, the values for all the design parameters N and $\mathbf{X}_n = \{I_n, \psi_n, x_n, y_n, z_n\}$ for $n = 1$ to N are to be determined.

2.1.2 Design of Linear Phase FIR Filter

The frequency response of a L-tap linear phase FIR filter is characterized by its transfer function

$$H(\theta) = \sum_{l=0}^{L-1} h(l) e^{-jl\theta} \quad \text{for} \quad 0 \leq \theta \leq \pi, \tag{2.8}$$

where θ is the dimensionless digital frequency and $h(l)$ is the impulse response. Depending on whether L is odd or even, and whether $h(l)$ is symmetric or antisymmetric, there are four special types of linear phase FIR filters. The amplitude response of these filters is written as

$$A(\theta) = \sum_{k=0}^{K} b_k \, \mathrm{trig}(\theta, k), \tag{2.9}$$

where K and b_k are related to L and $h(l)$ respectively, and $\mathrm{trig}(\theta, k)$ is a sinusoidal function. In the work presented in this dissertation, filters with odd L and symmetric $h(l)$ are used as examples. For this type of filter, the amplitude response is expressed as

$$A(\theta) = \sum_{k=0}^{K} b_k \cos(k\theta), \tag{2.10}$$

where $K = (L-1)/2$ and

$$b_k = \begin{cases} h(K) & \text{for} \quad k = 0 \\ 2h(K-k) & \text{for} \quad k = 1, 2, \ldots, K \end{cases} . \tag{2.11}$$

If $b_k = 0$, then tap k is unused.

To enable the automatic determination of used and unused taps, an atomic form of the amplitude response model is required. To obtain an atomic model for the amplitude response, Eq. (2.10) is rewritten as

$$A(\theta) = \sum_{n=1}^{N} c_n \cos(T_n \theta), \tag{2.12}$$

where T_n takes on the values of the integer tap-position index, k in Eq. (2.10). In Eq. (2.10), k is not a parameter. It is the use of T_n as a parameter in Eq. (2.12) that allows automatic tap use determination.

The following expressions yield values for the parameters in Eq. (2.10) given values of the parameters in Eq. (2.12):

$$K = \max\{T_n\} \tag{2.13}$$

and

$$b_k = \sum_{n:T_n=k} c_n \, . \tag{2.14}$$

The sum in Eq. (2.14) is necessary because the values of T_n for different values of n are not necessarily unique. Eq. (2.14) states that $b_k = 0$ if $T_n \neq k$ for $n = 1$ to N. Using Eq. (2.13), the filter length can be written as

$$L = 2\max\{T_n\} + 1, \tag{2.15}$$

and the total number of taps used, J is

$$J = 2 \times \text{total number of nonzero } b_k - 1. \tag{2.16}$$

In practice, the filter coefficients, b_k, of a linear phase FIR filter are limited in dynamic range and accuracy. For a linear phase FIR filter that have filter coefficients expressed as a sum of signed power-of-two (SPoT) terms, the amplitude response in Eq. (2.12) can be rewritten as

$$A(\theta) = \sum_{n=1}^{N} \pm 2^{-p_n} \cos(T_n\theta), \tag{2.17}$$

where p_n denotes the integer power. The use of SPoT terms constrains the filter coefficients, b_k, to have a discrete set of values, which are expressed as a sum of one or more of the following SPoT terms:

$$\text{SPoT}_n = \{-1, -2^{-1}, -2^{-2}, -2^{-3}, \cdots, -2^{-P}, 2^{-P}, \cdots, 2^{-3}, 2^{-2}, 2^{-1}, 1\}, \tag{2.18}$$

where P denotes the maximum integer power. The parameter N in Eq. (2.17) is related to the total number of SPoT terms used, J by

$$J = 2N - \text{total number of } T_n = 0. \tag{2.19}$$

The filter length remains the same as L in Eq. (2.15).

Figure 2.4 illustrates the desired amplitude response in decibels of a lowpass filter using upper and lower bounds at a total of M designated frequencies, θ_m. As in the design of an antenna array, the upper and lower bounds of the design specifications at the frequency θ_m are denoted by $B_U(\theta_m)$ and $B_L(\theta_m)$ respectively. In Figure 2.4, θ_p, θ_s, δ, and β denote the passband and stopband edge

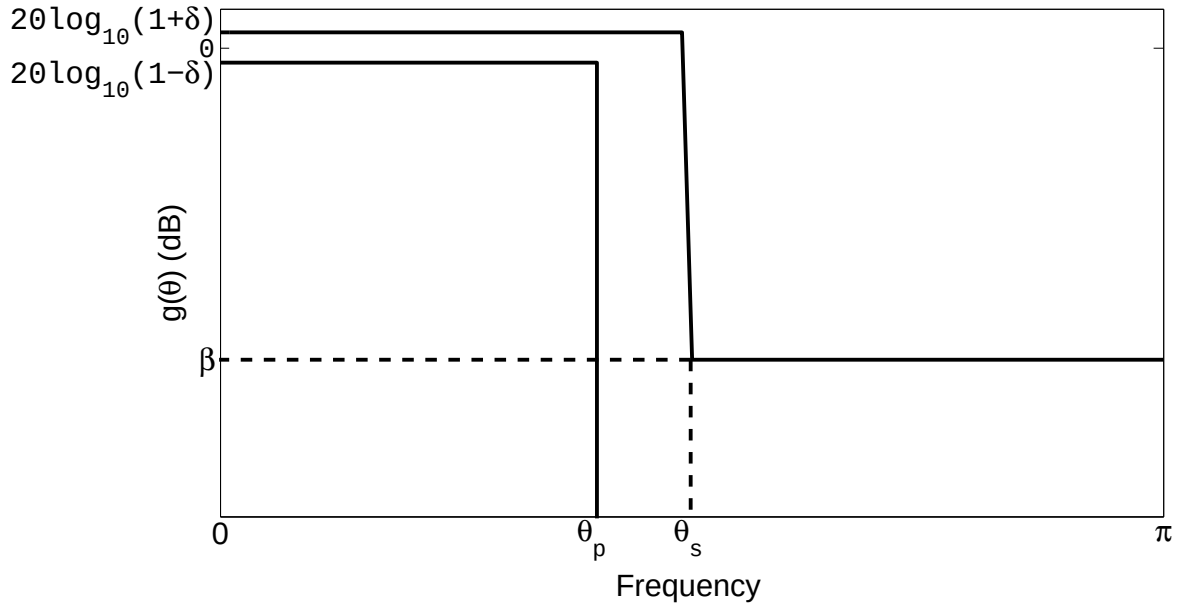

Figure 2.4: Design specifications for a lowpass log filter.

frequencies, the maximum passband ripple and the minimum stopband attenuation, respectively. Given the filter model

$$g(\theta) = 10 \log_{10} |A(\theta)|^2 \quad \text{for} \quad 0 \leq \theta \leq \pi, \tag{2.20}$$

the design goal is to determine the values for all the design parameters, N and $\mathbf{X}_n = \{T_n, c_n\}$ or $\mathbf{X}_n = \{T_n, \text{SPoT}_n\}$ for $n = 1$ to N, to produce a filter design with amplitude response that falls between the desired upper and lower limits.

2.2 Bayesian Inference Framework

2.2.1 Bayes' Theorem

The foundation of Bayesian inference lies with the powerful Bayes' theorem. In the context of both antenna array and linear phase FIR filter designs, Bayes' theorem can be expressed in the following form:

$$p(N, \mathbf{X}_N | \mathbf{B}_U, \mathbf{B}_L, \boldsymbol{\sigma}, E) \propto p(N, \mathbf{X}_N | E) p(\mathbf{B}_U, \mathbf{B}_L | N, \mathbf{X}_N, \boldsymbol{\sigma}, E). \tag{2.21}$$

$\mathbf{X}_N = \{I_1, \psi_1, x_1, y_1, z_1, I_2, \psi_2, x_2, y_2, z_2, \cdots, I_N, \psi_N, x_N, y_N, z_N\}$ are the parameters of the antenna elements while $\mathbf{X}_N = \{c_0, T_0, c_1, T_1, \ldots, c_N, T_N\}$ or $\mathbf{X}_N = \{\text{SPoT}_0, T_0, \text{SPoT}_1, T_1, \ldots, \text{SPoT}_N, T_N\}$ are the coefficients and tap numbers of a FIR filter. In both antenna array and linear phase FIR filter designs, the quantity $\sigma_m \in \{\sigma_1, \sigma_2, \sigma_3, \cdots, \sigma_M\}$ indicates the required degree of compliance between the desired and achieved radiation pattern or frequency response at the designated angle or frequency θ_m. The values of all σ_m are specified by the designer based on the understanding that a smaller value produces a greater degree of compliance. More explanations on the assignment of a value to σ_m are presented in Section 4.2.

A probability distribution function (*pdf*) can be in the discrete, continuous or mixed form. A discrete *pdf* has parameters that can only take a discrete number of values while a continuous *pdf* has parameters that are defined over a continuous interval. A mixed *pdf* has a combination of both the discrete and continuous *pdfs*. To simplify the notation, the symbol p is used to represent all three types of *pdfs* in this dissertation. Additionally, the symbol E that denotes the relevant background information about the design problem of interest is suppressed since every *pdf* is conditioned on the background information. However, it is of great importance to keep in mind its existence in all *pdfs* that follow.

Every term in Eq. (2.21) has a formal name. The term $p(N, \mathbf{X}_N)$ is called the prior *pdf* because it is only conditioned on the background information at hand. Based on the background information, there is no basis for asserting any dependency between N and $\mathbf{X}_N$ or between any two of the parameters of $\mathbf{X}_N$. Thus, all design parameters are treated as independent to avoid asserting information that is not known. Applying the product rule and treating all design parameters as independent, the term $p(N, \mathbf{X}_N)$ can be expanded to

$$p(N, \mathbf{X}_N) = p(N)p(\mathbf{X}_N), \tag{2.22}$$

where

$$p(\mathbf{X}_N) = p(N) \prod_{n=1}^{N} p(I_n)p(\psi_n)p(x_n)p(y_n)p(z_n) \tag{2.23}$$

for the antenna array design and

$$p(\mathbf{X}_N) = p(N) \prod_{n=1}^{N} p(c_n)p(T_n) \quad \text{or} \quad p(N) \prod_{n=1}^{N} p(\text{SPoT}_n)p(T_n) \tag{2.24}$$

for the linear phase FIR filter design. All the prior *pdfs* in Eq. (2.23) and Eq. (2.24) are assigned by the designer based on the design requirements and/or the background information at hand. In the case of antenna array design, these requirements and information could, for example, include the minimum and maximum number of antenna array elements that are required to meet specific design requirements, and the range of values for the element parameters. As for the case of linear phase FIR filter design, the requirements and prior information could include the maximum acceptable filter length and the possible range of values for the filter coefficients. The term $p(\mathbf{B}_U, \mathbf{B}_L|N, \mathbf{X}_N, \boldsymbol{\sigma})$ is called the likelihood function and its derivation will be discussed in Section 2.2.2. Having assigned a *pdf* to all priors and obtained the likelihood function, the posterior *pdf* $p(N, \mathbf{X}_N|\mathbf{B}_U, \mathbf{B}_L, \boldsymbol{\sigma})$ can be approximated computationally using an appropriate sampling technique.

2.2.2 The Likelihood

The derivation of the likelihood begins with the assignment of a *pdf* to the error between the desired and realized radiation pattern or frequency response. At every angle or frequency θ_m for $1 \leq m \leq M$, the error is assigned heuristically the following Laplacian *pdf*:

$$p(B_U, B_L|N, \mathbf{X}_N, \sigma_m) \propto \exp\left[-Q_m/\sigma_m\right], \tag{2.25}$$

where

$$Q_m = \begin{cases} B_L(\theta_m) - g(\theta_m) & \text{for} \quad g(\theta_m) < B_L(\theta_m) \\ g(\theta_m) - B_U(\theta_m) & \text{for} \quad g(\theta_m) > B_U(\theta_m) \\ 0 & \text{otherwise} \end{cases} . \tag{2.26}$$

As mentioned in Section 2.2.1, the value for each σ_m is assigned by the designer. The assigned value indicates the width of the error *pdf* for θ_m. Through the assignment of σ_m, a designer can specify,

based on design preferences, a different degree of compliance between the desired and achieved radiation pattern or frequency response for different regions. Because of logical independence, applying the product rule yields the following likelihood function:

$$p(\mathbf{B}_U, \mathbf{B}_L | N, \mathbf{X}_N, \boldsymbol{\sigma}) = \prod_{m=1}^{M} p(B_U, B_L | N, \mathbf{X}_N, \sigma_m)$$
$$\propto \exp\left[- \sum_{m=1}^{M} Q_m / \sigma_m \right]. \tag{2.27}$$

In addition to the Laplacian *pdf* in Eq. (2.25), another error *pdf*, the Gaussian *pdf*

$$p(B_U, B_L | N, \mathbf{X}_N, \sigma_m) \propto \exp\left[-Q_m^2 / 2\sigma_m^2 \right] \tag{2.28}$$

is used as well. For the Gaussian *pdf*, the likelihood function is of the form

$$p(\mathbf{B}_U, \mathbf{B}_L | N, \mathbf{X}_N, \boldsymbol{\sigma}) = \prod_{m=1}^{M} p(B_U, B_L | N, \mathbf{X}_N, \sigma_m)$$
$$\propto \exp\left[- \sum_{m=1}^{M} Q_m^2 / 2\sigma_m^2 \right]. \tag{2.29}$$

It has been observed that either likelihood can be used in any given design problem, and both likelihoods produce comparable results for the same design problem. In most of the research work presented here, the Gaussian likelihood is employed since it is normally used in Bayesian inference problems.

2.2.3 Sampling of the Posterior

The posterior distribution in Eq. (2.21), which is a function of the design parameters N and $\mathbf{X}_N$, cannot be determined in a closed form. The solution to this problem is to obtain a Monte Carlo approximation of the posterior distribution. In the Monte Carlo approximation, a reasonable number of samples are drawn from the posterior distribution using an appropriate sampling technique. In the work presented here, a program called BayeSys [59] which employs the MCMC method is used to draw W samples from the posterior distribution. In the context of antenna or filter design, each sample drawn from the posterior distribution represents a design candidate or a potential solution

to the design problem of interest. The drawn samples form an approximation to the posterior distribution so that

$$p(N, \mathbf{X}_N | \mathbf{B}_U, \mathbf{B}_L, \boldsymbol{\sigma}) \approx \frac{1}{W} \sum_{w=1}^{W} \epsilon(N - N^w) \delta(\mathbf{X}_N - \mathbf{X}_{N^w}^w) \tag{2.30}$$

where N^w is the number of atoms of the wth sample, δ is the Dirac delta function and

$$\epsilon(N - N^w) = \begin{cases} 1 & \text{for} \quad N = N^w \\ 0 & \text{otherwise} \end{cases} . \tag{2.31}$$

Eq. (2.30) can be used to approximate the expected values of functions under the posterior distribution. Using this property yields the following:

$$\langle N \rangle \approx \frac{1}{W} \sum_{w=1}^{W} N^w \tag{2.32}$$

and

$$p(N | \mathbf{B}_U, \mathbf{B}_L, \boldsymbol{\sigma}) \approx \frac{1}{W} \sum_{w=1}^{W} \epsilon(N - N^w) \tag{2.33}$$

which are the expected value of, and the posterior probabilities for N respectively. Eq. (2.33) comes from $p(N_o | \mathbf{B}_U, \mathbf{B}_L, \boldsymbol{\sigma}) = \langle N - N_o \rangle$ where N_o is some value of N.

2.2.4 Selecting the Final Design

The Bayesian inference portion of the design process ends with the drawing of the design candidates from the posterior distribution. All of the W design candidates are sampled from regions of the posterior distribution where its values are close to or equal to the maximum. As a result, all W design candidates satisfy the prescribed design specifications and requirements with minimal or no error. If a design problem has conditions such as design specifications and requirements of immense complexity, and adverse constraints on the values of the design parameters that render zero-error design unrealizable, then all W design candidates will have error close to the possible minimum error. Because all W design candidates have the potential to become the final design of a design problem, a designer has to choose a single final design from all the design candidates based upon priorities, judgement or additional criteria.

In the design of antenna arrays, if the first priority is to minimize the production cost followed by design performance as the second priority, an antenna designer must first choose all the design candidates that use the fewest number of elements. Among all the selected candidates, the antenna designer can then select the design that has the minimum error as the final design. If an antenna designer decides to prioritize the design performance over production cost, then the designer can choose, among all design candidates that have the minimum error, the design that uses the fewest number of elements as the final design. The article [65] describes another way of obtaining a final design that is to first choose the value of W that has the highest posterior probability value, and of all the design candidates that have the same chosen value of W, the design candidate with the least error is selected as the final design.

Like an antenna designer, a filter designer has to go through a selection process to acquire a final design. The sequence of a selection process depends on how the filter designer prioritizes design criteria such as the design performance, the total number of taps used and the filter length. If the priorities are in the order of design performance, total number of taps used and followed lastly by the filter length, a filter designer must first choose all the design candidates that have the smallest error. Among all the selected candidates, the designer can then narrow down the choices to those designs that use the fewest number of taps. After that, the designer can acquire a final design by selecting the design candidate that has the shortest filter length.

The above methods of selecting the final design may not be useful or practical for any actual design problem. For an actual design problem, the decision-making process may be much more complicated and involve many more factors and criteria. The designer must determine the factors and criteria based on the specifics of the application for which an antenna array or a linear phase FIR filter is being designed, and will presumably be built. In the end, the selection of the final design lies with the designer.

2.3 Ockham's Razor in the Inference Framework

The Bayesian inference framework for design has the ability to design physical systems that have design complexity appropriate to the design specifications and requirements. This is because the Bayesian inference framework embodies the principle of parsimony and quantitatively implements the Ockham's razor principle to render designs that have higher design complexity than required less probable. The Ockham's razor implicit in the Bayesian inference framework ensures that a design that has lower design complexity is preferred to one with higher design complexity, if both designs yield the same degree of compliance between the desired and achieved radiation pattern or frequency response. This property, acting through the posterior probability for the number of atoms $p(N|\mathbf{B}_U, \mathbf{B}_L, \boldsymbol{\sigma})$, allows automatic determination of the design complexity. The automatic determination of the number of atoms is equivalent to Bayesian model selection. The mechanism by which Ockham's razor operates in Bayesian model selection is discussed at length in, among other places, [60, Ch. 3], [61, Ch. 4] and [62, Ch. 28]. This dissertation provides, in the following explanations, an intuitive description of the Ockham's Razor principle in the context of design.

In a design problem, the posterior probability for a design that has design complexity corresponding to N can be written as

$$p(N|\mathbf{B}_U, \mathbf{B}_L, \boldsymbol{\sigma}) = \frac{p(N)p(\mathbf{B}_U, \mathbf{B}_L|N, \boldsymbol{\sigma})}{p(\mathbf{B}_U, \mathbf{B}_L)} \tag{2.34}$$

where

$$\begin{aligned} p(\mathbf{B}_U, \mathbf{B}_L|N, \boldsymbol{\sigma}) &= \int p(\mathbf{X}_N)p(\mathbf{B}_U, \mathbf{B}_L|N, \mathbf{X}_N, \boldsymbol{\sigma})d\mathbf{X}_N \\ &\approx \frac{1}{(\triangle_{prior})^{\alpha N}} (\triangle_{posterior})^{\alpha N} \, max\{p(\mathbf{B}_U, \mathbf{B}_L|N, \mathbf{X}_N, \boldsymbol{\sigma})\} \end{aligned} \tag{2.35}$$

since the peak of the likelihood $p(\mathbf{B}_U, \mathbf{B}_L|N, \mathbf{X}_N, \boldsymbol{\sigma})$ is generally significantly higher than the peak of the priors $p(\mathbf{X}_N)$. In Eq. (2.35), α denotes the number of model parameters when $N = 1$ while $\triangle_{prior}$ and $\triangle_{posterior}$ indicate respectively the width of the priors and posterior in each dimension. For two designs that have design complexity corresponding to N and $N + 1$, comparison is made

by taking the ratio

$$\begin{aligned}\frac{p(N+1|\mathbf{B}_U,\mathbf{B}_L,\boldsymbol{\sigma})}{p(N|\mathbf{B}_U,\mathbf{B}_L,\boldsymbol{\sigma})} &= \frac{p(N+1)p(\mathbf{B}_U,\mathbf{B}_L|N+1,\boldsymbol{\sigma})}{p(N)p(\mathbf{B}_U,\mathbf{B}_L|N,\boldsymbol{\sigma})} \\ &= \frac{p(\mathbf{B}_U,\mathbf{B}_L|N+1,\boldsymbol{\sigma})}{p(\mathbf{B}_U,\mathbf{B}_L|N,\boldsymbol{\sigma})} \\ &\approx \frac{max\{p(\mathbf{B}_U,\mathbf{B}_L|N+1,\mathbf{X}_{N+1},\boldsymbol{\sigma})\}}{max\{p(\mathbf{B}_U,\mathbf{B}_L|N,\mathbf{X}_N,\boldsymbol{\sigma})\}} \left(\frac{\triangle_{posterior}}{\triangle_{prior}}\right)^{\alpha}. \end{aligned} \tag{2.36}$$

Eq. (2.36) is obtained using Eq. (2.35) and the notion of $p(N+1) = p(N)$ which comes from the principle of indifference. In the context of design, this principle states that neither the design that has design complexity corresponding to N or the design with design complexity corresponding to $N+1$ is preferred to the other. From Eq. (2.36), it can be observed that the design with design complexity corresponding to $N+1$ is preferred to the design that has design complexity corresponding to N if the former design has much smaller error or higher likelihood value than the latter design. This is because the ratio of the peak likelihood value in Eq. (2.36) is more than one and becomes the dominant term. In the case where two designs have zero error or the same maximum likelihood value, the design with lower design complexity is preferred since $\triangle_{posterior}$ is generally smaller than $\triangle_{prior}$. The term $\left(\frac{\triangle_{posterior}}{\triangle_{prior}}\right)^{\alpha}$ in Eq. (2.36) is referred to as the Ockham's factor which penalizes designs that have higher design complexity. The Ockham's factor plays a crucial role in the Bayesian inference framework for producing designs that have appropriate design complexity.

CHAPTER 3

SAMPLING THE POSTERIOR DISTRIBUTION

The posterior distribution in Eq. (2.21) cannot be determined in a closed form; however, a Monte Carlo approximation of it can be obtained. In the approximation, a reasonable number of samples are drawn from the posterior distribution using an appropriate sampling algorithm. There are various algorithms that have been developed for efficiently sampling a probability distribution function in a multidimensional parameter space. The work presented in this dissertation employs the computer algorithm BayeSys [59]. BayeSys is a Markov chain Monte Carlo (MCMC) based algorithm written by John Skilling and made available as an open source code in 2004. Monte Carlo methods are computational techniques that make use of random numbers to generate samples from a given probability distribution function such as a posterior distribution. A Markov chain Monte Carlo algorithm uses Markov chains to simulate random walks in the parameter space. The Markov chains evolve by transitions from one state to another state, and eventually converge to the desired posterior distribution. BayeSys has a number of important features. In BayeSys, a multidimensional parameter space is mapped into one dimension using a Hilbert space-filling curve [66]. The exploration along a Hilbert curve is performed using binary slice sampling, which can adaptively scale the exploration steps. Multiple exploration engines are provided so that if one or more engines are thwarted, a different engine can help the system to overcome the obstacle. The convergence of a sampling process to the posterior distribution is difficult. To overcome this difficulty, selective annealing is used to achieve progressive convergence from the prior to the

posterior. Communication among multiple Markov chains or trial objects is facilitated to catalyze each other's sampling progress. An overview of the underlying theory behind BayeSys, which includes all of the above features, is provided in this chapter.

3.1 Atoms and Attributes

The ultimate objective of Bayesian inference is to recover an object of interest from the observations or data. In the context of antenna array and linear phase FIR filter design, the objects of interest are respectively an antenna array design and a linear phase FIR filter design that comply with the design specifications and requirements. These objects are complicated and have many degrees of freedom. Due to the high complexity, it is fitting to decompose the object of interest into some number of parts, which are referred to as atoms in BayeSys. Every atom has a specific number of attributes and is scattered with certain locations over the domain of interest. These locations determine if additional attributes or atoms are required to model the object of interest. In the context of the two design applications of interest, an atom represents an array element, a pair of antenna elements, a filter tap or a SPoT term. The attributes of an atom are the position and complex current of an array element, or the position and coefficient value of a filter tap or SPoT term. The decomposition of the object of interest into a number of atoms, the allowed variation of the number of atoms, coupled with the implicit Ockham's razor principle in Bayesian inference, are the reasons why physical systems that have design complexity appropriate to the design specifications and requirements can be produced by the Bayesian inference framework using BayeSys.

The change in the number of atoms in BayeSys is restricted to the birth or death of only one atom at a time, even though multiple births or deaths are feasible in a MCMC algorithm [67]. The decay time of an atom is chosen to be unit mean of a lifetime, yielding a death rate of

$$p(N-1|N) = Ndt \tag{3.1}$$

in an infinitesimal interval dt of artificial time. The reason for choosing this decay rate is that after

a unit time, most of the atoms would have been altered. It follows from detailed balance, which is explained in Eq. (3.4) on the next page, that the birth rate is

$$\begin{aligned} p(N|N-1) &= \frac{p(N-1|N)p(N)}{p(N-1)} \\ &= \frac{p(N)}{p(N-1)} N dt, \end{aligned}$$

which leads to

$$p(N+1|N) = \Gamma_N dt = \frac{p(N+1)}{p(N)}(N+1)dt. \tag{3.2}$$

If the number of atoms at the start is N, the time to the next birth or death, in the ratio of $\Gamma_N : N$, is exponentially distributed as follows:

$$p(\Delta t) = (\Gamma_N + N) \exp\left[-\left(\Gamma_N + N\right) \Delta t\right]. \tag{3.3}$$

The number of atoms is typically assigned a uniform, geometric or Poisson probability distribution. The choice of prior depends on the degree of complexity that is expected, and the uncertainty of the estimate.

An atom has a certain number of attributes or parameters, which are known as the dimensionality, d. In BayeSys, all parameters are restricted to the range $[0, 1]$, and the priors are uniform over the unit hypercube, $[0, 1]^d$. Because of this restriction, the samples supplied by BayeSys are required to be transformed according to their individual prior *pdf's*, so that sets of parameters that are required in the computation of the likelihood can be obtained. In addition to the restriction, all parameter values in BayeSys are enforced to be an odd multiple of $2^{-(WL+1)}$, where WL is the word length of a computer. The use of this integer representation facilitates the application of binary slice sampling in BayeSys, a topic which is presented in Section 3.3.

3.2 Markov chain Monte Carlo

The Markov chain Monte Carlo algorithm in BayeSys generates samples by using multiple Markov chains to explore the parameter space. Starting at the prior, multiple Markov chains evolve

by transitions from one state to another state, and eventually converge to the desired posterior distribution after going through a certain number of intermediate states. Generally, a transition to the next state depends only on the current state as a Markov chain gradually forgets its earlier states as it evolves. The Markov chains used in BayeSys observe detailed balance

$$p(X = i|X = j)p(X = j) = p(X = j|X = i)p(X = i), \tag{3.4}$$

where $p(X = i)$ and $p(X = j)$ are the equilibrium probabilities of X being in states i and j respectively, and $p(X = j|X = i)$ is the transition probability for the process of X in state $i \rightarrow X$ in state j. Eq. (3.4) states that the transition from states i to j is as probable as the transition from states j to i. This property is of interest in a MCMC simulation because detailed balance implies invariance of the probability distribution, $p(X)$, under the constructed Markov chain, which is a necessary condition for the convergence to $p(X)$.

The posterior distribution is located via the likelihood function. Given that the likelihood is $p(\mathbf{B}_U, \mathbf{B}_L|N_i, \mathbf{X}_{N_i}, \boldsymbol{\sigma})$ and $p(\mathbf{B}_U, \mathbf{B}_L|N_j, \mathbf{X}_{N_j}, \boldsymbol{\sigma})$ at states i and j respectively, the transition from states i to j is accepted if and only if

$$p(\mathbf{B}_U, \mathbf{B}_L|N_j, \mathbf{X}_{N_j}, \boldsymbol{\sigma}) \geq U\left(0, p(\mathbf{B}_U, \mathbf{B}_L|N_i, \mathbf{X}_{N_i}, \boldsymbol{\sigma})\right), \tag{3.5}$$

where U indicates that a random sample is drawn from the uniform distribution over the stated range. The above method is known as the Metropolis Hastings algorithm [68, 69], which satisfies detailed balance. The Metropolis Hastings algorithm can be inefficient if the magnitude of change, $\Delta\mathbf{X}$, is not set to the correct scale in the transitions. If the values used are too large, most of the proposed transitions will be rejected, resulting in the failure to converge to the desired posterior distribution. On the other hand, if the step sizes are too small, the rate of progress will be unnecessarily slow. The solution to this issue is to utilize binary slice sampling which facilitates self-tuning of the step sizes.

3.3 Binary Slice Sampling and Hilbert Curve

Slice sampling [70] originates from the observation that a univariate distribution can be sampled by first drawing sample points uniformly from the region under the curve of its probability distribution function, and then looking only at the horizontal coordinates of the sample points. This method of sampling can adaptively scale the magnitude of change, $\Delta\mathbf{X}$, as illustrated by the following procedure for single-parameter slice sampling:

1. Draw a value, y, uniformly from $(0, p^*(X_{old}))$, where X_{old} is the current point, and $p^*(X)$ is proportional to the target distribution.

2. Define a horizontal slice: $S = \{X : p^*(X) > y\}$.

3. Find an interval around X_{old} that contains all or much of the horizontal slice, S.

4. Draw a new point, X_{new}, from the part of the horizontal slice that is within this interval.

In practice, a slice sampling algorithm requires more detailed steps [70] than the above procedure. The above procedure is presented to provide a basic understanding of slice sampling and a stepping stone to the description of binary slice sampling.

In binary slice sampling, the parameter, X, that is being slice-sampled is represented by a b-bit integer, x, taking on one of 2^b integer values, $x \in \{0, 1, 2, 3, \cdots, 2^b - 1\}$. Given a current point, x_{old}, the basic implementation of binary slice sampling in BayeSys is as follows:

$ro \leftarrow U[0, 2^b)$	Define a random non-zero origin
Do $\{$	Loop
$\quad x_{new} \leftarrow \Big((x_{old} - ro) \oplus U[0, 2^b)\Big) + ro$	Propose a trial point, x_{new}, around x_{old}
$\quad b \leftarrow b - 1$	Shrink the interval around x_{old}

$\}$ While x_{new} is out of range or $p^*(x_{new}) < U\,(0, p^*(x_{old}))$

where $\oplus$ represents the binary bitwise exclusive-OR operation.

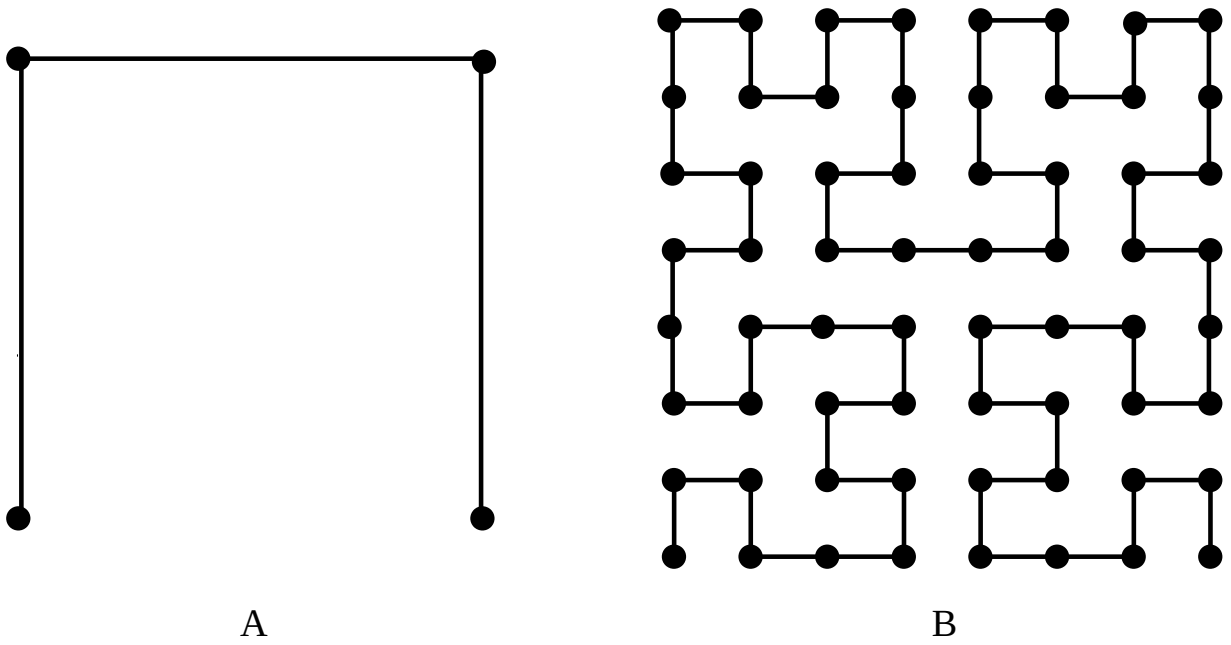

Figure 3.1: First and third level two dimensional Hilbert curves.

The transition scheme in a single-parameter slice sampling algorithm is to alter the current value, X_{old}, by an appropriate ΔX. The same transition scheme can be adapted and used in a binary slice sampling algorithm, by randomizing a certain number of least significant bits of x_{old}. In a slice sampling algorithm, the process of finding an interval around X_{old} may require subsequent broadening of the initial interval so that all or much of the horizontal slice are contained. This interval enlargement process is not required in the binary slice sampling algorithm in BayeSys. This is because as shown in the procedure above, the randomization of x_{old} begins with all b-bits and continues with one fewer most significant bit every time a proposed trial point is rejected. This randomization process is equivalent to shrinking the interval around x_{old}, which is initially very wide, repeatedly by half while locating an acceptable new point. There appear to be barriers to free movement which make it difficult for x to move from one location to another. For example, the movement between two adjacent integers represented by $0111\cdots1111$ and $1000\cdots0000$ requires all b bits to change. These barriers can be overcome by introducing a random non-zero origin denoted by, ro, into the randomization process.

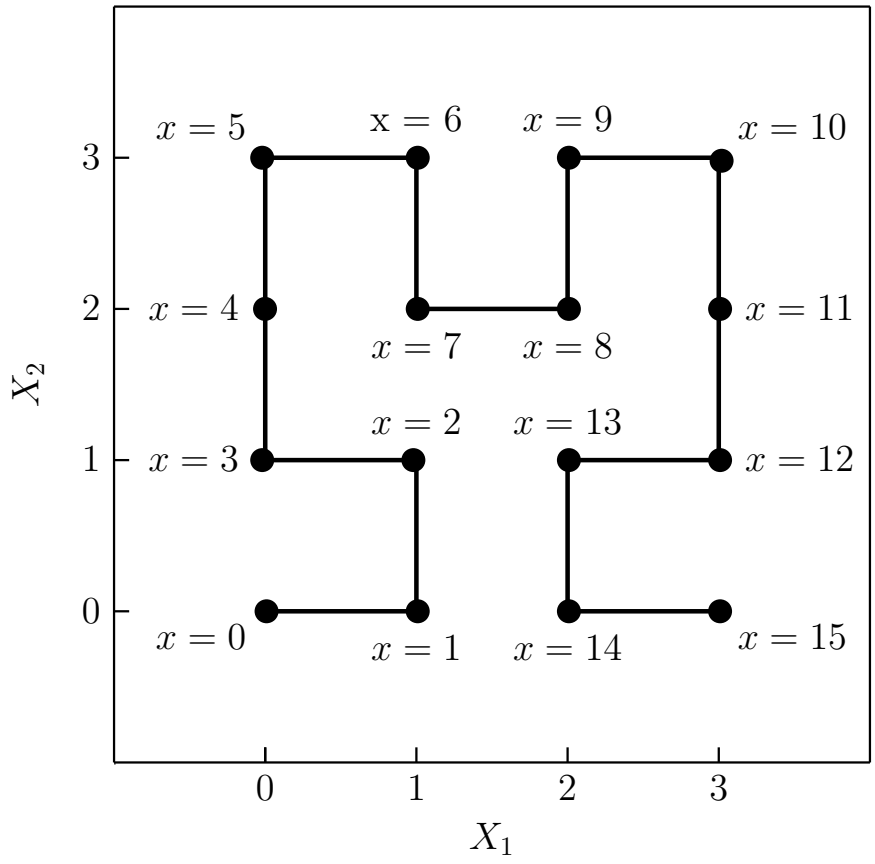

Figure 3.2: Second level two dimensional Hilbert curve.

A prominent advantage of using integer representation is that two or more parameters, $X_1, X_2, X_3, \cdots$, can be represented by a single integer, x, using a reasonable number of additional bits. The integer, x, can be mapped to $X_1, X_2, X_3, \cdots$ using a space-filling Hilbert curve. A Hilbert curve uniformly covers the interior of a d-dimensional hypercube [66]. In addition, a Hilbert curve preserves both locality and continuity. The former indicates that contiguity along the line implies contiguity in the parameter space while the latter means that a probability distribution function that is continuous in the parameter space must also be continuous along the line.

A Hilbert curve can be constructed recursively using its generator. Figure 3.1A shows the two dimensional generator, which is used to construct subsequent levels of Hilbert curve such as the second and third level Hilbert curves plotted in Figure 3.2 and Figure 3.1B respectively. Figure 3.2 illustrates the mapping of a 2-bit integer, x, to two parameters, X_1 and X_2. For example, the integer,

$x = 11$, is mapped to $X_1 = 3$ and $X_2 = 2$. Through the use of a space-filling Hilbert curve, the multidimensional slice sampling can be performed using the same algorithm as for one dimension.

3.4 Selective Annealing

The significant portion of a posterior distribution generally occupies only a tiny fraction of the prior. Almost all of the samples that are drawn from the prior are located at the far ends of the posterior. This feature renders the desired convergence to the posterior very difficult, especially if the posterior distribution is multimodal, which is the case for a design problem since multiple designs that completely satisfy the prescribed design specifications and requirements are conceivable. To solve this problem of "locating a needle in a haystack", BayeSys uses a variant of the simulated annealing technique [71], called selective annealing.

In selective annealing, a sampling process converges progressively from the prior to the posterior distribution. This gradual process can be implemented by introducing an annealing parameter, τ, to the posterior distribution in Eq. (2.21) as follows:

$$\begin{aligned} p(N, \mathbf{X}_N | \mathbf{B}_U, \mathbf{B}_L, \boldsymbol{\sigma}, \tau) &\propto p(N, \mathbf{X}_N) \left[p(\mathbf{B}_U, \mathbf{B}_L | N, \mathbf{X}_N, \boldsymbol{\sigma}) \right]^\tau \\ &\propto p(N, \mathbf{X}_N) \mathcal{L}^\tau (\mathbf{X}_N) , \end{aligned} \tag{3.6}$$

where $\mathcal{L}(\mathbf{X}_N) = p(\mathbf{B}_U, \mathbf{B}_L | N, \mathbf{X}_N, \boldsymbol{\sigma})$ is employed to simplify the notation for the likelihood function. For $\tau = 0$ and $\tau = 1$, the modified posterior in Eq. (3.6) is

$$p(N, \mathbf{X}_N | \mathbf{B}_U, \mathbf{B}_L, \boldsymbol{\sigma}, \tau) \propto \begin{cases} p(N, \mathbf{X}_N) & \text{for } \tau = 0 \\ p(N, \mathbf{X}_N) \mathcal{L}^\tau (\mathbf{X}_N) & \text{for } \tau = 1 \end{cases} . \tag{3.7}$$

Therefore, by gradually increasing τ from zero to one, a sampling process will converge progressively from the prior to the posterior distribution. The problem now is how to increase τ appropriately. In BayeSys, τ is increased adaptively and the overall numerical rate of increase is controlled by the user. The following explanation describes adaptive annealing.

For an ensemble of $\mathcal{J}$ objects, the normalized weight of an object is given by

$$\mathtt{W}_j = \mathcal{J}\frac{\mathtt{w}_j}{\sum_{j=1}^{\mathcal{J}}\mathtt{w}_j}, \quad \text{for} \;\; j = 1, 2, 3, \cdots, \mathcal{J}, \tag{3.8}$$

where

$$\mathtt{w}_j = (\mathcal{L}_j)^{\Delta\tau}, \quad \text{for} \;\; j = 1, 2, 3, \cdots, \mathcal{J}, \tag{3.9}$$

given that $\Delta\tau$ is the magnitude of increase in τ. The computed normalized weights are ranked in an increasing order and after sorting, the integer weights, $\mathcal{W}_j$, for $j = 1, 2, 3, \cdots, \mathcal{J}$ are determined by Eq. (25) in [72], which is

$$\mathcal{W}_j = \sum_{k=0}^{\mathcal{J}-1}\left[\mathcal{U}\left(u + k - \sum_{i=1}^{j-1}\mathtt{W}_i\right) - \mathcal{U}\left(u + k - \sum_{i=1}^{j}\mathtt{W}_i\right)\right], \tag{3.10}$$

where $u \in U[0, 1]$ and

$$\mathcal{U}(x) = \begin{cases} 1 & \text{for} \;\; x > 0 \\ 0 & \text{otherwise} \end{cases}. \tag{3.11}$$

For illustration, $\mathcal{J} = 5$ objects are used and their normalized weights at τ_{old} are listed in Table 3.1. If $u = 0.3$, then the sequence $\{u, u+1, u+2, u+3, u+4\} = \{0.3, 1.3, 2.3, 3.3, 4.3\}$ precedes the cumulative weight at $j = \{2, 3, 4, 5, 5\}$. These results indicate that objects 2, 3, and 4 are each picked once while object 5 is picked twice, and the corresponding $\mathcal{W}_j = \{0, 1, 1, 1, 2\}$ agrees with Eq. (3.10). The net effect is object 1 is replaced by object 5 at $\tau_{new} = \tau_{old} + \Delta\tau$.

The above procedure is called resampling. After resampling, some objects may have the same locations, and the independency among these objects is lost. To regain independent objects, a sufficient number of Metropolis Hastings transitions must occur. It is desirable to have most $\mathcal{W}_j$ being one, and important to avoid discarding most of the objects and replacing them with a few objects that have the highest weights. These goals can be achieved by using

$$\begin{aligned} \Delta\tau &\propto \frac{1}{ln(\mathcal{L}_{max}) - ln\left(\overline{\mathcal{L}}\right)} \\ &= \frac{Rate}{ln(\mathcal{L}_{max}) - ln\left(\overline{\mathcal{L}}\right)}, \end{aligned} \tag{3.12}$$

Table 3.1: Illustration of selective annealing using 5 objects.

Object j	$\mathtt{W}_j$	Cumulative Weight
1	0.2	0.2
2	0.6	0.8
3	0.8	1.6
4	1.3	2.9
5	2.1	5.0

where $\overline{\mathcal{L}}$ is the mean of all $\mathcal{J}$ likelihoods. The quantity, $Rate$, is a positive real value that is assigned by the user. The recommended values for $Rate$ are $0 < Rate \leq 0.5$, where a smaller value results in slower annealing speed.

Selective annealing has a prominent advantage in that resampling facilitates the relocation of an object from its current low likelihood location to a high likelihood location that has been currently discovered. This important feature can assist an object that is trapped in a local minima to escape without having to search for a geometrical exit route. In a problem that has multiple modes, selective annealing becomes even more useful as only one object is required to find a mode, and other objects will follow. Finally, all "good" objects are retained as only the "bad" objects are replaced.

3.5 MCMC Exploration Engines

BayeSys has several MCMC exploration engines and they are LifeStory1, LifeStory2, GuidedWalk, LeapFrog1, LeapFrog2, Chameleon1 and Chameleon2. The reason for having several engines is that any individual engine can be thwarted by a particular form of likelihood, and even if convergence is achieved, the rate of progress may be impractically slow. An alternative engine might overcome the deficiency, only to be trapped in another location. Having multiple engines may not prevail all the time, but a total defeat is less likely given that the engines can help out each other when one or more engines are hindered in their progress.

All of the MCMC exploration engines in BayeSys operate in the environment of an ensemble which has $\mathcal{J}$ objects. An ensemble is considered as a supersystem that has numbers of atoms,

attributes, ensemble prior, ensemble likelihood, and ensemble posterior, all of which are expressed in sequence in the following:

$$\begin{aligned}
\boldsymbol{N} &= \{N_1, N_2, N_3, \cdots, N_{\mathcal{J}}\}, \\
\boldsymbol{X} &= \{\boldsymbol{\mathcal{X}}_1, \boldsymbol{\mathcal{X}}_2, \boldsymbol{\mathcal{X}}_3, \cdots, \boldsymbol{\mathcal{X}}_{\mathcal{J}}\}, \\
p\left(\boldsymbol{X}\right) &= p\left(\boldsymbol{\mathcal{X}}_1\right) p\left(\boldsymbol{\mathcal{X}}_2\right) p\left(\boldsymbol{\mathcal{X}}_3\right) \cdots p\left(\boldsymbol{\mathcal{X}}_{\mathcal{J}}\right), \\
\boldsymbol{L}\left(\boldsymbol{X}\right) &= \mathcal{L}\left(\boldsymbol{\mathcal{X}}_1\right) \mathcal{L}\left(\boldsymbol{\mathcal{X}}_2\right) \mathcal{L}\left(\boldsymbol{\mathcal{X}}_3\right) \cdots \mathcal{L}\left(\boldsymbol{\mathcal{X}}_{\mathcal{J}}\right), \\
\boldsymbol{P}\left(\boldsymbol{X}\right) &= \mathcal{P}\left(\boldsymbol{\mathcal{X}}_1\right) \mathcal{P}\left(\boldsymbol{\mathcal{X}}_2\right) \mathcal{P}\left(\boldsymbol{\mathcal{X}}_3\right) \cdots \mathcal{P}\left(\boldsymbol{\mathcal{X}}_{\mathcal{J}}\right),
\end{aligned}$$

where in the context of design,

$$\begin{aligned}
\boldsymbol{\mathcal{X}}_j &= \mathbf{X}_{N_j}, \\
p\left(\boldsymbol{\mathcal{X}}_j\right) &= p(\mathbf{X}_{N_j}), \\
\mathcal{L}\left(\boldsymbol{\mathcal{X}}_j\right) &= p(\mathbf{B}_U, \mathbf{B}_L | N_j, \mathbf{X}_{N_j}, \boldsymbol{\sigma}),
\end{aligned}$$

and

$$\mathcal{P}\left(\boldsymbol{\mathcal{X}}_j\right) = p(N_j, \mathbf{X}_{N_j} | \mathbf{B}_U, \mathbf{B}_L, \boldsymbol{\sigma}),$$

for $j = 1, 2, 3, \cdots, \mathcal{J}$.

3.5.1 LifeStory Engines

The LifeStory1 engine operates on only one object in the ensemble. This engine combines the processes of birth, death and movement along a Hilbert curve. When an atom is born, it is given a random coordinate or location. In the event of a death, an atom is randomly chosen to be removed. The increase or decrease in the number of atoms is subject to Metropolis Hastings acceptance. Prior to the acceptance or rejection by Metropolis Hastings, movement of the newly born atom or the atom under the death sentence due to binary slice sampling has most likely occurred. If a newly born atom is accepted, a change has been made to the object, and binary slice sampling has likely improved the initial location. On the contrary, no change is observed if rejection occurs. If a death

event is accepted, a randomly selected atom is removed from the object, indicating a change has been made. A change is also observed in the rejection of a death event since the atom that has survived the cut has most likely moved.

The LifeStory2 engine is similar to LifeStory1 except that one of the neighboring atoms is also permitted to move. A neighboring atom can move aside to make room for the birth of an atom, or move nearer to compensate for the loss of an atom. When a newborn atom is accepted, binary slice sampling has likely improved its initial location, and the compensatory location of a neighbor. If a newborn atom is rejected, a change is still observed because a neighbor almost certainly has moved. When a randomly chosen atom survives the cut, it is most likely that this atom and one of its neighbors have both moved. If an atom is indeed removed, a neighboring atom will have moved to compensate for the removal. Overall, useful changes are almost always observed in LifeStory2, making it more powerful than LifeStory1.

3.5.2 Guided Walk and LeapFrog Engines

Both LifeStory engines offer roughly isotropic exploration which can be inefficient in high-dimensional likelihood function. This inefficiency can be overcome by using atoms of different objects. Let L and R represent the left and right neighbors of the atom of interest, X. All three atoms are presumed to come from different objects and represent some feature of the local likelihood, in which they are located. An appropriate trial location can be proposed for X as follows:

$$\mathbf{X}^{trial} = \mathbf{X} + s\left(\mathbf{R} - \mathbf{L}\right),$$

where s is an adjustable scalar, which is kept nearly optimal using binary slice sampling. The above proposition corresponds to a guided walk in the direction of $\pm\left(\mathbf{R} - \mathbf{L}\right)$, which allows an atom to move geometrically within a hypercube space. The use of guided walk helps an ensemble to learn about and utilize the shape of a likelihood function.

BaysSys provides two more engines that are similar to guided walk. These engines, namely LeapFrog1 and LeapFrog2, are simpler to implement. The LeapFrog1 engine uses either the left or

right neighboring atom, which can be from the same object, or preferably from another object. The trial position is given by either

$$\mathbf{X}^{trial} = 2\mathbf{L} - \mathbf{X}, \qquad \text{or} \qquad \mathbf{X}^{trial} = 2\mathbf{R} - \mathbf{X},$$

without any adjustable scalar. The LeapFrog2 engine uses both left and right neighbors, which can be from the same object, or preferably from different objects. The trial position in the LeapFrog2 engine is

$$\mathbf{X}^{trial} = \mathbf{L} + \mathbf{R} - \mathbf{X}.$$

3.5.3 Chameleon Engines

The Chameleon1 engine allows a randomly chosen atom to jump from one object to another. The rationale for having this facility is that an atom might be better placed in another object than its source. In addition, this facility could occasionally rescue the destination object out of a trap. Based on the Metropolis Hastings rule, a proposed jump is accepted if and only if

$$\mathbf{\mathit{L}}_{new} \geq U\left(0, \mathbf{\mathit{L}}_{old}\right),$$

where $\mathbf{\mathit{L}}_{old}$ and $\mathbf{\mathit{L}}_{new}$ are respectively the ensemble likelihood prior to and after the jump. In the event of a jump, only the source and destination likelihoods are changed.

The Chameleon2 engine is an extension of Chameleon1 in that pairs of atoms are allowed to swap ensemble memberships. After an exchange, both atoms retain their attribute values from the source object. To encourage synergy between a pair of jumps, the two selected atoms should be close together as if they are neighbors of the same object. As in the Chameleon1 engine, a proposed switch is accepted if and only if

$$\mathbf{\mathit{L}}_{new} \geq U\left(0, \mathbf{\mathit{L}}_{old}\right).$$

CHAPTER 4

DESIGN OF ANTENNA ARRAY

The Bayesian inference framework for design has been applied to the design of antenna arrays. In this chapter, several antenna array design examples are presented. An antenna array design problem generally has three main aspects: the desired radiation pattern, the type of antenna array used and the practical design requirements that are required to be incorporated. The design problems presented in this chapter use different types of antenna arrays such as symmetric linear array with real-valued currents, asymmetric linear array with complex currents, reconfigurable linear array and planar array to realize various desired radiation patterns while satisfying certain prescribed practical design requirements. The radiation patterns of interest include two broadside patterns, an end-fire pattern, a shaped beam pattern which is the sector beam pattern, and a three-dimensional radiation pattern. In practice, apart from the design pattern specifications, a design problem consists of additional practical design requirements such as a minimum spacing between two adjacent array elements, limitations in the dynamic range and accuracy of the current amplitudes and phases, and the ability to maintain a desired radiation pattern over a frequency band. A much more challenging requirement is the ability to maintain a desired radiation pattern when one or more array elements are defective or failing. The above examples of practical design requirements have all been implemented and are shown in the design problems presented in Section 4.3.

In the Bayesian inference framework for design, the process of solving an antenna array design problem generally consists of the following steps. The first step is to specify the desired radiation

pattern and the type of antenna array to be used. The second step is to assign either a Laplacian or Gaussian *pdf* to the error between the desired and achieved radiation pattern. Following the assignment of an error distribution, the likelihood function can be obtained. The third step is to assign a *pdf* to all design parameters which include the number of array elements or element pairs, N, and the parameters of all antenna elements, $\mathbf{X}_N$. This is followed by the assignment of a value to all σ_m which denote the degree of compliance between the desired and achieved radiation pattern. At this stage, the likelihood function, $p(\mathbf{B}_U, \mathbf{B}_L | N, \mathbf{X}_N, \boldsymbol{\sigma})$, and the prior *pdf*, $p(N, \mathbf{X}_N)$, in Eq. (2.34) are determined. Hence, the next step is to approximate the posterior *pdf*, $p(N, \mathbf{X}_N | \mathbf{B}_U, \mathbf{B}_L, \boldsymbol{\sigma})$, by drawing a reasonable number of samples from it. The design process concludes with the selection of a design candidate from all the drawn posterior samples as the final design.

All of the above procedures have been explained at length in Chapter 2 with the exception of a detailed description of how the assignment of a *pdf* to the design parameters and the assignment of a value to σ_m are made. Prior to the presentation of the design examples, the following discussions describe how the design parameters are assigned a *pdf* and how σ_m is assigned a value based on the background information which encompasses some practical design requirements.

4.1 Assignments for the Design Parameters

The design parameters of an antenna array design problem include the number of array elements or element pairs, N, the current amplitudes and phases, $\{I_1, \psi_1, I_2, \psi_2, \cdots, I_N, \psi_N\}$, and the positions of the array elements, $\{x_1, y_1, z_1, x_2, y_2, z_2, \cdots, x_N, y_N, z_N\}$. For the parameter N, a discrete uniform distribution, $U[N^{min}, N^{max}]$, is generally assigned for it when only the minimum and maximum acceptable values are known. The integer N^{max} indicates the maximum number of antenna elements or element pairs that is allowed in a design problem. Generally, N^{max} can be given any positive value; however, in practice, the assignment of N^{max} could be dictated by the antenna array production cost since the use of more antenna elements results in higher production

cost. The integer N^{min}, which is often given the value 1, denotes the minimum number of antenna elements or element pairs that is acceptable in a design problem. It is possible for a designer to assign a larger value to N^{min} if the designer is sure that the desired radiation pattern cannot be realized using a N value that is less than N^{min}. Otherwise, giving N^{min} a too large value will result in the failure to acquire antenna array designs that have design complexity appropriate to the design specifications and requirements.

The positions of the array elements of a linear antenna array are denoted by $\{z_1, z_2, z_3, \cdots, z_N\}$. For the parameter z_n, a continuous uniform distribution, $U[z_n^{min}, z_n^{max}]$, is generally assigned for it when only the range of the z_n values is known. In an asymmetric linear antenna array, the real-valued z_n^{min} and z_n^{max} indicate the positions that are allowed in a design problem for the placement of the first and last antenna elements respectively. A common practical design requirement is a maximum aperture width that is allowed in a linear antenna array design. This practical design requirement can be incorporated into the values assigned to z_n^{min} and z_n^{max}, because the maximum aperture width that a designed asymmetric linear antenna array can have is equal to $z_n^{max} - z_n^{min}$. For a symmetric linear antenna array, z_n^{min} and z_n^{max} must both be positive or negative. The quantity z_n^{max} indicates the position that is allowed for the placement of the last pair of antenna elements. Since the maximum aperture width that a designed symmetric linear antenna array can have is $2 \times z_n^{max}$, a designer can incorporate the maximum acceptable aperture width specified in a design problem into the value assigned to z_n^{max}. The quantity z_n^{min} indicates the position that is allowed for the placement of the first pair of antenna elements. In practice, a minimum spacing is required between two adjacent array elements. To ensure that the spacing between the first pair of array elements satisfies the minimum spacing requirement, z_n^{min} is often given a value equal to half of the minimum spacing value.

For a planar array that has antenna elements placed in the xy plane, the positions of the array elements are denoted by $\{x_1, y_1, x_2, y_2, \cdots, x_N, y_N\}$. When only the range of the x_n and y_n values are known, the parameters x_n and y_n are both assigned a continuous uniform distribution which

is denoted by $U[x_n^{min}, x_n^{max}]$ and $U[y_n^{min}, y_n^{max}]$ respectively. The real-valued x_n^{min}, x_n^{max}, y_n^{min} and y_n^{max} denote the minimum and maximum x and y positions that are allowed for the placement of an array element on the xy plane. Since $x_n^{max} - x_n^{min}$ and $y_n^{max} - y_n^{min}$ equal to the maximum length and width that a designed planar array can have, a designer can incorporate the maximum acceptable planar array dimensions specified in a design problem into the values assigned to x_n^{min}, x_n^{max}, y_n^{min} and y_n^{max}.

The assignment of a *pdf* to a current value depends on whether the current value is real or complex. For a real-valued current, the current amplitude I_n is assigned a uniform distribution, $U[I_n^{min}, I_n^{max}]$, if the only information possessed are the minimum and maximum acceptable values that are denoted by I_n^{min} and I_n^{max} respectively. The ranges of the current amplitudes depend on the phases of the current sources. If the current sources have a uniform phase, the current amplitudes can either be all positive or negative. If one or more current sources have a phase shift of $180°$, $I_n^{min} = -I_n^{max}$ given that I_n^{max} is positive. The parametric model in Eq. (2.2) corresponds to the unnormalized radiation pattern. When a parametric model representing a radiation pattern that is not normalized with respect to its peak level is used, I_n^{min} and I_n^{max} are generally given a value such that a peak level of 0 dB can be realized when $N = 1$. For a complex-valued current, the *pdf* assigned to the current value is in the shape of a cylinder. The magnitude of a complex current is uniformly distributed over the specified range of $|I_n|$ while the phase is uniformly distributed over $[0, 2\pi]$. The program BayeSys [59, Section 5.1.2] facilitates a subroutine that draws samples from the cylindrical distribution. To use the subroutine, the range of $|I_n|$ has to be specified. The drawn samples are represented by their real and imaginary values which are $|I_n| \cos \psi_n$ and $|I_n| \sin \psi_n$ respectively.

In a design problem, the determined values of a design parameter are generally required to be in an acceptable range. As described in this section, this type of practical design requirement can be treated as prior information and is incorporated into the prior *pdfs*. There are other practical design requirements such as those described at the start of this chapter. The incorporation of these practical

design requirements requires the modifications of the likelihood function which will be addressed in the presentation of the design examples.

4.2 Assignments for σ_m

As explained in Section 2.2.2, a Laplacian or Gaussian *pdf* is assigned to the error between the desired and realized radiation patterns at each angle θ_m. The width of the error distribution for θ_m is denoted by σ_m, a quantity which has to be assigned a value. Depending on the complexity of a design problem which includes the desired radiation pattern, practical design requirements, and constraints on the design parameters, the obtained error distribution for θ_m is not guaranteed to have the specified width, or even the shape of the assigned distribution. In the context of antenna array design, the ultimate goal is to acquire designs that meet the design pattern specifications and practical design requirements with minimal or no error, rather than to obtain an error distribution that has the specified shape and width for every θ_m. Since a smaller σ_m value results in a greater degree of compliance between the desired and realized radiation patterns, the values that are assigned to all σ_m should be as small as possible so that designs that have minimal or zero error can be realized. However, the assignment of smaller values to σ_m narrows the width of or sharpens the posterior distribution. Consequently, the sampling of the posterior distribution becomes harder and requires higher computational cost. In order to solve a design problem within a reasonable amount of computational time, the key is to assign all σ_m with the largest possible values that can still yield full compliance between the desired and achieved radiation patterns.

Investigations have been conducted to find out how to determine the appropriate values for all σ_m. The findings reveal that the assignment of a value to σ_m depends on many aspects of a design problem. These aspects include the desired radiation pattern, the parametric model or array factor that is used and the practical design requirements. In a desired radiation pattern, there are regions that have smaller margins for error and the σ_m at these angles should all be assigned a smaller value. The values that are assigned to σ_m also hinge on the type of antenna array used in a design

problem. If both symmetric and asymmetric linear antenna arrays are used to solve the same design problem, the σ_m in the latter case should be assigned a smaller value. This is because the parametric model of an asymmetric linear antenna array is more complicated and generally contains more design parameters. The complexity of the practical design requirements also plays a crucial role in the value assignments for σ_m. If one design problem requires a designed linear antenna array to have the ability to achieve the desired radiation pattern over a frequency band and another design problem requires a minimum spacing to exist between two adjacent array elements, smaller values should be assigned to the σ_m in the former case. This is because maintaining the performance of an antenna array over a frequency band is more difficult than enforcing a minimum spacing between two adjacent elements. The above findings all point to the conclusion that the σ_m in a more complex design problem should be assigned smaller values.

The above findings have proved to be helpful when solving an antenna design problem. Nevertheless, a systematic procedure for determining the appropriate values for all σ_m remains the most desirable tool to have for assigning values to σ_m. This tool has not been discovered in the investigations because the difficulty and complexity involved in finding the appropriate σ_m values is very high. In order to devise the tool, a much more extensive and exhaustive study is required. In all the design problems presented in this chapter, the values for all σ_m are assigned based on experience, intuition and, in some cases, trial and error.

4.3 Design Problems

This section presents the results for several antenna array design problems. In all the presented design problems, the Gaussian likelihood in Eq. (2.29) is used and the number of samples drawn from the posterior distribution is $W = 3000$. Each of the 3000 samples represents a design candidate. For all the design examples presented here, the final design is selected using a multistep process. The selection process begins by first selecting the design candidates that have zero or the minimum error. The next step is to narrow down the selected design candidates to those designs

that use the fewest number of array elements. Of all the remaining design candidates, the design candidate with the smallest antenna aperture dimension is chosen as the final design.

4.3.1 Sector Beam Pattern

The first design problem to be presented is the sector beam pattern [15] whose design pattern specifications are indicated by the dashed lines in Figure 4.1. There are basically two regions in the radiation pattern. The first region that falls in the range of $78.3^\circ \leq \theta \leq 101.7^\circ$ contains ripples that have to be smaller than 0.5 dB. The second region, that is in the range of $0^\circ \leq \theta \leq 69.3^\circ$ and $110.7^\circ \leq \theta \leq 180^\circ$, has desired sidelobe levels that are lower than -25 dB. For this design problem, the goal is to produce a radiation pattern that completely satisfies the desired pattern specifications using a symmetric linear antenna array with real-valued current sources. The parametric model used in the inference framework is Eq. (2.7) and the number of equally spaced angles used is $M = 101$. Since the array factor is symmetric about $\theta = 90^\circ$, the 101 predefined angles need to cover only the range of $0^\circ \leq \theta_m \leq 90^\circ$. Sections 4.1 and 4.2 have explained how assignments can be made for the design parameters and σ_m. For the current design problem, the assignments are

$$p(N) = U[1, 20],$$

$$p(I_n) = U[-0.5, 0.5],$$

$$p(z_n/\lambda) = U[0.25, 4.75],$$

and

$$\sigma_m = \begin{cases} 1/2 \text{ dB} & \text{for } \ 0^\circ < \theta_m < 78.3^\circ \\ 1/5 \text{ dB} & \text{for } \ 78.3^\circ \leq \theta_m \leq 90.0^\circ \end{cases}.$$

The current amplitudes for this problem are allowed to have negative and positive values because a shaped beam pattern such as the sector beam pattern cannot be realized using currents that have a uniform phase.

The obtained results are summarized in Table 4.1, Table 4.2 and Figure 4.1. The final design for this design example is not chosen based on the multistep process described at the beginning of

Table 4.1: Estimated posterior probability for the number of element pairs for the sector beam pattern. In this case, $\langle N \rangle = 6.65$.

N	$p(N\|\mathbf{B}_U, \mathbf{B}_L, \boldsymbol{\sigma})$
5	0.137000
6	0.402667
7	0.244000
8	0.127000
9	0.070667
10	0.016667
11	0.002000

Table 4.2: Current amplitudes and positions of the antenna elements for the final design of the sector beam pattern.

Element Number	I_n	z_n/λ
1	0.360296	0.351589
2	0.184328	1.050703
3	-0.000144	2.205824
4	-0.066528	2.417333
5	-0.034567	3.035362
6	0.030780	4.152995

Section 4.3. Instead, the final design is chosen to illustrate that, since the positions of the antenna elements are not fixed and without a constraint on the spacing between two adjacent antenna elements, it is possible to have two adjacent array elements placed too close to each other as shown in Table 4.2. Even though the produced radiation pattern at the 101 predefined angles fully satisfies the design pattern specifications as shown in Figure 4.1, this linear antenna array design is physically not realizable because the 3rd and 4th array elements are too close to each other. To avoid having physically unrealizable linear antenna array designs, a constraint must be imposed on the spacing between two adjacent array elements. The following section presents a design problem that requires a certain minimum spacing to exist between two adjacent antenna elements.

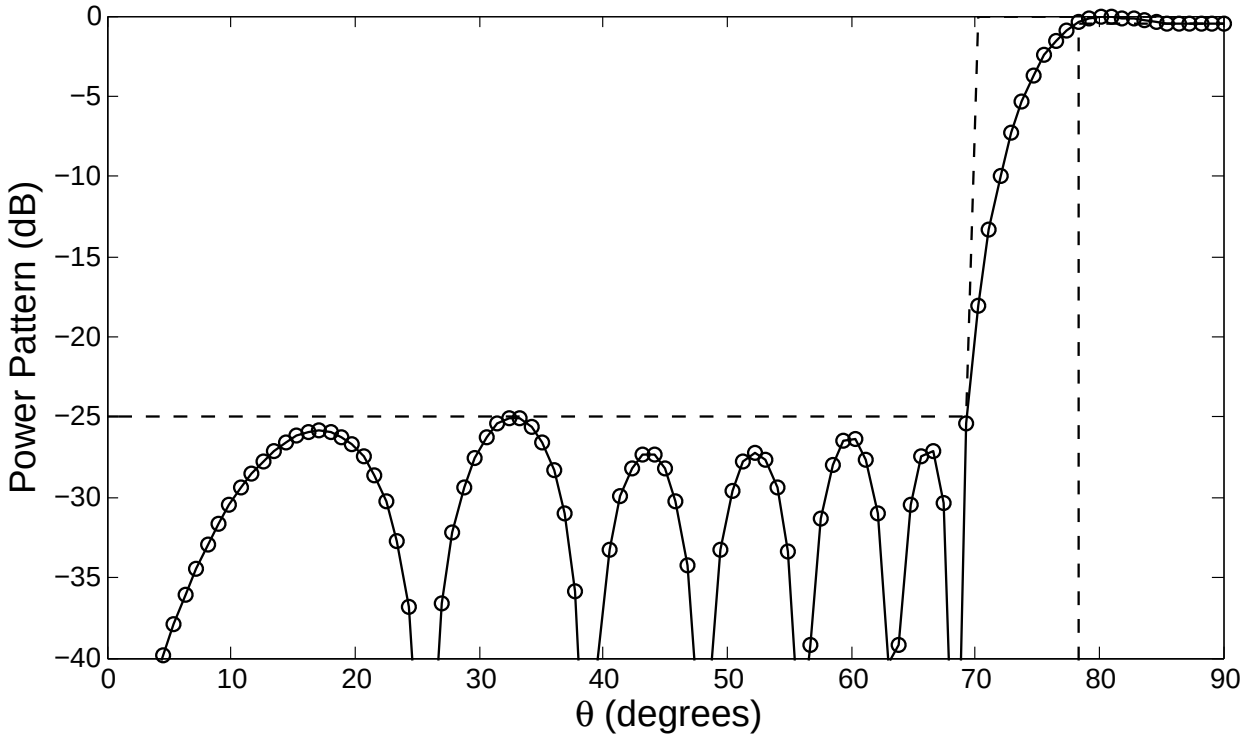

Figure 4.1: Achieved sector beam pattern using the inference framework. $\boldsymbol{B_U}$ and $\boldsymbol{B_L}$ are denoted by dashed lines.

4.3.2 Sector Beam Pattern with a Minimum Element Spacing

To ensure that any two adjacent antenna elements are not placed too close to each other, a desired minimum value, Δz_{min}, is imposed on the spacing between two adjacent antenna elements. Since BayeSys requires the prior *pdf* for all z_n to have the same functional form, the constraint on the element spacing cannot be incorporated into the prior *pdf* for z_n. Instead, the practical design requirement of having a minimum spacing between two adjacent antenna elements is imposed by modifying the Gaussian likelihood in Eq. (2.29) as follows:

$$p(\mathbf{B}_U, \mathbf{B}_L | N, \mathbf{X}_N, \boldsymbol{\sigma}) \propto \exp\left[-Q_z^2/2\sigma_z^2 - \sum_{m=1}^{M} Q_m^2/2\sigma_m^2\right], \tag{4.1}$$

where

$$Q_z = \begin{cases} \Delta z_{min} - \min(z_{i+1} - z_i) & \text{for } \min(z_{i+1} - z_i) < \Delta z_{min}\,, \;\; i = 1, 2, \ldots, N-1 \\ 0 & \text{otherwise} \end{cases} \tag{4.2}$$

and similar to σ_m, σ_z is a quantity that has to be assigned a value. The assignment of σ_z depends on the relative importance of two design objectives which are realizing the desired radiation pattern and achieving the minimum required element spacing. Generally, these two design goals can be satisfied concurrently in a linear antenna array design problem, and thus, σ_z can be given any reasonable value. If these two design goals cannot be achieved concurrently, a compromise is required and the relative importance of these two design objectives can be reflected through the relative values assigned to σ_m and σ_z.

To illustrate the implementation of the design requirement of having a minimum spacing between two adjacent antenna elements, the previous sector beam pattern design problem is used. For this design problem, Δz_{min} is specified to be 0.5λ and the following assignments are made:

$$p(N) = U[1, 20],$$
$$p(I_n) = U[-0.5, 0.5],$$
$$p(z_n/\lambda) = U[0.25, 4.75],$$
$$\sigma_z = 1/100,$$

and

$$\sigma_m = \begin{cases} 1/2 \text{ dB} & \text{for } \ 0^\circ < \theta_m < 78.3^\circ \\ 1/5 \text{ dB} & \text{for } \ 78.3^\circ \leq \theta_m \leq 90.0^\circ \end{cases}.$$

Table 4.3, Table 4.4 and Figure 4.2 summarize the obtained results. As in the previous design problem, many of the design candidates obtained here have zero error. While numerous design candidates with zero error in the previous design problem are physically unrealizable, all the design candidates with zero error in the current design problem are physically realizable. This is because zero error in the current design problem indicates that not only the design pattern specifications are fully satisfied, all the spacings between two adjacent antenna elements are at least 0.5λ.

The parameter values of the antenna elements for the final design are displayed in Table 4.4. Using these values, the radiation pattern at the 101 predefined angles is plotted in Figure 4.2. The final design uses 5 pairs of antenna elements which is two pairs fewer than the 7 pairs obtained

Table 4.3: Estimated posterior probability for the number of element pairs for the sector beam pattern with a minimum element spacing of 0.5λ. $\langle N \rangle = 5.20$ for $\sigma_m = 1/2$ or $1/5$ while $\langle N \rangle = 4.08$ for $\sigma_m = 2.5$ or 1.0.

$\sigma_m = 1/2$ or $1/5$		$\sigma_m = 2.5$ or 1.0	
N	$p(N\|\mathbf{B}_U, \mathbf{B}_L, \boldsymbol{\sigma})$	N	$p(N\|\mathbf{B}_U, \mathbf{B}_L, \boldsymbol{\sigma})$
4	0.000667	3	0.015714
5	0.802667	4	0.893929
6	0.190667	5	0.088571
7	0.006000	6	0.001786

Table 4.4: Current amplitudes and positions of the antenna elements for the final design of the sector beam pattern with a minimum element spacing of 0.5λ.

	$\sigma_m = 1/2$ or $1/5$		$\sigma_m = 2.5$ or 1.0	
Element Number	I_n	z_n/λ	I_n	z_n/λ
1	-0.369432	0.355845	0.357544	0.361559
2	-0.187986	1.070300	0.187923	1.083078
3	0.057547	2.404585	-0.070778	2.471254
4	0.036646	2.971623	-0.033291	3.114672
5	-0.030678	4.112518	0.026269	4.252864

Table 4.5: The error points produced by the final design for $\sigma_m = 2.5$ or 1.0.

θ (degrees)	$B_L(\theta)$ (dB)	$B_U(\theta)$ (dB)	Achieved Power (dB)
65.7	$-\infty$	-25.0	-24.88
66.6	$-\infty$	-25.0	-24.06
78.3	-0.5	0.0	-0.61
86.4	-0.5	0.0	-0.51
87.3	-0.5	0.0	-0.55
88.2	-0.5	0.0	-0.57
89.1	-0.5	0.0	-0.58
90.0	-0.5	0.0	-0.58

in [15] that uses fixed positions. In fact, many of the 3000 design candidates that have zero error use only 5 pairs of array elements. Another notable comparison between these two results is that the design parameters here do not include the phase of a driving current, ψ_n. Instead, the real-valued currents are allowed to have negative values. The use of this property along with the positions of the array elements are sufficient to realize the desired sector beam radiation pattern.

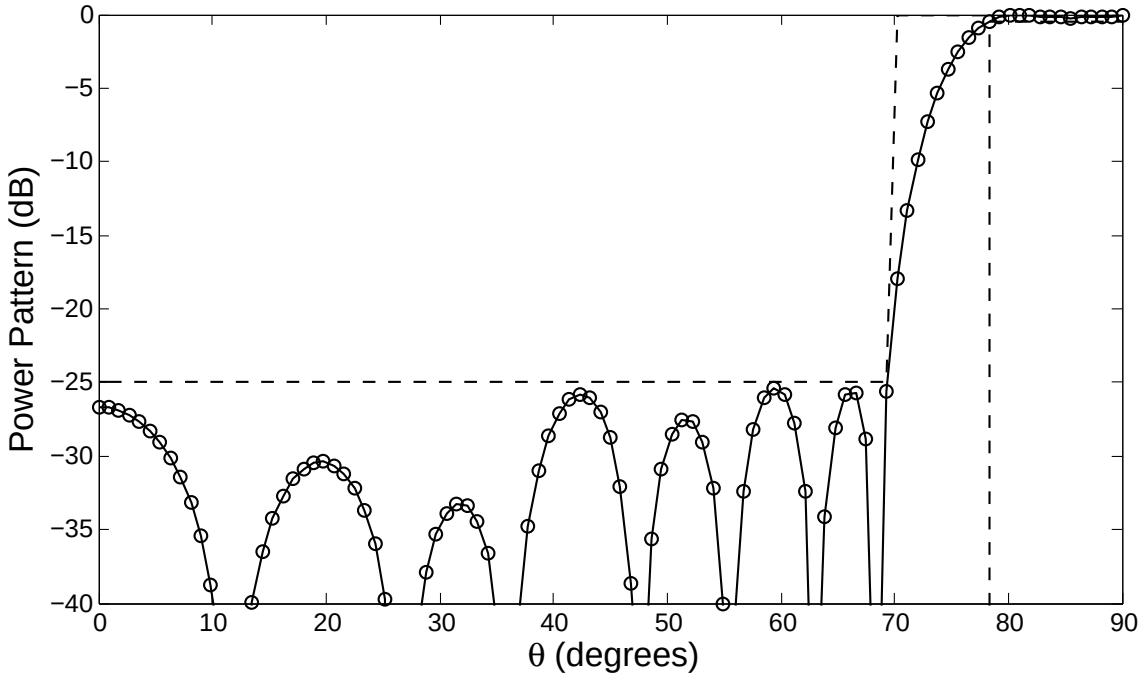

Figure 4.2: Achieved sector beam pattern with a minimum element spacing of 0.5λ using the inference framework for $\sigma_m = 1/2$ or $1/5$. $\boldsymbol{B_U}$ and $\boldsymbol{B_L}$ are denoted by dashed lines.

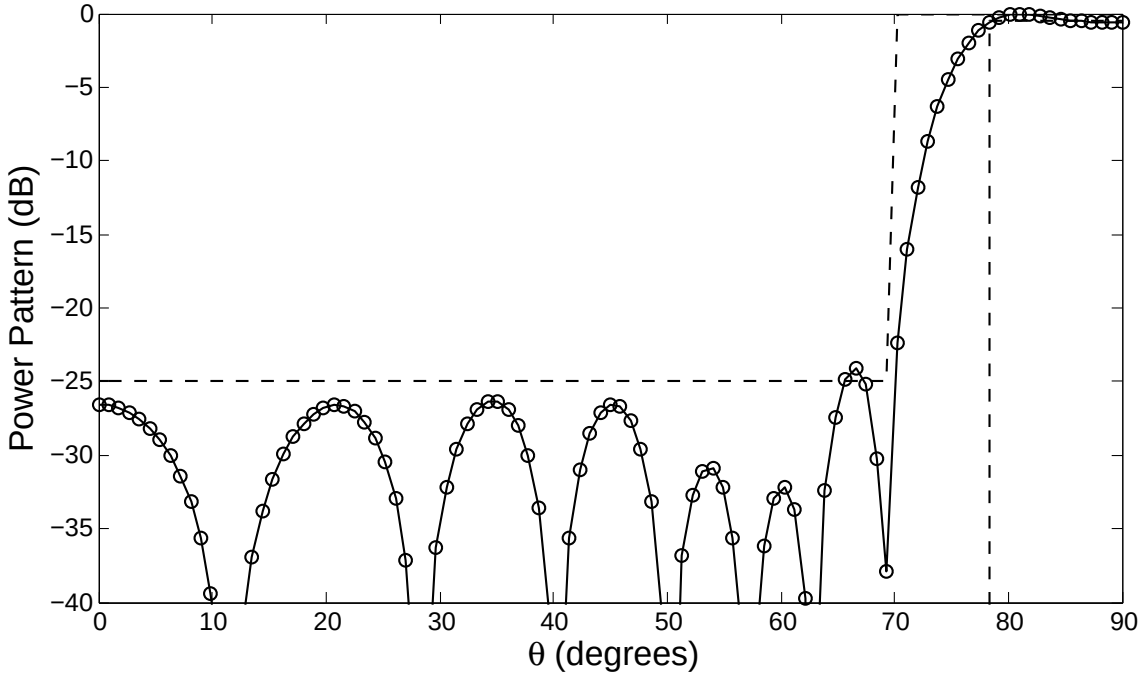

Figure 4.3: Achieved sector beam pattern with a minimum element spacing of 0.5λ using the inference framework for $\sigma_m = 2.5$ or 1.0. $\boldsymbol{B_U}$ and $\boldsymbol{B_L}$ are denoted by dashed lines.

Section 4.2 discusses the importance of assigning an appropriate value to all σ_m. If the assigned values are too large, none of the 3000 design candidates will have zero error. This observation is illustrated by the design example in which

$$\sigma_m = \begin{cases} 2.5 \text{ dB} & \text{for } \ 0^\circ < \theta_m < 78.3^\circ \\ 1.0 \text{ dB} & \text{for } \ 78.3^\circ \leq \theta_m \leq 90.0^\circ \end{cases} .$$

For this design example, the design candidate that has the minimum error is chosen as the final design. The parameter values of the antenna elements for the final design are displayed in Table 4.4. Using these values, the radiation pattern at the 101 predefined angles is plotted in Figure 4.3 which shows that the design pattern specifications are not fully met. There are 8 points that fall outside the envelopes and they are listed in Table 4.5. The results of this design example show that all σ_m must be assigned an appropriate value in order to acquire designs that have zero error.

Having successfully incorporated the design requirement of having a minimum spacing between two adjacent antenna elements, this practical design requirement is included in all the remaining linear antenna array design problems that are going to be presented. This is because in practice, any two adjacent antenna elements are required to have a minimum separation between them.

4.3.3 Chebyshev Pattern

The article [29] discusses the importance of designing linear antenna arrays using as few antenna elements as possible. This article presents a method which can reproduce the radiation pattern generated by an existing design using a linear antenna array that has fewer antenna elements. It is interesting to compare the results obtained by the method in [29] with the results produced by the Bayesian inference framework for design. For results comparison, the broadside Chebyshev pattern, which is Example 1 of [29], is used. The original Chebyshev pattern that was produced using 10 pairs of uniformly spaced antenna elements has desired sidelobe levels that are lower than -30 dB. The beam widths at -30 dB and -3 dB are desired to be less than 16.0° and at least 6.3° respectively. Since the Chebyshev pattern is symmetric, the parametric model in Eq.

Table 4.6: Estimated posterior probability for the number of element pairs for the Chebyshev pattern design. In this case, $\langle N \rangle = 6.00$.

N	$p(N\|\mathbf{B}_U, \mathbf{B}_L, \boldsymbol{\sigma})$
6	1.000000

Table 4.7: Current amplitudes and positions of the antenna elements obtained by the inference framework and matrix pencil method for the Chebyshev pattern.

	Inference Framework			Matrix Pencil Method	
Element Number	I_n	Normalized I_n	z_n/λ	I_n	z_n/λ
1	-0.131249	1.000000	0.430382	1.00000	0.4254
2	-0.118172	0.900365	1.299538	0.91407	1.2755
3	-0.100142	0.762992	2.155145	0.75974	2.1236
4	-0.070234	0.535120	3.024240	0.56719	2.9671
5	-0.048651	0.370677	3.874108	0.37122	3.8011
6	-0.029490	0.224687	4.718745	0.26841	4.6371

(2.7) and 101 uniformly spaced angles over the range of $0^\circ \leq \theta_m \leq 90^\circ$ are used. To strictly enforce the beam widths at -30 dB and -3 dB, the sample points $B_U(\theta = 81.9^\circ) = -30$ dB and $B_L(\theta = 86.4^\circ) = -3$ dB are replaced by new sample points $B_U(\theta = 82.0^\circ) = -30$ dB and $B_L(\theta = 86.85^\circ) = -3$ dB respectively. For this design problem, Δz_{min} is specified to be 0.5λ and the following assignments are made:

$$p(N) = U[1, 50],$$

$$p(I_n) = U[-0.5, 0.5],$$

$$p(z_n/\lambda) = U[0.25, 4.75],$$

$$\sigma_z = 1/100,$$

and

$$\sigma_m = \begin{cases} 1/2 \text{ dB} & \text{for } 0^\circ < \theta_m < 86.85^\circ \\ 1/5 \text{ dB} & \text{for } 86.85^\circ \leq \theta_m \leq 90.0^\circ \end{cases}.$$

The achieved results are summarized in Table 4.6, Table 4.7 and Figure 4.4. The posterior probability distribution for the number of element pairs approximated by 3000 drawn samples

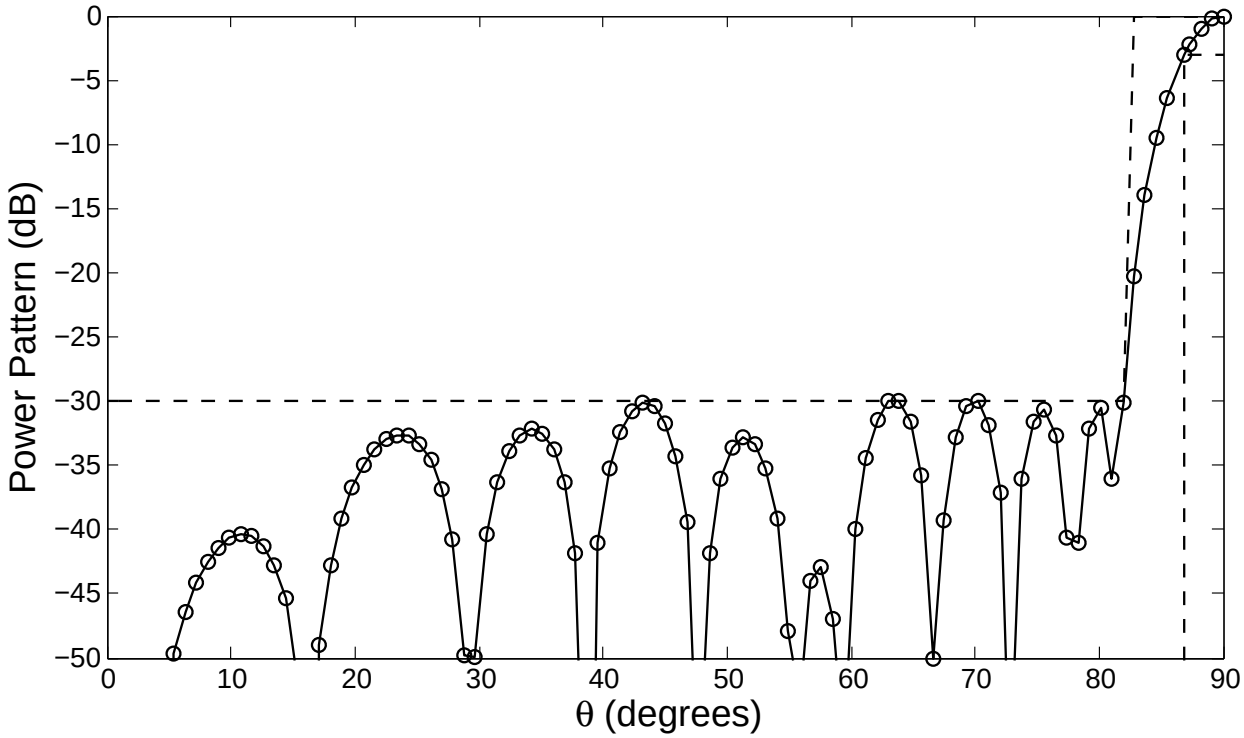

Figure 4.4: Achieved Chebyshev pattern using the inference framework. $\boldsymbol{B_U}$ and $\boldsymbol{B_L}$ are denoted by dashed lines.

is shown in Table 4.6. This table reports that all 3000 design candidates use 6 pairs of antenna elements. The parameter values of the antenna elements for the final design are listed in the 1st and 3rd columns of Table 4.7. These parameter values are used to plot the radiation pattern at the 101 predefined angles. The plot is graphed in Figure 4.4 which indicates that the design pattern specifications are fully met.

Table 4.7 indicates that the final designs produced by the method in [29] and the Bayesian inference framework are comparable to each other. In addition to having the same number of elements, 12, the values of the position and normalized current amplitude of each element are comparable as well. While the method in [29] manages to reproduce the original Chebyshev pattern using fewer antenna elements, the Bayesian inference framework manages to produce a number of linear antenna array designs that realize the desired pattern specifications using the same number of elements, though as many as 50 pairs of antenna elements are allowed in a design. The results

comparison proves that the Bayesian inference framework for design has the ability to produce linear antenna array designs that have design complexity appropriate to the design pattern specifications and requirements.

4.3.4 Pattern with Tapered Sidelobes

Having demonstrated that the designs produced by the Bayesian inference framework have design complexity that is appropriate to the design pattern specifications and requirements, this section presents a design example that has more demanding design pattern specifications than the previously presented design problems. To achieve the desired radiation pattern, linear antenna array designs that have higher design complexity are required. This design problem, which is picked from [20], has tapered sidelobes that decrease linearly from -40 dB to -50 dB and a beam width smaller than 9.5° at -40 dB. For this design problem, the parametric model in Eq. (2.7), which represents a symmetric linear antenna array with real-valued currents, is used. Since the array factor is symmetric, the 1001 uniformly spaced angles used in this problem need to cover only the range of $0^\circ \leq \theta_m \leq 90^\circ$. To strictly enforce the beam width at -40 dB, the sample point $B_U(\theta = 4.77^\circ) = -40$ dB is replaced by a new sample point $B_U(\theta = 4.75^\circ) = -40$ dB. For this design problem, Δz_{min} is specified to be 0.5λ and the following assignments are made:

$$
\begin{aligned}
p(N) &= U[1, 50], \\
p(I_n) &= U[-0.5, 0.5], \\
p(z_n/\lambda) &= U[0.25, 40.00], \\
\sigma_z &= 1/100,
\end{aligned}
$$

and

$$
\sigma_m = \begin{cases} 1/20 \text{ dB} & \text{for } \theta_m = 0^\circ \\ 1/2.5 \text{ dB} & \text{for } \theta_m > 0^\circ \end{cases} .
$$

Table 4.8: Estimated posterior probability for the number of element pairs for the pattern with tapered sidelobes. In this case, $\langle N \rangle = 13.01$.

N	$p(N\|\mathbf{B}_U, \mathbf{B}_L, \boldsymbol{\sigma})$
13	0.988667
14	0.011333

Table 4.9: Current amplitudes and positions of the antenna elements for the final design of the pattern with tapered sidelobes.

Element Number	I_n	z_n/λ	Element Number	I_n	z_n/λ
1	0.072165	0.437571	8	0.030456	6.357680
2	0.069616	1.308480	9	0.024484	7.190383
3	0.064988	2.174159	10	0.018069	8.038896
4	0.059376	3.034273	11	0.013107	8.885740
5	0.052246	3.878529	12	0.008447	9.777309
6	0.044633	4.706074	13	0.004978	10.543368
7	0.037177	5.532226			

Table 4.8, Table 4.9 and Figure 4.5 summarize the achieved results. Table 4.9 lists the parameter values of the antenna elements for the final design. Using these parameter values, the radiation pattern at the 1001 predefined angles is plotted. The plot is illustrated in Figure 4.5 which indicates that the design pattern specifications are fully satisfied.

The results presented here reiterate the importance of having the ability to determine automatically the design complexity that is appropriate to the design pattern specifications and requirements. The final design produced by the Bayesian inference framework uses only 13 pairs of antenna elements which are significantly fewer than the 20 pairs used in [20]. In fact, more than 98% of the 3000 design candidates use 13 pairs of antenna elements and some of these design candidates have zero error as well. Even though the antenna aperture width of the final design is around 8.14% larger, the 35% reduction in the number of antenna elements used represents a great coup.

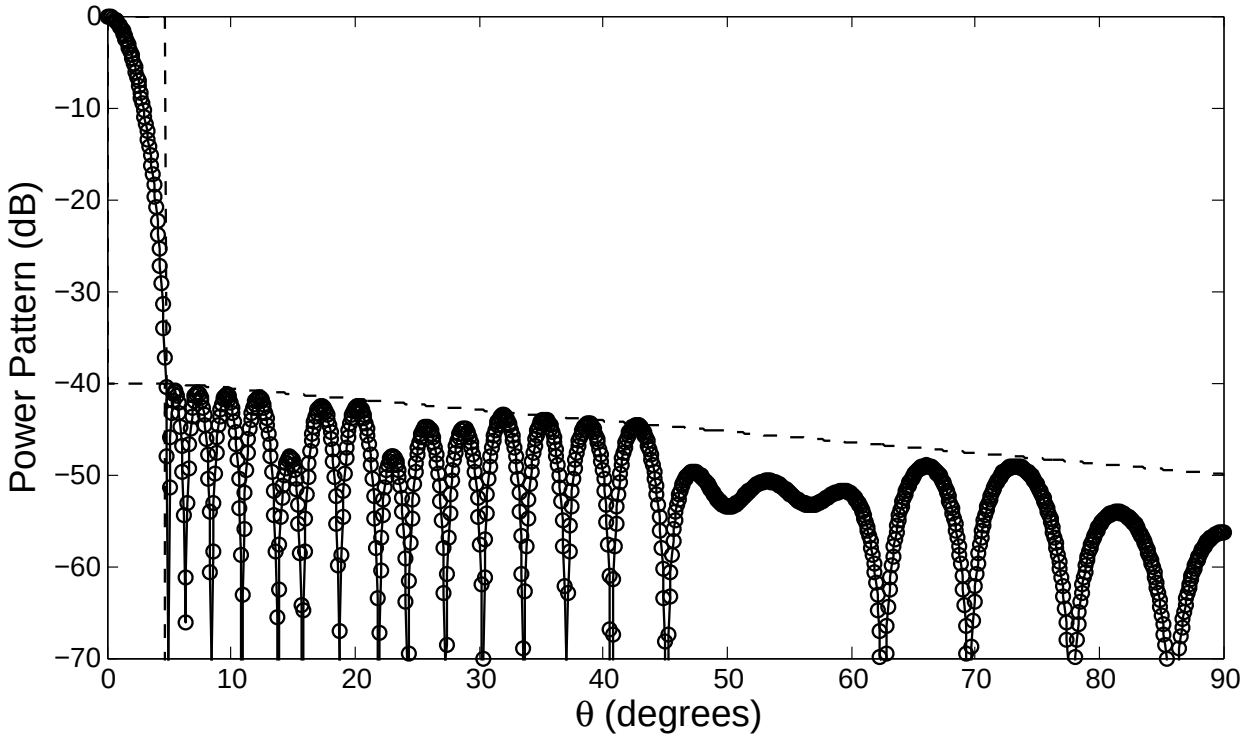

Figure 4.5: Achieved pattern with tapered sidelobes using the inference framework. $\boldsymbol{B_U}$ and $\boldsymbol{B_L}$ are denoted by dashed lines.

4.3.5 Sector Beam Pattern Using Asymmetric Array with Complex Valued Currents

This next design example to be presented demonstrates the design of an asymmetric linear antenna array with complex valued driving currents. When an asymmetric linear antenna array is used, the number of antenna elements that is required to realize the desired radiation pattern is expected to be fewer than using a symmetric linear antenna array. For comparison purpose, the sector beam pattern design problem is used. Here, the parametric model in Eq. (2.5) and 101 uniformly spaced angles over the range of $0^\circ \leq \theta_m \leq 180^\circ$ are used since the produced radiation pattern is asymmetric. To strictly enforce the width of the region that contains ripples, the sample points $B_L(\theta = 79.2^\circ) = -$Inf dB and $B_L(\theta = 100.8^\circ) = -$Inf dB are replaced by new sample points $B_L(\theta = 78.3^\circ) = -0.5$ dB and $B_L(\theta = 101.7^\circ) = -0.5$ dB respectively. For this design

Table 4.10: Estimated posterior probability for the number of array elements for the sector beam pattern using an asymmetric array with complex valued currents. In this case, $\langle N \rangle = 8.05$.

N	$p(N\|\mathbf{B}_U, \mathbf{B}_L, \boldsymbol{\sigma})$
8	0.949000
9	0.051000

Table 4.11: Complex currents and positions of the antenna elements for the final design of the sector beam pattern using an asymmetric array with complex valued currents.

Element Number	$\|I_n\| \cos(\phi_n)$	$\|I_n\| \sin(\phi_n)$	z_n/λ
1	0.013537	−0.091263	−3.668621
2	0.013126	−0.130003	−2.975687
3	−0.030088	0.240415	−1.524411
4	−0.043003	0.394155	−0.817944
5	−0.037316	0.323476	−0.096799
6	−0.016426	0.117691	0.596490
7	−0.000772	0.050263	2.789045
8	−0.005216	0.042619	3.506913

problem, Δz_{min} is specified to be 0.5λ and the following assignments are made:

$$p(N) = U[1, 50],$$

$$p(|I_n|) = U[0.0, 0.5],$$

$$p(z_n/\lambda) = U[-4.75, 4.75],$$

$$\sigma_z = 1/100,$$

and

$$\sigma_m = \begin{cases} 1/12.5 \text{ dB} & \text{for } \ 78.3^\circ \leq \theta_m \leq 101.7^\circ \\ 1/4 \text{ dB} & \text{otherwise} \end{cases} .$$

The values assigned to all σ_m are smaller in this problem than those used in Section 4.3.2 because as mentioned in Section 4.2, the current problem uses the parametric model of an asymmetric linear antenna array, which is more complicated and contains more design parameters.

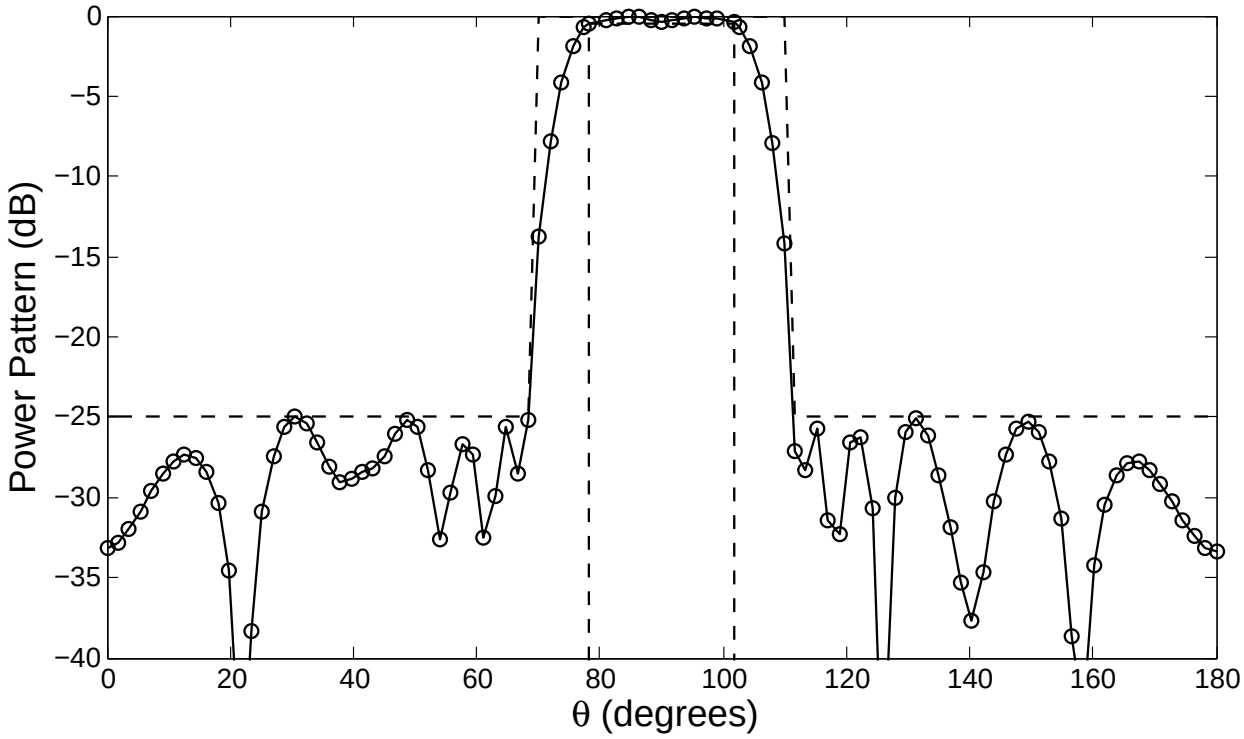

Figure 4.6: Achieved sector beam pattern using an asymmetric array with complex valued currents. $\boldsymbol{B_U}$ and $\boldsymbol{B_L}$ are denoted by dashed lines.

Table 4.10, Table 4.11 and Figure 4.6 summarize the obtained results. The parameter values of the antenna elements for the final design are listed in Table 4.11. The plot of the radiation pattern produced by the final design at the 101 predefined angles is shown in Figure 4.6. This figure indicates that the design pattern specifications are fully satisfied.

The final design in the current design problem uses 8 antenna elements which are fewer than the 5 pairs of antenna elements used in the symmetric linear antenna array with real-valued currents. In addition, the antenna aperture width is reduced by about 1.05λ. This outcome meets the expectation of producing a linear antenna array design that has lower design complexity. If the results in [15] are used for comparison, the number of elements used here is 6 fewer or about 42.86% less. This significant reduction of antenna elements used reaffirms the prominent advantages that the Bayesian inference framework possesses.

4.3.6 End-Fire Pattern

The examples of desired radiation pattern that have been presented so far are broadside and shaped beam patterns. This section presents an end-fire pattern design problem that uses an asymmetric linear antenna array with complex currents. The dashed lines in Figure 4.7 indicates the desired radiation pattern which is inspired by the Hansen-Woodyard end-fire array example in [73, Ch. 6]. The maximum radiation is desired to be at the direction of 180° with sidelobe levels constrained to be less than -10 dB. The beam widths at -3 dB and -10 dB are desired to be at least 36.0° and less than 60.0° respectively. To ensure that the power level of the achieved pattern at $\theta = 180^\circ$ is close to 0 dB, $B_L(\theta = 180^\circ)$ is set to -0.001 dB. For this design problem, the parametric model in Eq. (2.5) and 101 uniformly spaced angles over the range of $0^\circ \leq \theta_m \leq 180^\circ$ are used. To strictly enforce the beam width at -10 dB, the sample point $B_U(\theta = 149.4^\circ) = -10$ dB is replaced by a new sample point $B_U(\theta = 150.0^\circ) = -10$ dB.

The Hansen-Woodyard end-fire array example in [73, Ch. 6] uses a uniform element spacing of 0.25λ. For this design problem, Δz_{min} is specified to be 0.25λ, and the following assignments are made:

$$p(N) = U[1, 50],$$
$$p(|I_n|) = U[0.0, 1.0],$$
$$p(z_n/\lambda) = U[-5.0, 5.0],$$
$$\sigma_z = 1/100,$$

and

$$\sigma_m = \begin{cases} 1/4 \text{ dB} & \text{for } \ 0^\circ < \theta_m < 162.0^\circ \\ 1/20 \text{ dB} & \text{for } \ 162.0^\circ \leq \theta_m < 180.0^\circ \\ 1/100 \text{ dB} & \text{for } \ \theta_m = 180.0^\circ \end{cases} .$$

Table 4.12: Estimated posterior probability for the number of array elements for the end-fire pattern design. In this case, $\langle N \rangle = 6.00$.

N	$p(N|\mathbf{B}_U, \mathbf{B}_L, \boldsymbol{\sigma})$
6	0.997000
7	0.003000

Table 4.13: Complex currents and locations of the antenna elements for the final design for the end-fire pattern.

Element Number	$\lvert I_n \rvert \cos(\phi_n)$	$\lvert I_n \rvert \sin(\phi_n)$	z_n/λ
1	-0.241997	-0.152666	0.497200
2	0.611562	0.168843	0.836637
3	-0.881787	-0.108559	1.100791
4	0.882620	-0.095218	1.420520
5	-0.612047	0.062371	1.738349
6	0.257120	-0.148767	2.047627

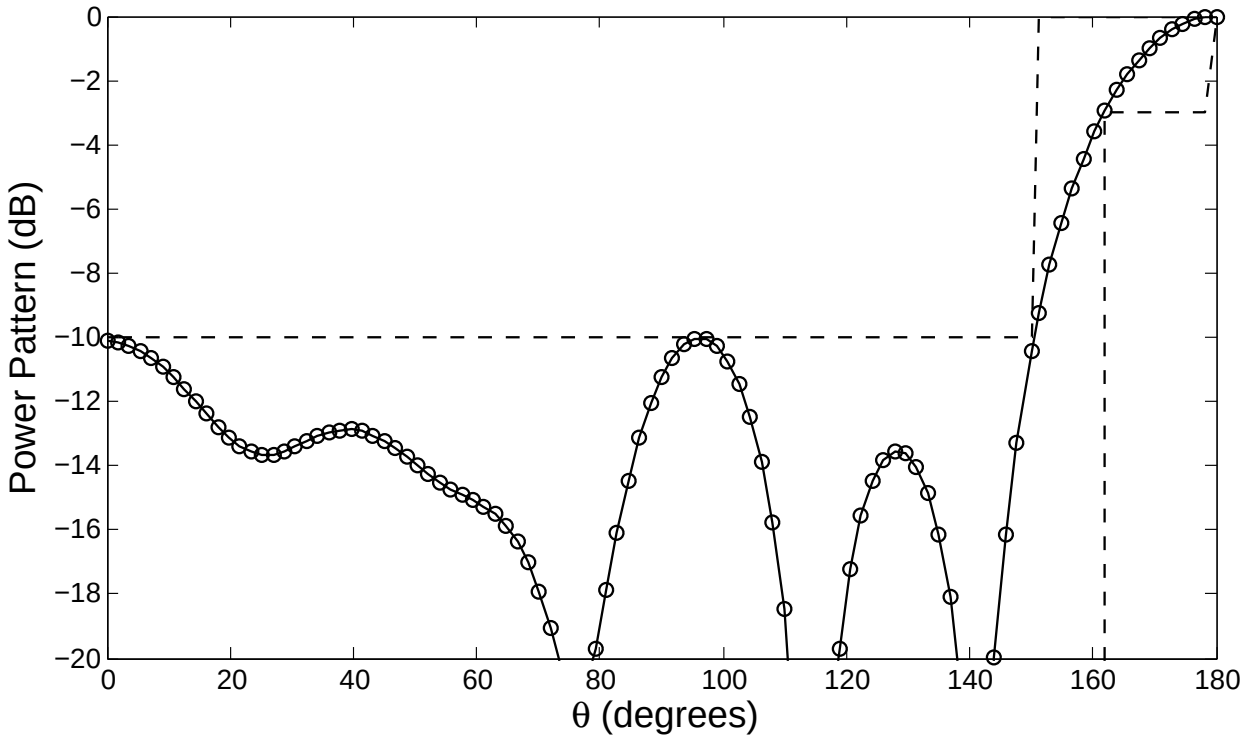

Figure 4.7: Achieved end-fire pattern using the inference framework. $\boldsymbol{B_U}$ and $\boldsymbol{B_L}$ are denoted by dashed lines.

Table 4.12, Table 4.13 and Figure 4.7 summarize the obtained results. Table 4.13 displays the parameter values of the array elements for the final design. Using these parameter values, the radiation pattern at the 101 predefined angles is plotted in Figure 4.7. This plot shows that the design pattern specifications are fully satisfied. The final design uses 6 antenna elements which are fewer than the 10 array elements used in [73, Ch. 6]. The results presented here demonstrate that the Bayesian inference approach can be successfully applied to an end-fire pattern design problem.

4.3.7 Dual-Pattern with Digital Attenuators

This section presents the design of a symmetric linear antenna array with real-valued currents that can produce two different radiation patterns. The two desired radiation patterns are the sector beam and Chebyshev patterns presented previously. Here, the design pattern specifications of both radiation patterns are slightly modified. The modifications made to the sector beam pattern are the reduction of the beam width at -25 dB from 41.4° to 40.0°, and the increase in the width of the ripple region from 23.4° to 24.0°. As for the Chebyshev pattern, the changes are the increase in the beam widths at -30 dB and -3 dB from 16° to 20° and from 6.3° to 6.4° respectively. In this design problem, the real-valued current amplitudes are allowed to be reconfigurable so that a dual-pattern can be realized. In order to incorporate an additional radiation pattern, the likelihood in Eq. (4.1) is modified to

$$p(\mathbf{B}_U, \mathbf{B}_L | N, \mathbf{X}_N, \boldsymbol{\sigma}) \propto \exp\left[-Q_z^2/2\sigma_z^2 - \sum_{m=1}^{M} \left(Q_{SBm}^2/2\sigma_{SBm}^2 + Q_{PBm}^2/2\sigma_{PBm}^2\right)\right], \qquad (4.3)$$

where Q_{SBm} denotes the error between the achieved and desired sector beam patterns, and Q_{PBm} denotes the error between the realized and desired Chebyshev patterns.

In practice, the current amplitudes are limited in the dynamic range and accuracy. This practical design requirement is included in the current design problem with the current amplitudes constrained to discrete values that are represented by a fixed number of bits. Due to the discrete nature of the current amplitudes, the normalized antenna array pattern is used as the parametric model for both

Table 4.14: Estimated posterior probability for the number of element pairs for the dual-pattern design. $\langle N \rangle = 7.00$ for 6-bit representation and $\langle N \rangle = 8.00$ for 5-bit representation.

	6-bit Representation	5-bit Representation
N	$p(N\|\mathbf{B}_U, \mathbf{B}_L, \boldsymbol{\sigma})$	$p(N\|\mathbf{B}_U, \mathbf{B}_L, \boldsymbol{\sigma})$
7	1.000000	
8		0.996000
9		0.004000

Table 4.15: Current amplitudes and positions of the antenna elements for the final designs of the dual pattern.

	6-bit Representation			5-bit Representation		
Element Number	$I_n(SB)$	$I_n(PB)$	z_n/λ	$I_n(SB)$	$I_n(PB)$	z_n/λ
1	50	-55	0.304528	31	31	0.285408
2	33	-53	0.939185	19	26	0.798194
3	6	-51	1.613621	10	26	1.299276
4	-10	-40	2.293888	-1	23	1.836182
5	-8	-29	2.990451	-7	22	2.455469
6	1	-20	3.653564	-4	14	3.142585
7	6	-12	4.334831	2	7	3.916065
8				3	2	4.431656

radiation patterns. The parametric models, $g_{SB}(\theta)$ and $g_{PB}(\theta)$, are respectively written as

$$g_{SB}(\theta) = 10 \log_{10} \left[\frac{|AF_{SB}(\theta)|}{max\{|AF_{SB}(\theta)|\}} \right]^2 \quad \text{for} \quad 0 \leq \theta \leq \pi,$$

and

$$g_{PB}(\theta) = 10 \log_{10} \left[\frac{|AF_{PB}(\theta)|}{max\{|AF_{PB}(\theta)|\}} \right]^2 \quad \text{for} \quad 0 \leq \theta \leq \pi.$$

The number of bits used to represent the current amplitudes affects the design of a linear antenna array. Here, two cases, in which the number of bits used are respectively 6 and 5 excluding the sign bit, are presented. For both cases, 101 uniformly spaced angles over the range of $0^\circ \leq \theta_m \leq 90^\circ$ are used for each of the two desired radiation patterns. The value assigned to Δz_{min} remains 0.5λ,

and the following assignments are made:

$$
\begin{aligned}
p(N) &= U[1, 50], \\
p(z_n/\lambda) &= U[0.25, 30.00], \\
\sigma_z &= 1/100, \\
p(I_n) &= \begin{cases} U[-63, -62, -61, \cdots, 61, 62, 63] & \text{for 6-bit representation} \\ U[-31, -30, -29, \cdots, 29, 30, 31] & \text{for 5-bit representation} \end{cases}, \\
\sigma_{SBm} &= \begin{cases} 1/5 \text{ dB} & \text{for } 0^\circ < \theta_m < 78.0^\circ \\ 1/40 \text{ dB} & \text{for } 78.0^\circ \leq \theta_m \leq 90.0^\circ \end{cases},
\end{aligned}
$$

and

$$
\sigma_{PBm} = \begin{cases} 1/5 \text{ dB} & \text{for } 0^\circ < \theta_m < 86.8^\circ \\ 1/40 \text{ dB} & \text{for } 86.8^\circ \leq \theta_m \leq 90.0^\circ \end{cases}.
$$

The obtained results are summarized in Table 4.14, Table 4.15, Figure 4.8 and Figure 4.9. Using the parameter values of the array elements for the two final designs, the achieved radiation patterns at the 101 predefined angles are plotted in Figure 4.8 and Figure 4.9. All four plots show that the design pattern specifications are fully satisfied. Tables 4.14 and 4.15 provide some valuable insight into the effects of using different number of bits to represent the current amplitudes. The design complexity of the final design that uses 5-bit representation for the current amplitudes is higher than the one that uses 6 bits. The former final design uses one more pair of array elements and has an antenna aperture that is 0.116λ wider. The results presented here cannot be compared directly to the results in [35] because of the different nature of the two design problems. The reconfigurable linear antenna array documented in the literature [18, 32–35] has a variable phase shifter attached to each array element and uses the same power dividing network to produce the desired dual beams. Even though the reconfigurable linear antenna array designed here has variable digital attenuators which may render the antenna system more difficult to be built, the success in solving the current design problem provides an attractive alternative solution to those presented in the literature.

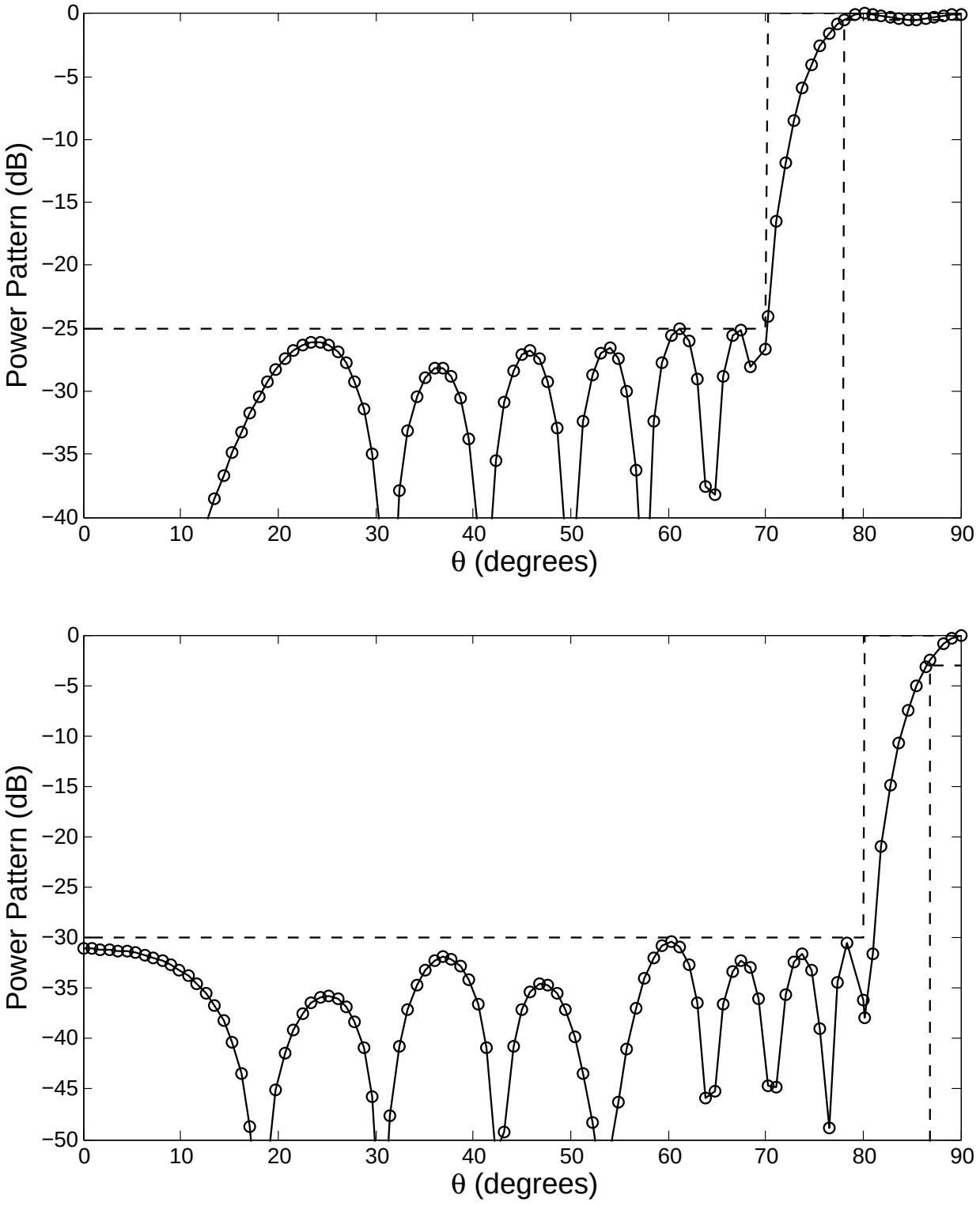

Figure 4.8: Achieved sector beam and Chebyshev patterns using a reconfigurable linear antenna array with 6-bit representation of the current amplitudes. $\boldsymbol{B_U}$ and $\boldsymbol{B_L}$ are denoted by dashed lines.

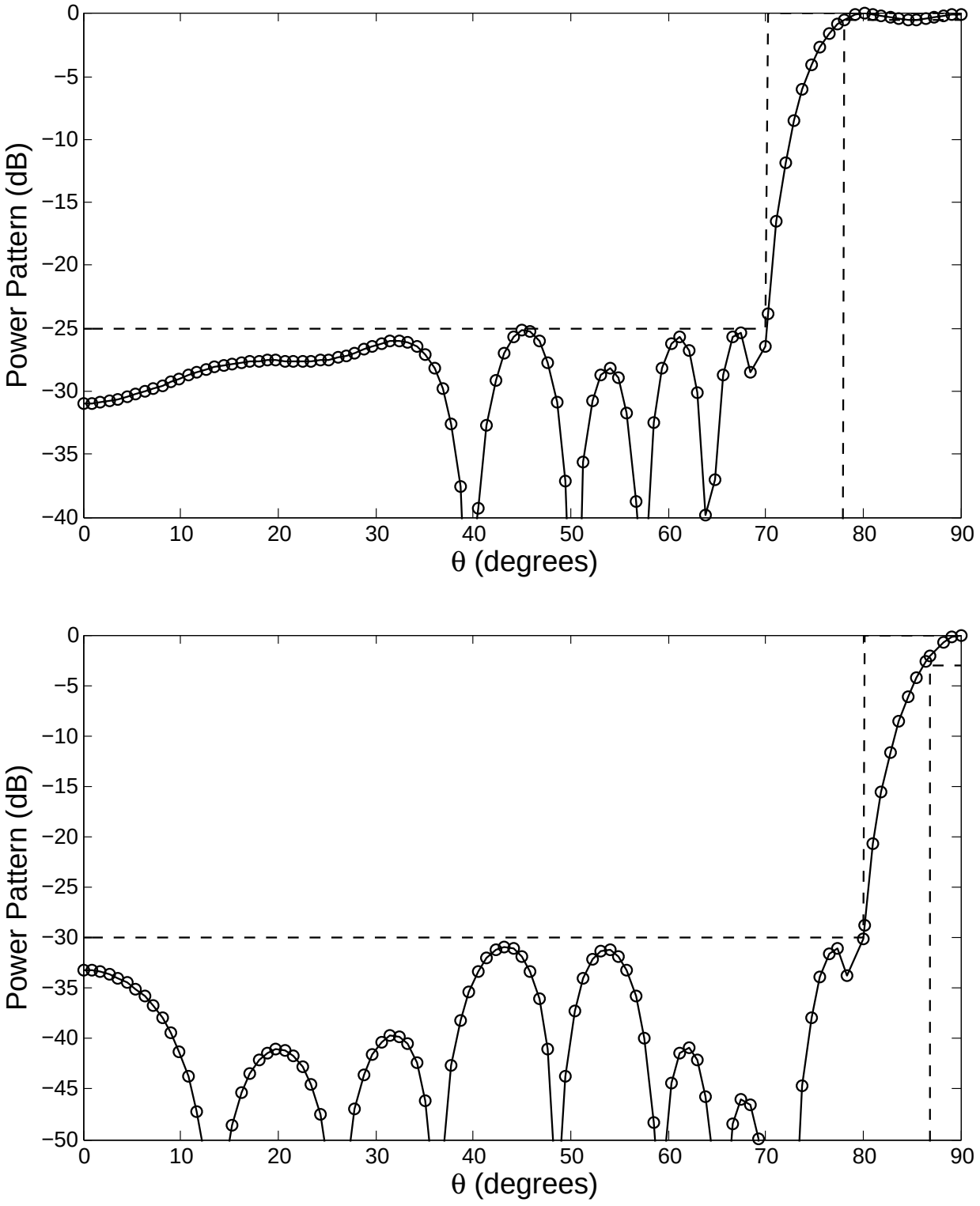

Figure 4.9: Achieved sector beam and Chebyshev patterns using a reconfigurable linear antenna array with 5-bit representation of the current amplitudes. $\boldsymbol{B_U}$ and $\boldsymbol{B_L}$ are denoted by dashed lines.

4.3.8 Sector Beam Pattern with a Frequency Bandwidth

In practice, an antenna has an operating frequency bandwidth that is defined as the range of frequencies within which the performance of an antenna conforms to a specified standard [73]. In linear antenna array design, the task is to ensure that all the radiation patterns produced by a single linear antenna array at different frequencies satisfy the design pattern specifications. This task is very challenging but can be solved by the Bayesian inference framework for design.

In order to incorporate the challenging practical design requirement, the likelihood in Eq. (4.1) has to be modified. The relative frequency bandwidth of a linear antenna array, BW, is defined as

$$BW = \frac{f_H - f_L}{f_C} \tag{4.4}$$

$$= \frac{2(f_C - f_L)}{f_C} = 2\left(1 - \frac{f_L}{f_C}\right) \tag{4.5}$$

$$= \frac{2(f_H - f_C)}{f_C} = 2\left(\frac{f_H}{f_C} - 1\right) \tag{4.6}$$

where f_H, f_L and f_C are the upper, lower and center frequencies respectively. If the wavelengths at f_H, f_L and f_C are denoted by λ_H, λ_L and λ_C respectively, one can write

$$\frac{\lambda_C}{\lambda_L} = \frac{f_L}{f_C} = 1 - \frac{BW}{2} \tag{4.7}$$

from Eq. (4.5) and

$$\frac{\lambda_C}{\lambda_H} = \frac{f_H}{f_C} = 1 + \frac{BW}{2} \tag{4.8}$$

from Eq. (4.6). For the lower and upper frequencies, the array factor in Eq. (2.5) can be rewritten as

$$\begin{aligned} AF_L(\theta) &= \sum_{n=1}^{N} |I_n| \exp(j\phi_n) \exp\left(j2\pi \frac{z_n}{\lambda_L} \cos\theta\right) \\ &= \sum_{n=1}^{N} |I_n| \exp(j\phi_n) \exp\left(j2\pi \frac{z_n}{\lambda_C} \frac{\lambda_C}{\lambda_L} \cos\theta\right) \\ &= \sum_{n=1}^{N} |I_n| \exp(j\phi_n) \exp\left[j2\pi \frac{z_n}{\lambda_C} \left(1 - \frac{BW}{2}\right) \cos\theta\right] \end{aligned} \tag{4.9}$$

and

$$\begin{aligned} AF_H(\theta) &= \sum_{n=1}^{N} |I_n| \exp(j\phi_n) \exp\left(j2\pi \frac{z_n}{\lambda_H} \cos\theta\right) \\ &= \sum_{n=1}^{N} |I_n| \exp(j\phi_n) \exp\left(j2\pi \frac{z_n}{\lambda_C} \frac{\lambda_C}{\lambda_H} \cos\theta\right) \\ &= \sum_{n=1}^{N} |I_n| \exp(j\phi_n) \exp\left[j2\pi \frac{z_n}{\lambda_C} \left(1 + \frac{BW}{2}\right) \cos\theta\right] \end{aligned} \tag{4.10}$$

respectively using Eq. (4.7) and Eq. (4.8). As for the center frequency, the array factor, $AF_C(\theta)$, is of the form in Eq. (4.10) with $BW = 0$. For a symmetric linear antenna array with either complex or real-valued currents, the same modifications are applied to the array factor. Specifically, the term $\frac{z_n}{\lambda}$ in Eq. (2.7) is replaced by $\frac{z_n}{\lambda_C}\left(1 - \frac{BW}{2}\right)$, $\frac{z_n}{\lambda_C}\left(1 + \frac{BW}{2}\right)$ and $\frac{z_n}{\lambda_C}$ for the lower, upper and center frequencies respectively. The likelihood in Eq. (4.1) can now be modified as follows:

$$p(\mathbf{B}_U, \mathbf{B}_L | N, \mathbf{X}_N, \boldsymbol{\sigma}) \propto \exp\left[-Q_z^2/2\sigma_z^2 - \sum_{m=1}^{M} \left(Q_{Lm}^2 + Q_{Hm}^2 + Q_{Cm}^2\right)/2\sigma_m^2\right] \tag{4.11}$$

where Q_{Lm}, Q_{Hm} and Q_{Cm} are defined as in Eq. (2.26) with $g(\theta_m)$ being either $10\log_{10}|AF_L(\theta_m)|^2$, $10\log_{10}|AF_H(\theta_m)|^2$ or $10\log_{10}|AF_C(\theta_m)|^2$.

For demonstration and comparison purposes, two design examples are presented here. The desired radiation pattern in both design examples has exactly the same design pattern specifications of the sector beam radiation pattern presented in Section 4.3.5. The difference is that the first example uses a symmetric linear antenna array with real-valued currents while the second example employs an asymmetric linear antenna array with complex currents. For both design problems, Δz_{min} and BW are specified to be 0.5λ and 0.1 respectively. The 101 sampling angles used in the first and second examples are identical to those used in Section 4.3.2 and Section 4.3.5 respectively. For the first example, the following assignments are made:

$$p(N) = U[1, 20],$$

$$p(I_n) = U[-0.5, 0.5],$$

$$p(z_n/\lambda) = U[0.25, 9.75],$$

$$\sigma_z = 1/100,$$

and

$$\sigma_m = \begin{cases} 1/2 \text{ dB} & \text{for } 0^\circ < \theta_m < 78.3^\circ \\ 1/5 \text{ dB} & \text{for } 78.3^\circ \leq \theta_m \leq 90.0^\circ \end{cases} .$$

As for the second example, the assignments are:

$$p(N) = U[1, 50],$$
$$p(|I_n|) = U[0.0, 0.5],$$
$$p(z_n/\lambda) = U[-10.0, 10.0],$$
$$\sigma_z = 1/100,$$

and

$$\sigma_m = \begin{cases} 1/12.5 \text{ dB} & \text{for } 78.3^\circ \leq \theta_m \leq 101.7^\circ \\ 1/4 \text{ dB} & \text{otherwise} \end{cases} .$$

The accomplished results are summarized in Table 4.16, Table 4.17, and Figures 4.10 – 4.15. Table 4.17 lists the parameter values of the antenna elements for the two final designs. Using these parameter values, the radiation patterns for the two final designs at f_C, f_L and f_H are plotted in Figures 4.10 – 4.15. The final design for the symmetric linear antenna array uses 7 pairs of antenna elements and has an antenna aperture width of about 11.65λ. Compared to the final design in Section 4.3.2, the increase in the number of antenna elements used and the width of the antenna aperture are expected because the antenna frequency bandwidth is included as an additional design requirement. The final asymmetric linear antenna array design uses 11 array elements and has an antenna aperture width of about 8.8λ. This outcome meets the expectation of using fewer array elements and having smaller antenna aperture width when an asymmetric, rather than a symmetric, linear antenna array is used.

The variation of the current phases with respect to the operating frequency has not been taken into consideration when devising the final designs above. Consequently, for the phase of each

Table 4.16: Estimated posterior probability for the value of N for the sector beam pattern with an operating frequency bandwidth. In this case, $\langle N \rangle = 6.39$ for the symmetric array and $\langle N \rangle = 11.00$ for the asymmetric array.

Symmetric Array		Asymmetric Array	
N	$p(N\|\mathbf{B}_U, \mathbf{B}_L, \boldsymbol{\sigma})$	N	$p(N\|\mathbf{B}_U, \mathbf{B}_L, \boldsymbol{\sigma})$
6	0.624000	11	1.000000
7	0.358000		
8	0.017667		
9	0.000333		

Table 4.17: Current values and positions of the antenna elements for the final designs of the sector beam pattern with an operating frequency bandwidth.

	Symmetric Array		Asymmetric Array		
Element Number	I_n	z_n/λ	$\|I_n\| \cos(\phi_n)$	$\|I_n\| \sin(\phi_n)$	z_n/λ
1	-0.362144	0.352190	0.014267	-0.037571	-1.506269
2	-0.192231	1.049156	-0.032003	0.073178	-0.143787
3	0.075076	2.485017	-0.043715	0.123767	0.522849
4	0.034992	3.227365	-0.022149	0.052751	1.108444
5	-0.025151	3.834026	0.052848	-0.132131	1.953265
6	-0.032361	4.600318	0.106740	-0.302139	2.590085
7	0.019051	5.822793	0.115945	-0.321821	3.250945
8			0.078095	-0.216468	3.922001
9			0.022396	-0.068040	4.613493
10			0.010118	-0.041224	6.611156
11			0.010943	-0.034671	7.294409

driving current, a different time delay is required to be implemented for each different operating frequency in the physical design. This requirement results in extremely high implementation costs and renders the above final designs impractical. The solution to this issue is to incorporate the variation of the current phases with respect to the operating frequency into the design problem by modifying the array factors $AF_L(\theta)$, $AF_C(\theta)$ and $AF_H(\theta)$. Given that a constant time delay requires

$$\frac{\phi_{nL}}{\phi_{nC}} = \frac{\lambda_C}{\lambda_L} = 1 - \frac{BW}{2}, \tag{4.12}$$

and

$$\frac{\phi_{nH}}{\phi_{nC}} = \frac{\lambda_C}{\lambda_H} = 1 + \frac{BW}{2}, \tag{4.13}$$

the array factors in Eq. (4.9) and Eq. (4.10) can be modified respectively to

$$\begin{aligned} AF_L(\theta) &= \sum_{n=1}^{N} |I_n| \exp(j\phi_{nL}) \exp\left[j2\pi \frac{z_n}{\lambda_C}\left(1-\frac{BW}{2}\right)\cos\theta\right] \\ &= \sum_{n=1}^{N} |I_n| \exp\left(j\phi_{nC}\frac{\phi_{nL}}{\phi_{nC}}\right) \exp\left[j2\pi \frac{z_n}{\lambda_C}\left(1-\frac{BW}{2}\right)\cos\theta\right] \\ &= \sum_{n=1}^{N} |I_n| \exp\left[j\phi_{nC}\left(1-\frac{BW}{2}\right)\right] \exp\left[j2\pi \frac{z_n}{\lambda_C}\left(1-\frac{BW}{2}\right)\cos\theta\right], \end{aligned} \tag{4.14}$$

and

$$\begin{aligned} AF_H(\theta) &= \sum_{n=1}^{N} |I_n| \exp(j\phi_{nH}) \exp\left[j2\pi \frac{z_n}{\lambda_C}\left(1+\frac{BW}{2}\right)\cos\theta\right] \\ &= \sum_{n=1}^{N} |I_n| \exp\left(j\phi_{nC}\frac{\phi_{nH}}{\phi_{nC}}\right) \exp\left[j2\pi \frac{z_n}{\lambda_C}\left(1+\frac{BW}{2}\right)\cos\theta\right] \\ &= \sum_{n=1}^{N} |I_n| \exp\left[j\phi_{nC}\left(1+\frac{BW}{2}\right)\right] \exp\left[j2\pi \frac{z_n}{\lambda_C}\left(1+\frac{BW}{2}\right)\cos\theta\right]. \end{aligned} \tag{4.15}$$

As for the center frequency, the array factor, $AF_C(\theta)$, is of the form in Eq. (4.15) with $BW = 0$.

For demonstration purposes, the second design example presented in this section is used. The type of antenna array used, design pattern specifications, form of the likelihood, sampling angles, and the values assigned to Δz_{min} and BW all remain unchanged. The current design example uses the normalized antenna array pattern as the parametric model. To ensure that the antenna power gain is constant with frequency, the radiation patterns obtained at the lower, center and upper frequencies are normalized with respect to the peak value of all three radiation patterns combined. The parametric model for the three frequency points, $g_L(\theta)$, $g_C(\theta)$ and $g_H(\theta)$, are respectively written as

$$g_L(\theta) = 10\log\left[\frac{|AF_L(\theta)|^2}{max\{|AF_L(\theta)|^2, |AF_C(\theta)|^2, |AF_H(\theta)|^2\}}\right] \quad \text{for} \quad 0 \le \theta \le \pi,$$

$$g_C(\theta) = 10\log\left[\frac{|AF_C(\theta)|^2}{max\{|AF_L(\theta)|^2, |AF_C(\theta)|^2, |AF_H(\theta)|^2\}}\right] \quad \text{for} \quad 0 \le \theta \le \pi,$$

and

$$g_H(\theta) = 10\log\left[\frac{|AF_H(\theta)|^2}{max\{|AF_L(\theta)|^2, |AF_C(\theta)|^2, |AF_H(\theta)|^2\}}\right] \quad \text{for} \quad 0 \le \theta \le \pi.$$

Table 4.18: Estimated posterior probability for the number of array elements for the sector beam pattern design problem that uses constant time delays to maintain the antenna array performance over an operating frequency bandwidth. In this case, $\langle N \rangle = 10.00$.

N	$p(N\|\mathbf{B}_U, \mathbf{B}_L, \boldsymbol{\sigma})$
10	0.999000
11	0.001000

Table 4.19: Complex currents and positions of the antenna elements for the final design of the sector beam pattern design problem that uses constant time delays to maintain the antenna array performance over an operating frequency bandwidth.

Element Number	$\|I_n\|$	ψ_n (degree)	z_n/λ
1	0.028765	26.736388	14.056151
2	0.048744	219.604180	15.341690
3	0.061396	219.133496	16.055467
4	0.069891	33.960985	17.435305
5	0.217387	216.964392	18.852676
6	0.448279	215.856177	19.549415
7	0.453841	216.333336	20.250519
8	0.240504	216.620675	20.948632
9	0.112236	35.191985	22.336131
10	0.083699	32.290011	23.036526

For this design example, the following assignments are made:

$$p(N) = U[1, 50],$$

$$p(|I_n|) = U[0.0, 0.5],$$

$$p(z_n/\lambda) = U[-40.0, 40.0],$$

$$\sigma_z = 1/100,$$

and

$$\sigma_m = \begin{cases} 1/100 \text{ dB} & \text{for } \ 78.3^\circ \leq \theta_m \leq 101.7^\circ \\ 1/8 \text{ dB} & \text{otherwise} \end{cases} .$$

Table 4.18, Table 4.19, and Figures 4.16 – 4.18 summarized the achieved results. The parameter values of the antenna elements for the final design are listed in Table 4.19. Using these parameter values, the radiation patterns at f_C, f_L and f_H are plotted in Figures 4.16, 4.17 and 4.18 respectively. The final design uses 10 antenna elements which are fewer than the 11 array elements used in the second example. The variation of the current phases with respect to the operating frequency has been successfully incorporated into the final design here. Compared with the second final design, this final design is much more practically useful because only a single time delay is required to implement the phase of each driving current.

All the plots presented in this section indicate that the final designs are able to produce radiation patterns that comply fully with the design pattern specifications at the center, lower and upper frequencies. In fact, all three final designs have been tested at 101 uniform sampling frequencies that fall within the range of $f_L \leq f \leq f_H$. The results of the tests show that all 303 radiation patterns satisfy the design pattern specifications completely. Tables 4.17 and 4.19 indicate that all the spacings between two adjacent elements meet the minimum requirement. These outcomes reaffirm the ability of the Bayesian inference framework in incorporating various practical and challenging design requirements in a single design problem. A notable comparison with the results obtained in [15] is that the linear antenna array designs here can maintain their performances over a frequency band using the same or even fewer array elements. This accomplishment is noteworthy because a 10% antenna bandwidth, which is desired in many applications, can be acquired using a network composed of a single amplitude and delay for each array element. The design of a linear antenna array that has wider antenna bandwidth is likely to require more amplitudes and delays, and this design problem can also be solved using the Bayesian inference framework.

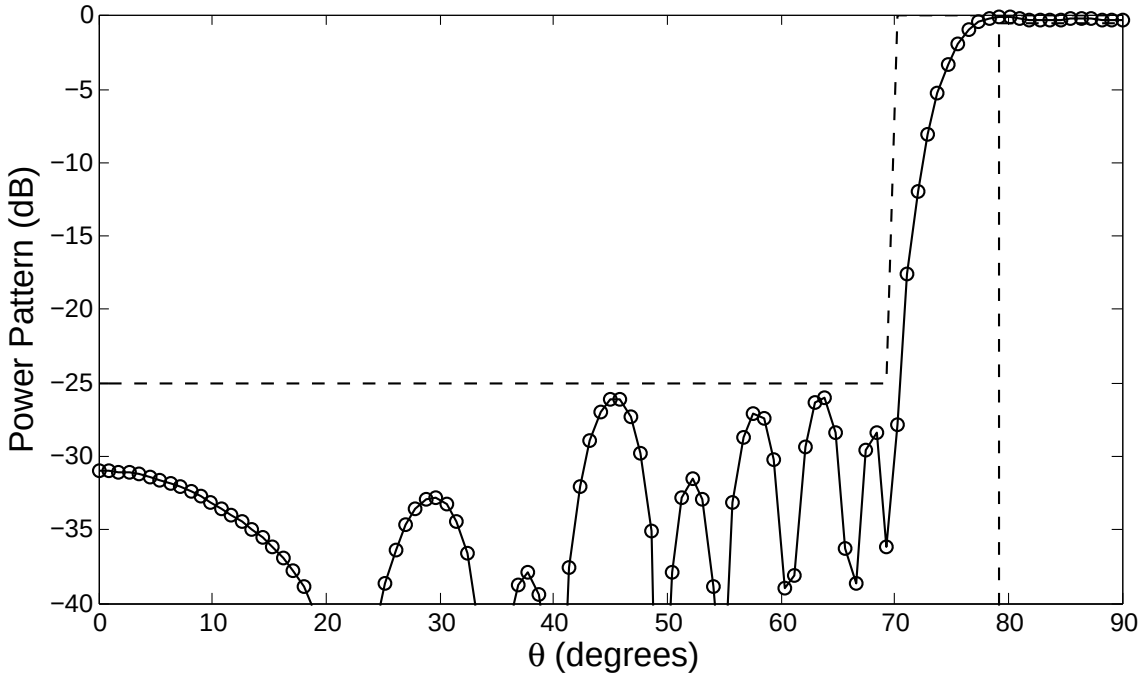

Figure 4.10: Achieved sector beam pattern at f_C using a symmetric linear antenna array. $\boldsymbol{B_U}$ and $\boldsymbol{B_L}$ are denoted by dashed lines.

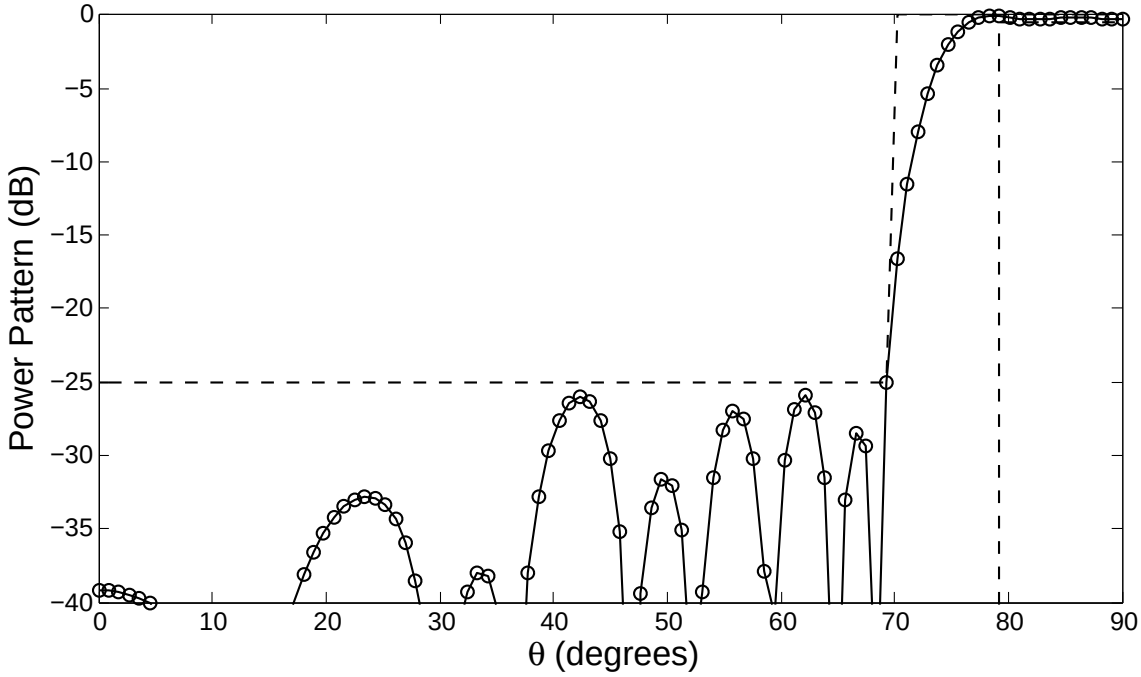

Figure 4.11: Achieved sector beam pattern at f_L using a symmetric linear antenna array. $\boldsymbol{B_U}$ and $\boldsymbol{B_L}$ are denoted by dashed lines.

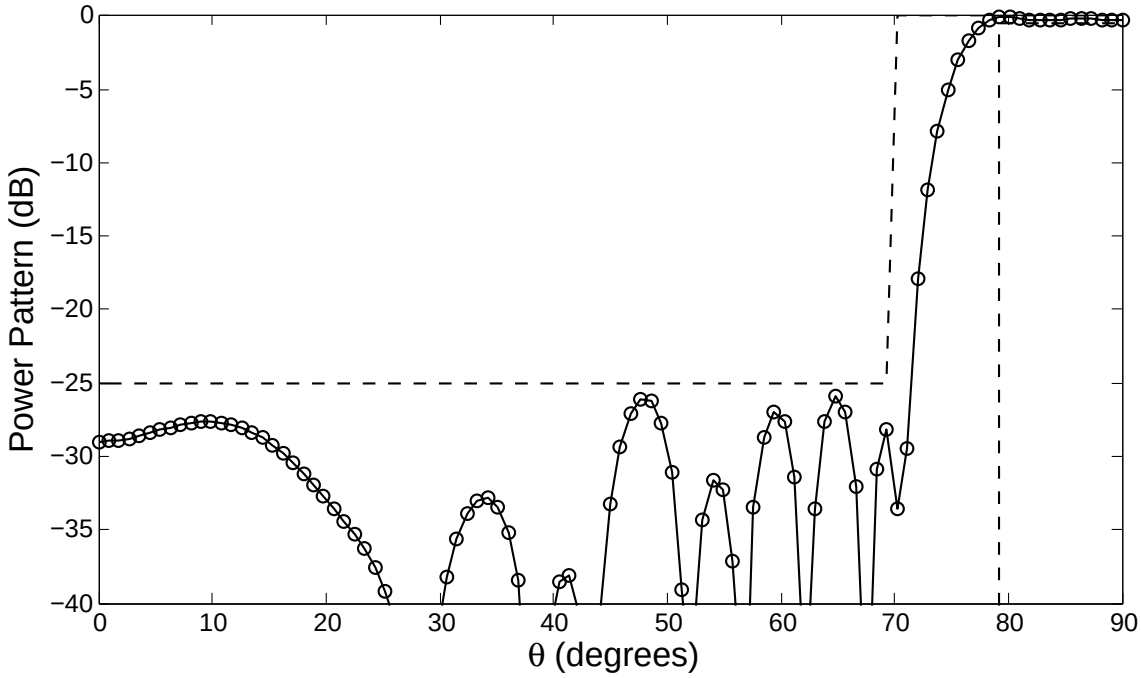

Figure 4.12: Achieved sector beam pattern at f_H using a symmetric linear antenna array. $\boldsymbol{B_U}$ and $\boldsymbol{B_L}$ are denoted by dashed lines.

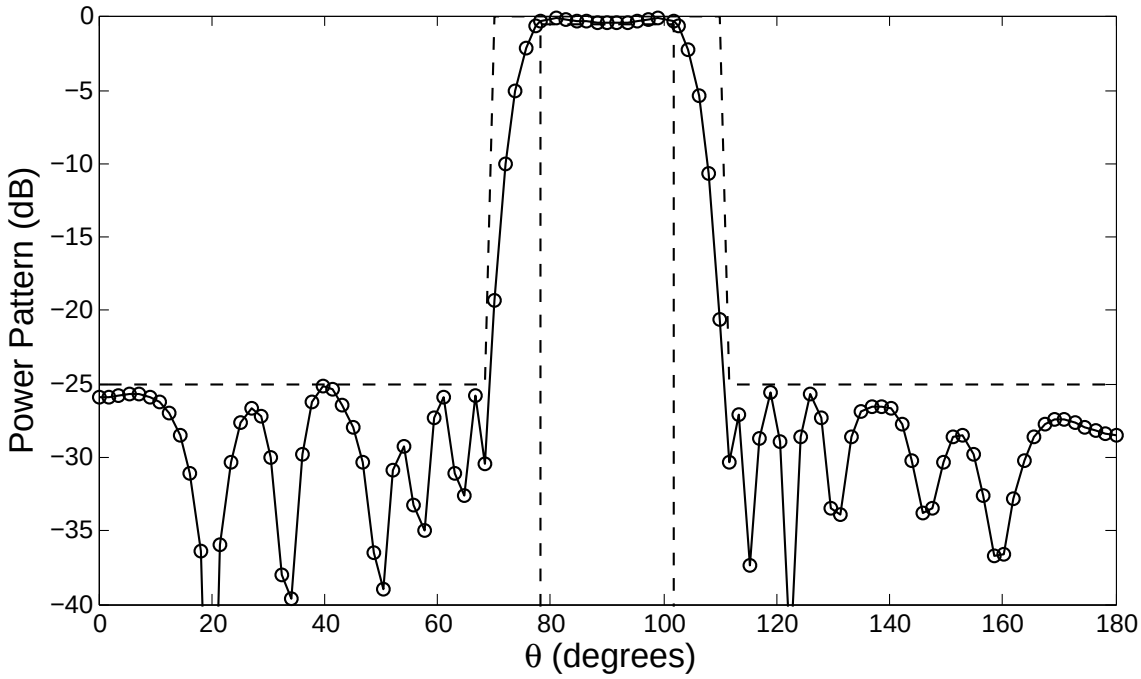

Figure 4.13: Achieved sector beam pattern at f_C using an asymmetric linear antenna array. $\boldsymbol{B_U}$ and $\boldsymbol{B_L}$ are denoted by dashed lines.

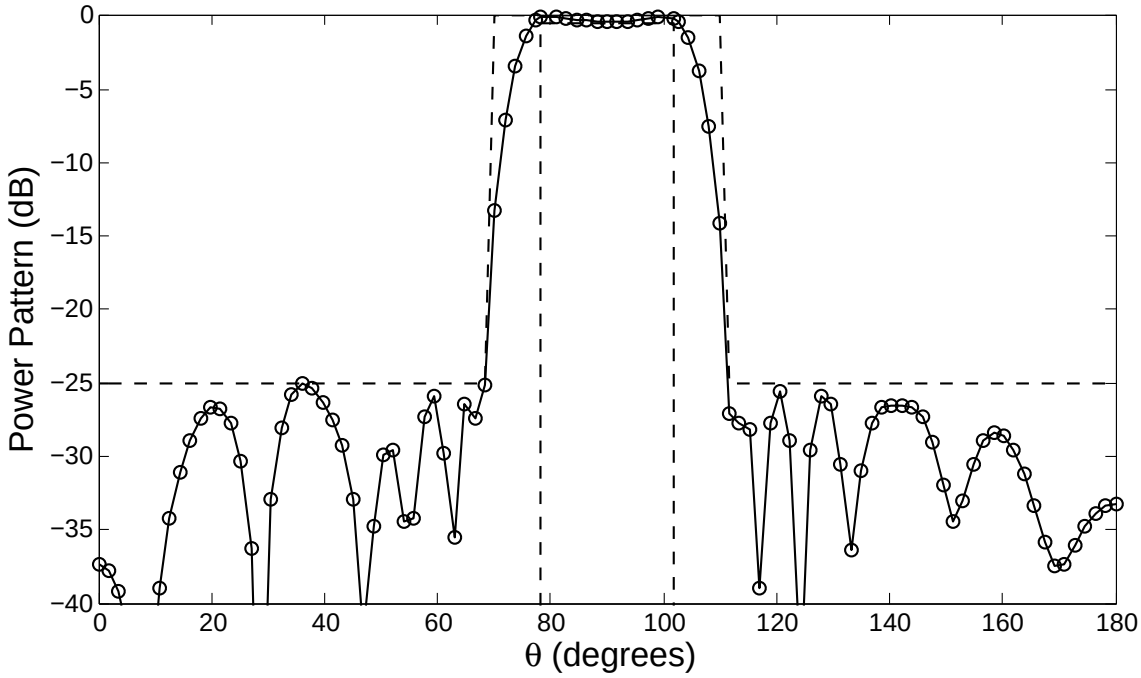

Figure 4.14: Achieved sector beam pattern at f_L using an asymmetric linear antenna array. $\boldsymbol{B_U}$ and $\boldsymbol{B_L}$ are denoted by dashed lines.

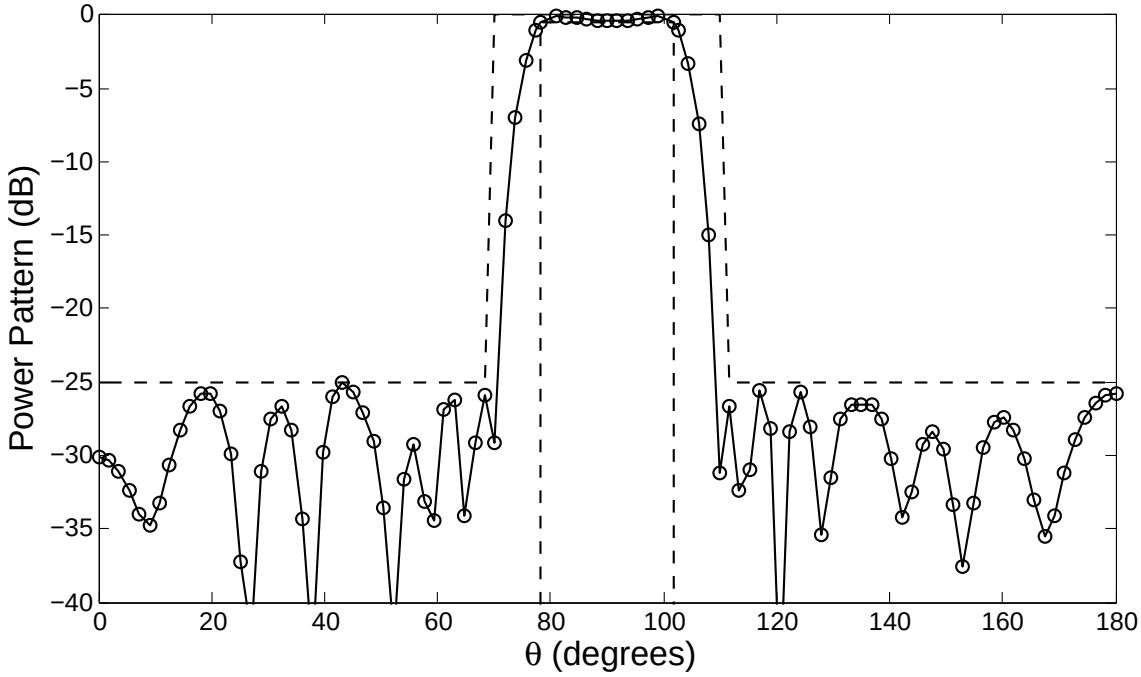

Figure 4.15: Achieved sector beam pattern at f_H using an asymmetric linear antenna array. $\boldsymbol{B_U}$ and $\boldsymbol{B_L}$ are denoted by dashed lines.

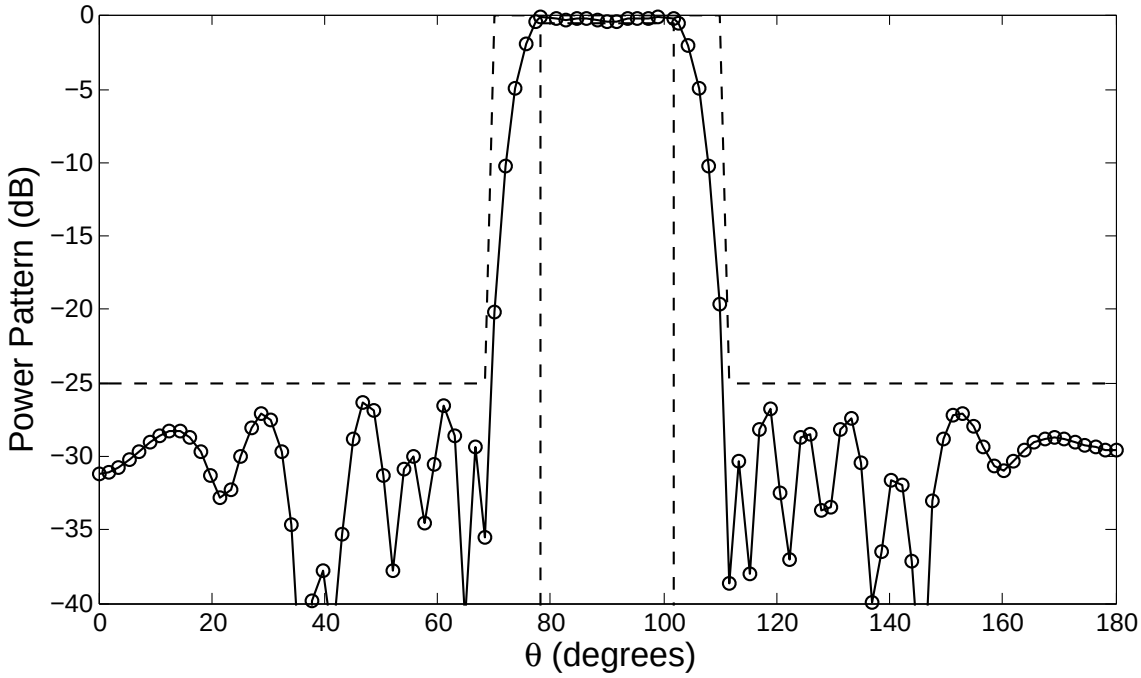

Figure 4.16: Achieved sector beam pattern at f_C using an asymmetric linear antenna array with constant time delays. $\boldsymbol{B_U}$ and $\boldsymbol{B_L}$ are denoted by dashed lines.

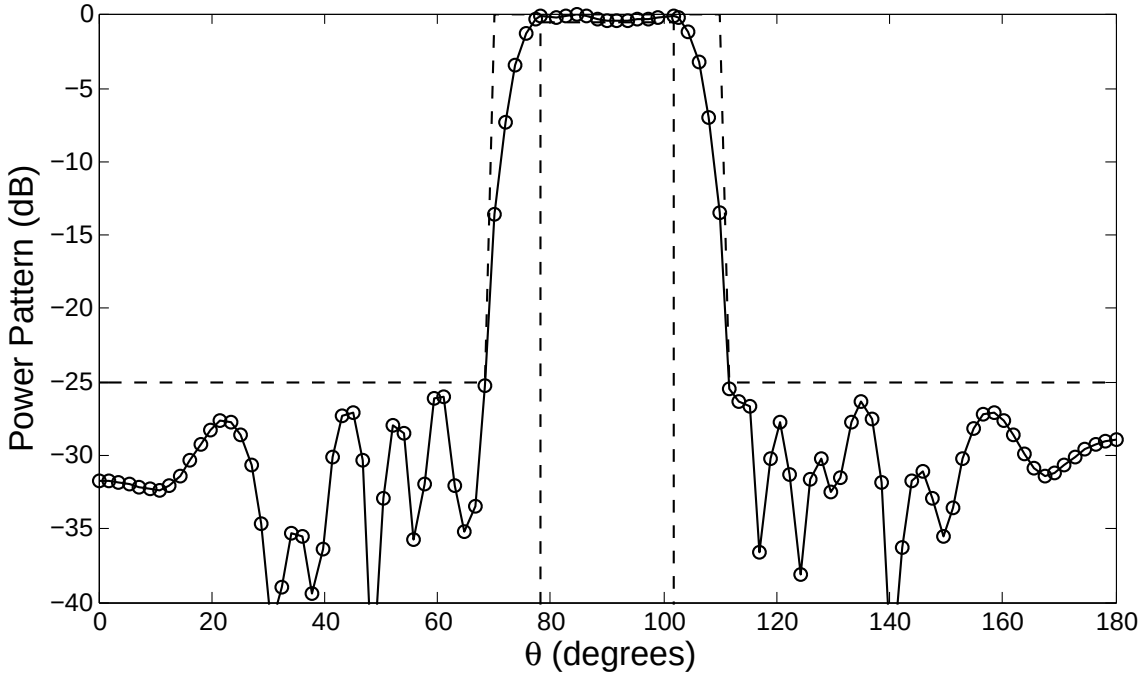

Figure 4.17: Achieved sector beam pattern at f_L using an asymmetric linear antenna array with constant time delays. $\boldsymbol{B_U}$ and $\boldsymbol{B_L}$ are denoted by dashed lines.

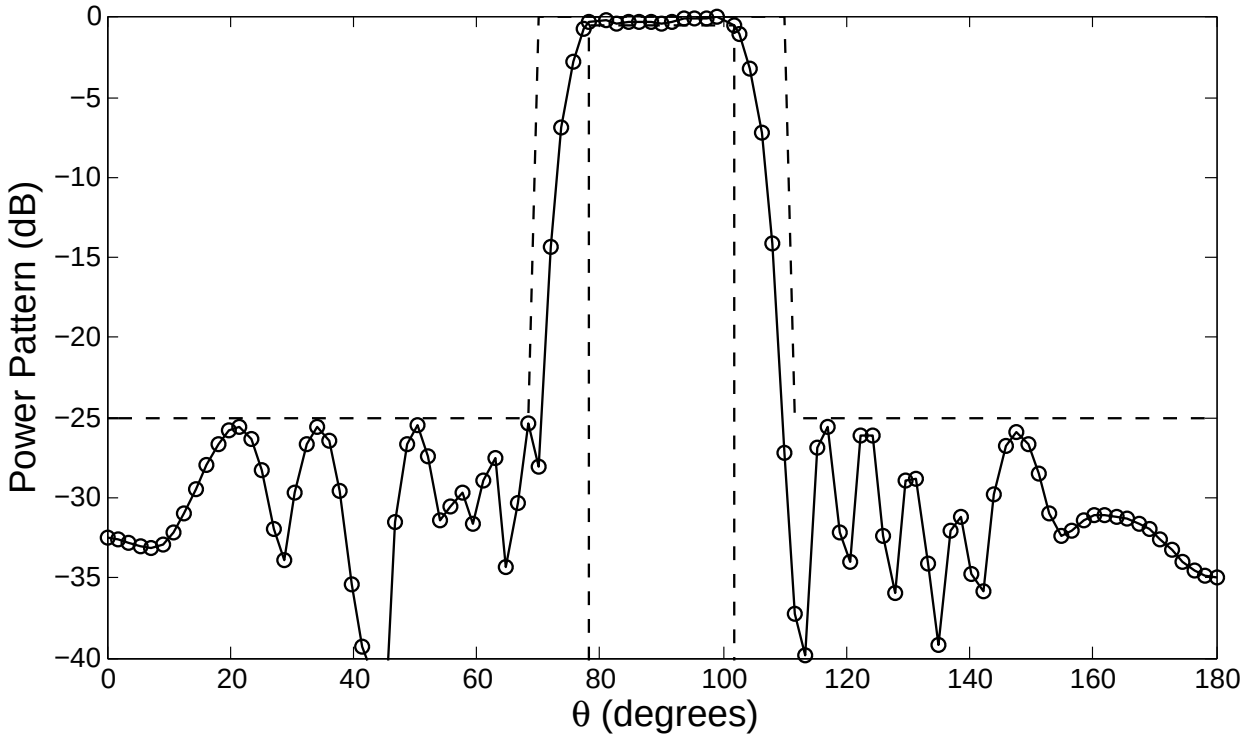

Figure 4.18: Achieved sector beam pattern at f_H using an asymmetric linear antenna array with constant time delays. $\boldsymbol{B_U}$ and $\boldsymbol{B_L}$ are denoted by dashed lines.

4.3.9 Linear Antenna Array with the Ability to Sustain the Loss of an Arbitrary Element

The performance of an antenna array deteriorates when one or more array elements become inoperable. Repairing or replacing a defective array element of an antenna array used in military or space applications may not be feasible at times. For these applications in which an antenna array is often subject to damage or failure of one or more array elements, it is desirable to design an antenna array that can maintain its performance at a reasonable level when one or more array elements are faulty. The following design example presents the design of a linear antenna array that has the ability to maintain the desired radiation pattern when an arbitrary array element becomes inoperable. The designed linear antenna array is required to maintain the desired radiation pattern without using any recovery measure such as reconfiguration of the element parameters.

Table 4.20: Estimated posterior probability for the number of array elements for the linear antenna array design that does not take into consideration the loss of an arbitrary array element. In this case, $\langle N \rangle = 8.84$.

N	$p(N\|\mathbf{B}_U, \mathbf{B}_L, \boldsymbol{\sigma})$
8	0.397333
9	0.408333
10	0.153667
11	0.035667
12	0.005000

Table 4.21: Complex currents and positions of the antenna elements for the final design of the linear antenna array design problem that does not take into consideration the loss of an arbitrary array element.

Element Number	$\|I_n\| \cos(\phi_n)$	$\|I_n\| \sin(\phi_n)$	z_n/λ
1	-0.269671	-0.141926	12.928013
2	-0.266663	-0.129406	13.722252
3	-0.322008	-0.128580	14.545142
4	-0.418296	-0.250193	15.404768
5	-0.305305	-0.110684	16.254164
6	-0.317826	-0.208315	17.165175
7	-0.286273	-0.111056	18.026896
8	-0.215835	-0.164148	18.789833

In the design problem presented here, an asymmetric linear antenna array with complex currents is used to realize a radiation pattern that has identical design pattern specifications to the Chebyshev pattern presented in Section 4.3.3, except that the maximum acceptable sidelobe level is relaxed to -15 dB. When an arbitrary array element becomes defective, the performance of a linear antenna array deteriorates in that the radiated power of the main beam is reduced and the sidelobe levels are increased. In the current design problem, the maximum power loss at $\theta = 90^\circ$ is limited to 1 dB. This design requirement can be implemented by setting $B_L(\theta = 90^\circ) = -1$ dB and using the following normalized parametric models:

$$g_\eta(\theta) = 10 \log \left[\frac{|AF_\eta(\theta)|^2}{max\{|AF_0(\theta)|^2\}} \right] \quad \text{for} \quad 0 \leq \theta \leq \pi, \quad 0 \leq \eta \leq N, \tag{4.16}$$

where $\eta = n$ denotes that the nth array element is defective, and $AF_0(\theta)$ is the array factor for

the primary radiation pattern that is obtained when all array elements are operating. Since the radiation pattern peak level is allowed to drop as much as 1 dB, the upper bound for the sidelobes are specified to be -16 dB to ensure that the sidelobe levels are at least 15 dB below the peak. The array factors $AF_\eta(\theta)$ are expressed as

$$AF_\eta(\theta) = \sum_{\substack{n=1 \\ n\neq\eta}}^{N} |I_n| \exp(j\psi_n) \exp\left[j2\pi \frac{z_n}{\lambda} \cos\theta\right], \tag{4.17}$$

and the likelihood in Eq. (4.1) is modified to

$$p(\mathbf{B}_U, \mathbf{B}_L | N, \mathbf{X}_N, \boldsymbol{\sigma}) \propto \exp\left[-Q_z^2/2\sigma_z^2 - \sum_{\eta=0}^{N}\sum_{m=1}^{M} Q_{\eta m}^2/2\sigma_m^2\right]. \tag{4.18}$$

For this design problem, Δz_{min} is specified to be 0.5λ, and the following assignments are made:

$$\begin{aligned} p(N) &= U[1, 50], \\ p(|I_n|) &= U[0.0, 0.5], \\ p(z_n/\lambda) &= U[-40.0, 40.0], \\ \sigma_z &= 1/100, \end{aligned}$$

and

$$\sigma_m = \begin{cases} 1/80 \text{ dB} & \text{for } \theta_m = 90.0^\circ \\ 1/20 \text{ dB} & \text{for } 86.85^\circ \leq \theta_m < 90.0^\circ \text{ and } 90.0^\circ < \theta_m \leq 93.15^\circ \\ 1/5 \text{ dB} & \text{otherwise} \end{cases}.$$

The obtained results are summarized in Table 4.22, Table 4.23, and Figures 4.21 – 4.37. The parameter values of the antenna elements for the final design are listed in Table 4.23. Using these parameter values, the radiation patterns that are produced when no antenna element or when an arbitrary array element is inoperable are plotted in Figures 4.21 – 4.37. For the case in which the loss of an arbitrary antenna element is not taken into consideration, the obtained results are summarized in Table 4.20, Table 4.21, and Figure 4.19. Table 4.21 lists the parameter values for the

Table 4.22: Estimated posterior probability for the number of array elements for the linear antenna array design that can maintain the desired radiation pattern when an arbitrary array element is inoperable. In this case, $\langle N \rangle = 16.30$.

N	$p(N\|\mathbf{B}_U, \mathbf{B}_L, \boldsymbol{\sigma})$
15	0.200000
16	0.423000
17	0.276000
18	0.084667
19	0.016000
20	0.000333

Table 4.23: Complex currents and positions of the antenna elements for the final design of the linear antenna array that can maintain the desired radiation pattern when an arbitrary array element is inoperable.

Element Number	$\|I_n\| \cos(\phi_n)$	$\|I_n\| \sin(\phi_n)$	z_n/λ
1	0.020378	−0.159873	−22.412249
2	0.020051	−0.404294	−21.836943
3	−0.036705	−0.438092	−21.302961
4	0.012136	−0.430679	−20.678771
5	−0.025168	−0.458153	−20.097629
6	0.024961	−0.456245	−19.574876
7	−0.012438	−0.450690	−19.073464
8	0.000515	−0.424054	−18.505450
9	−0.062079	−0.481467	−17.951211
10	−0.008858	−0.327190	−17.441321
11	0.007447	−0.344674	−16.772109
12	−0.004995	−0.439580	−16.051728
13	0.015775	−0.413209	−15.339305
14	−0.015106	−0.309285	18.107801
15	0.027221	−0.327962	18.698765
16	−0.006891	−0.090575	20.663559

final design while Figure 4.19 shows the achieved normalized radiation pattern produced by the final design. These results are obtained using the same assignments except that σ_m for the three regions are increased respectively from $1/80$ dB to $1/10$ dB, from $1/20$ dB to $1/2.5$ dB, and from $1/5$ dB to $1/1.25$ dB.

Figure 4.20 shows the radiation pattern produced by the final design that loses an arbitrary array element, specifically the 4th antenna element, for the case in which the loss of an arbitrary antenna element is not required to be compensated. This radiation pattern corresponds to the worst antenna performance that yields a power loss of 1.72 dB at $\theta = 90^{\circ}$ and a maximum sidelobe level of only 8.10 dB below the peak. When the loss of an arbitrary antenna element is required to be compensated, the required number of array elements of the final design doubles from 8 to 16 while the antenna aperture width increases from 5.86λ to 43.08λ. The maximum power loss at $\theta = 90^{\circ}$ is 0.73 dB, which stems from the loss of the 9th array element. The worst antenna performance is produced by the linear antenna array that loses the 8th array element. In this case, the achieved radiation pattern has a power loss of 0.64 dB at $\theta = 90^{\circ}$ and a maximum sidelobe level of 15.36 dB below the peak. The performance comparison suggests that if an antenna array, that is to be built, is often subject to damage or failure of an arbitrary array element, this antenna array should be designed in a way such that it is equipped with the ability to compensate for the loss of an arbitrary antenna element. The results presented here demonstrate that even after losing an arbitrary array element and without any recovery measure at hand, an antenna array that has the compensation ability can still perform at the required standard, at the expense of higher design complexity and production cost.

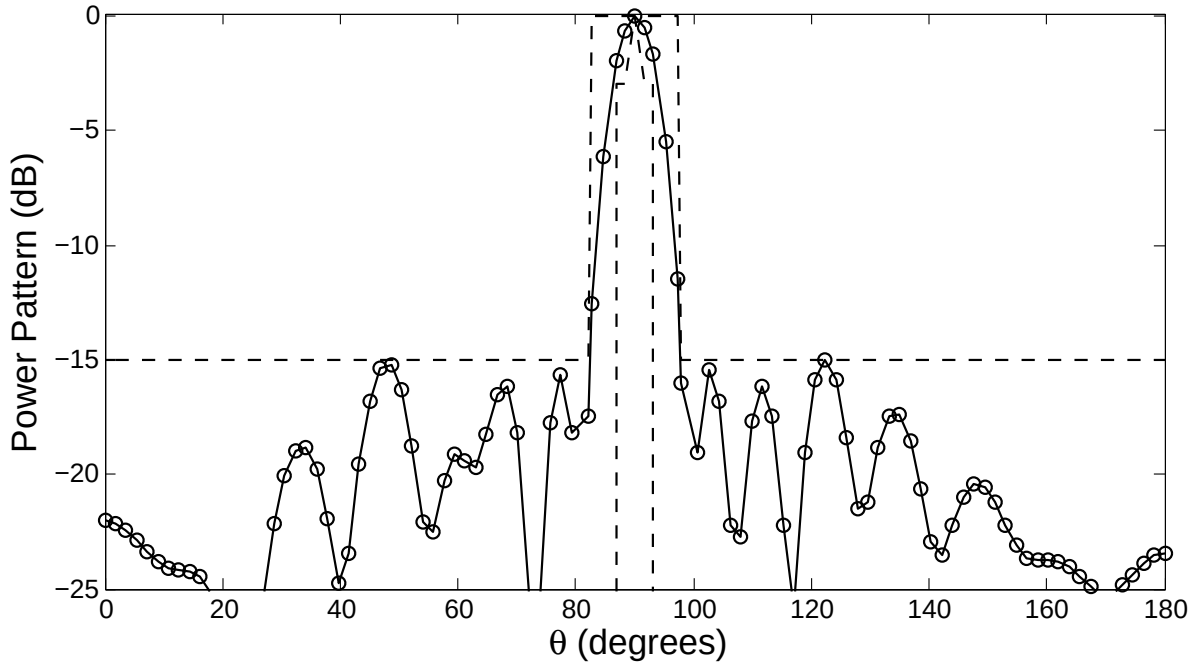

Figure 4.19: Achieved normalized radiation pattern by the final linear antenna array design for the case in which the loss of an arbitrary antenna element is not taken into consideration. $\boldsymbol{B_U}$ and $\boldsymbol{B_L}$ are denoted by dashed lines.

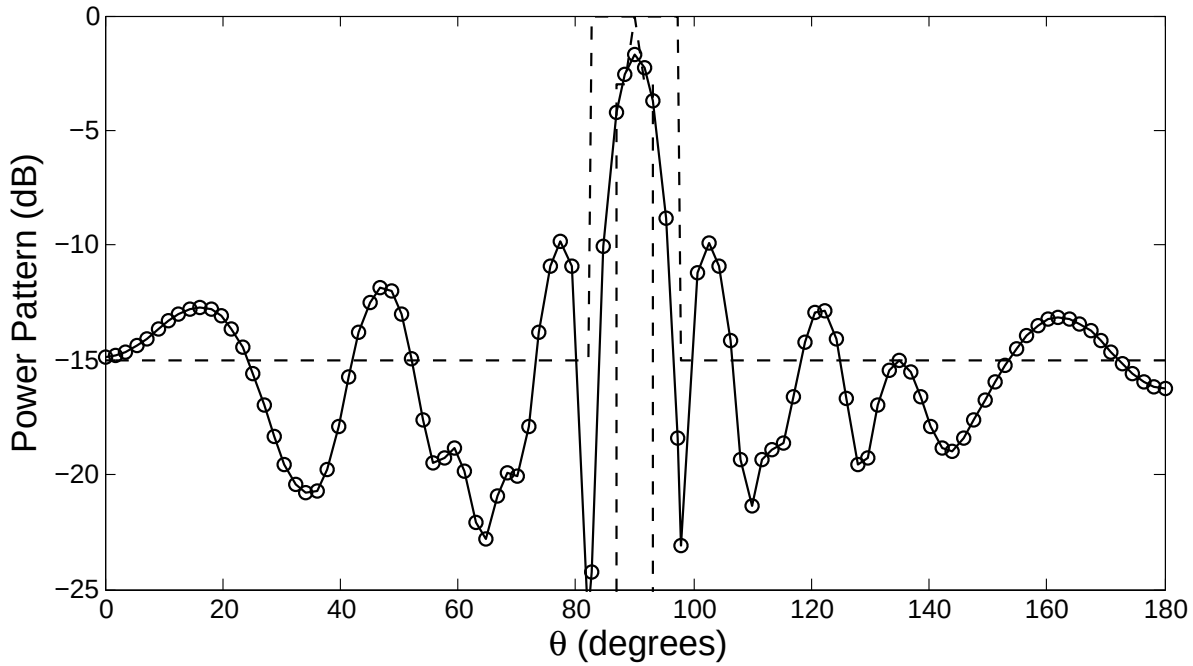

Figure 4.20: Achieved radiation pattern by the final linear antenna array design that loses the 4th array element for the case in which the loss of an arbitrary antenna element is not taken into consideration. $\boldsymbol{B_U}$ and $\boldsymbol{B_L}$ are denoted by dashed lines.

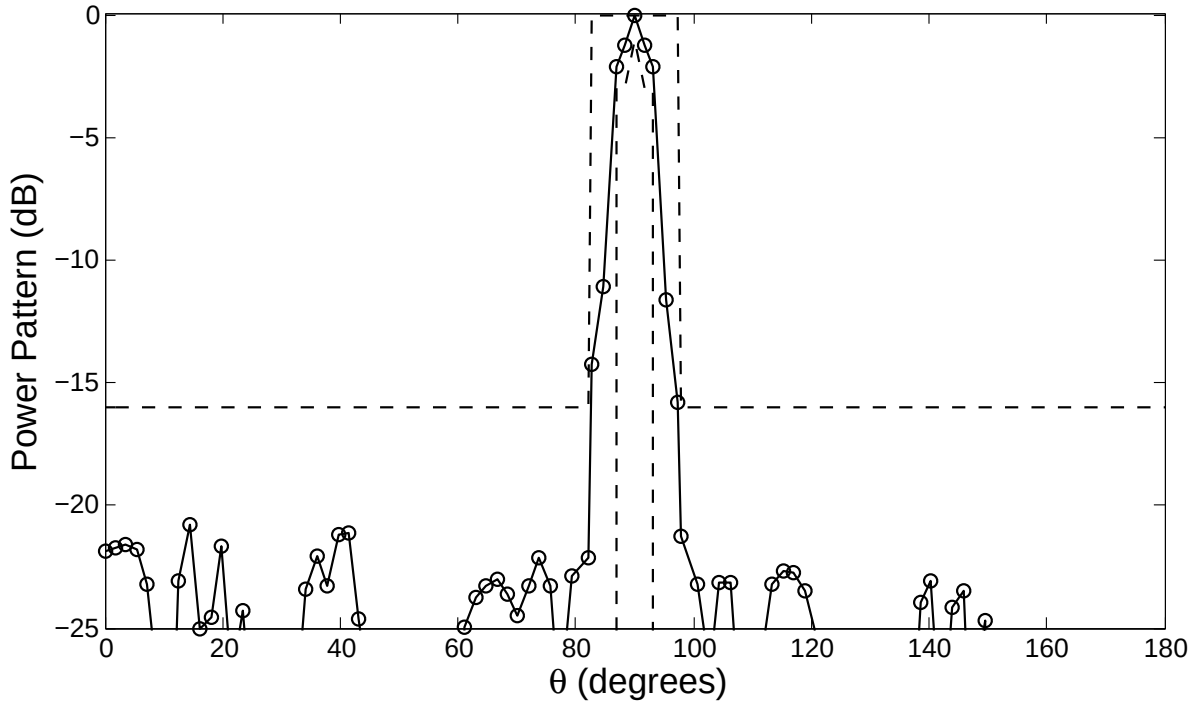

Figure 4.21: Achieved radiation pattern by the final linear antenna array design with all array elements functional. $\boldsymbol{B_U}$ and $\boldsymbol{B_L}$ are denoted by dashed lines.

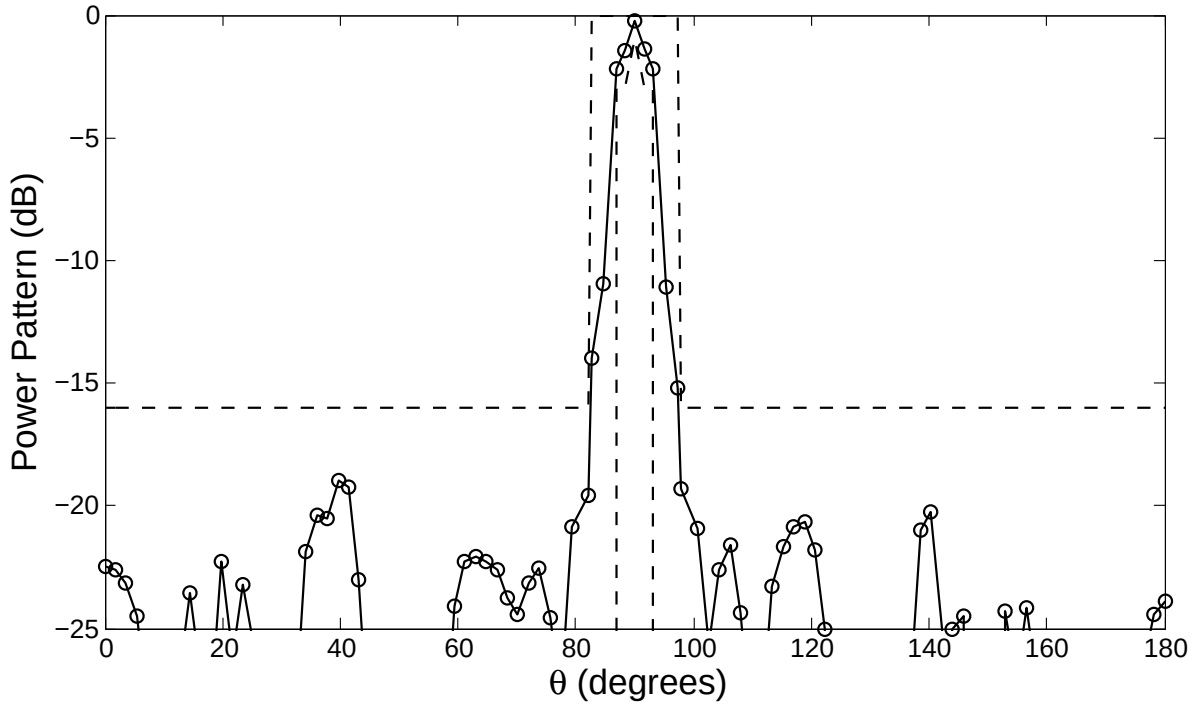

Figure 4.22: Achieved radiation pattern by the final linear antenna array design with the 1st array element being defective. $\boldsymbol{B_U}$ and $\boldsymbol{B_L}$ are denoted by dashed lines.

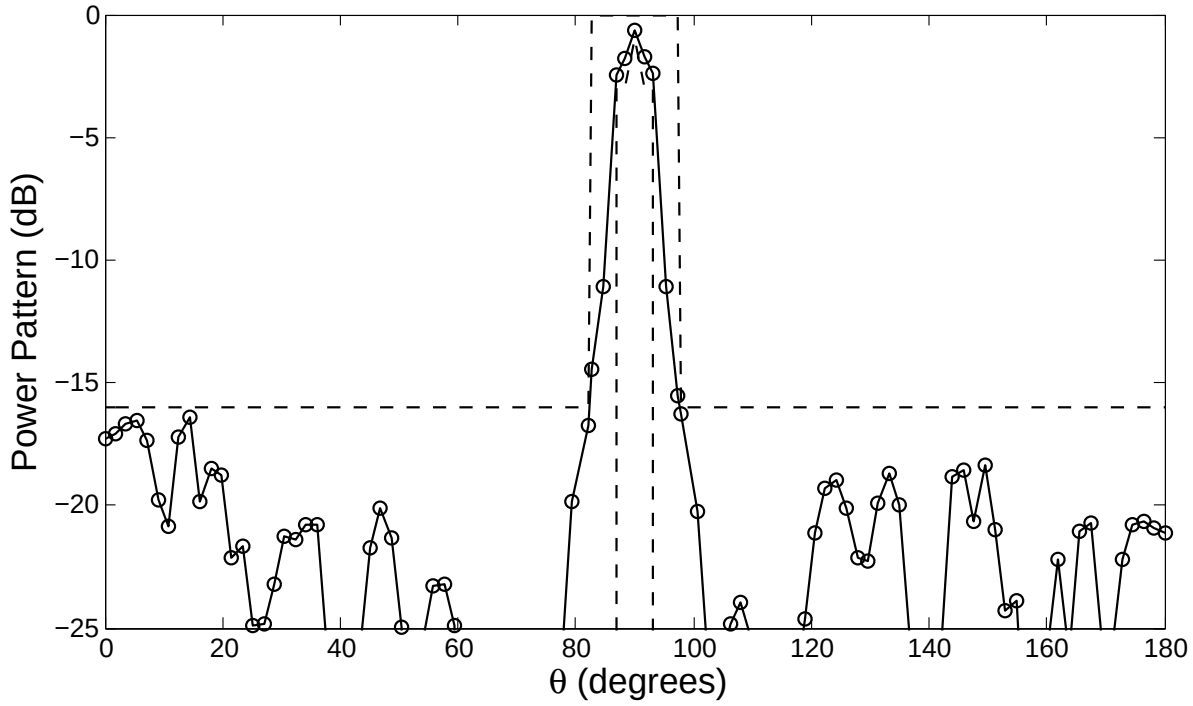

Figure 4.23: Achieved radiation pattern by the final linear antenna array design with the 2nd array element being defective. $\boldsymbol{B_U}$ and $\boldsymbol{B_L}$ are denoted by dashed lines.

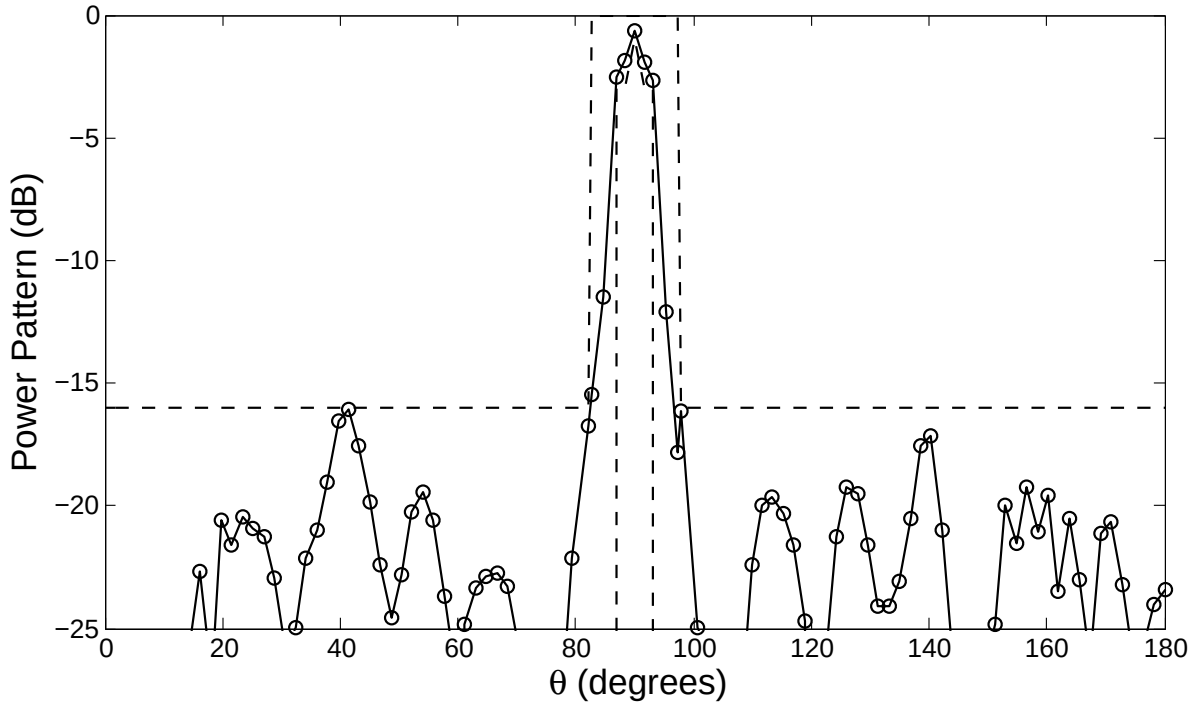

Figure 4.24: Achieved radiation pattern by the final linear antenna array design with the 3rd array element being defective. $\boldsymbol{B_U}$ and $\boldsymbol{B_L}$ are denoted by dashed lines.

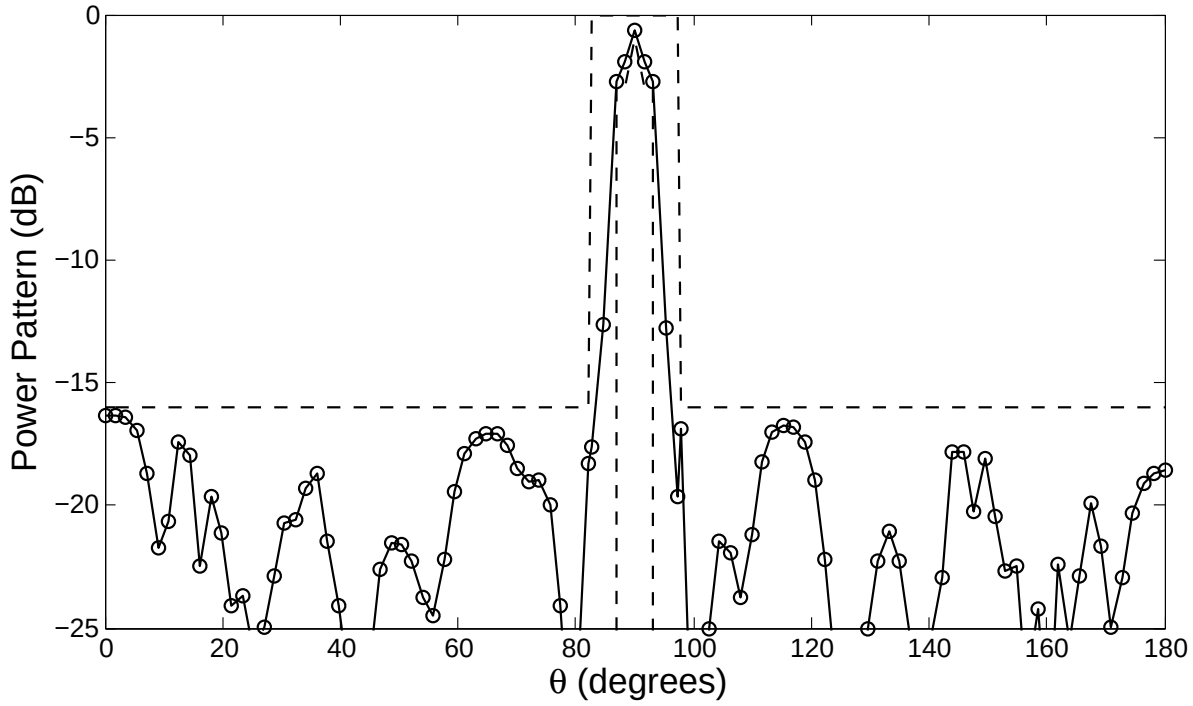

Figure 4.25: Achieved radiation pattern by the final linear antenna array design with the 4th array element being defective. $\boldsymbol{B_U}$ and $\boldsymbol{B_L}$ are denoted by dashed lines.

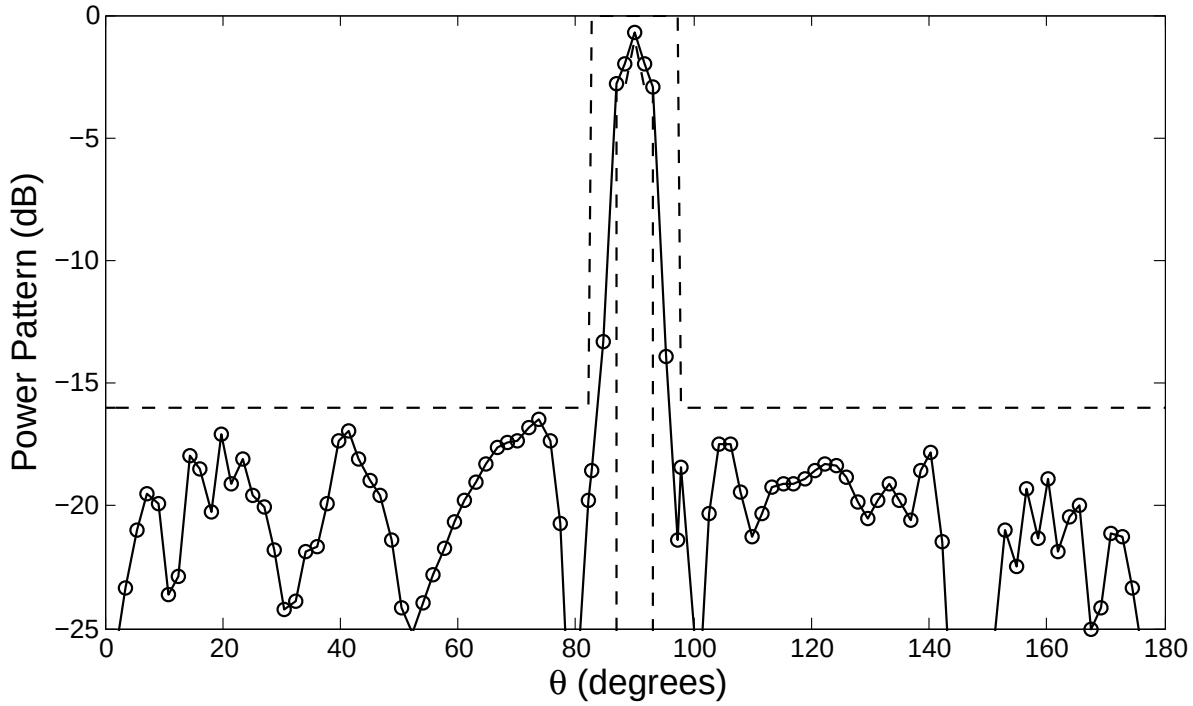

Figure 4.26: Achieved radiation pattern by the final linear antenna array design with the 5th array element being defective. $\boldsymbol{B_U}$ and $\boldsymbol{B_L}$ are denoted by dashed lines.

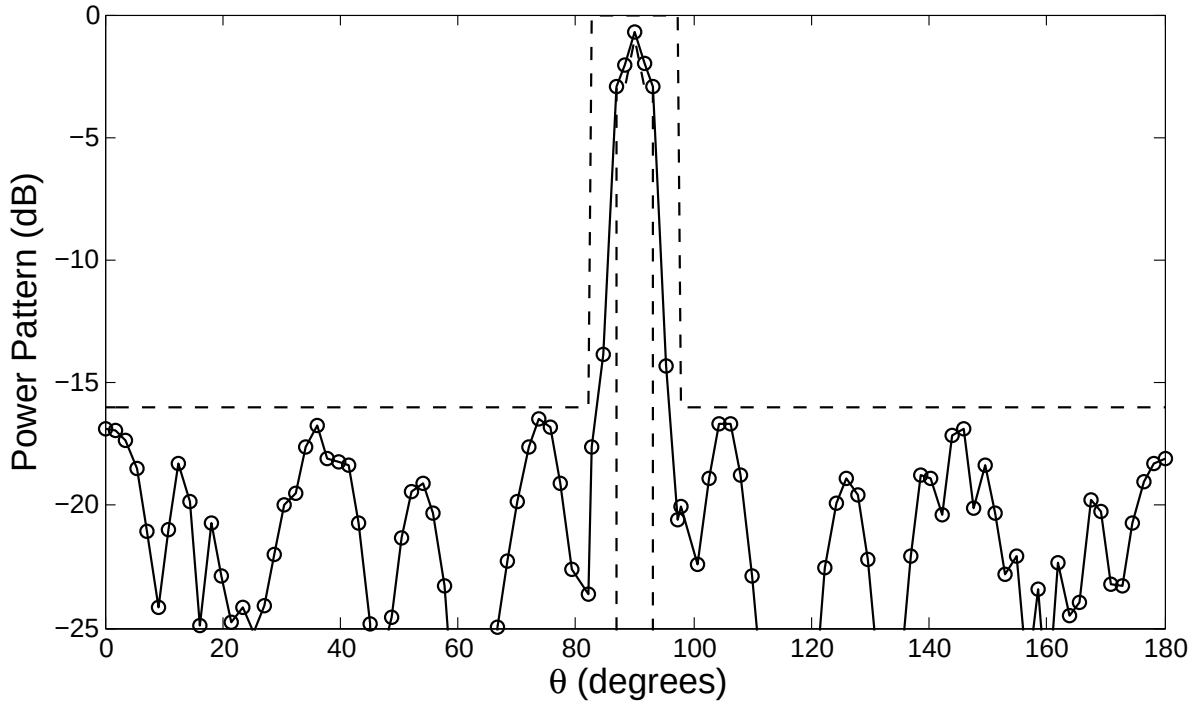

Figure 4.27: Achieved radiation pattern by the final linear antenna array design with the 6th array element being defective. $\boldsymbol{B_U}$ and $\boldsymbol{B_L}$ are denoted by dashed lines.

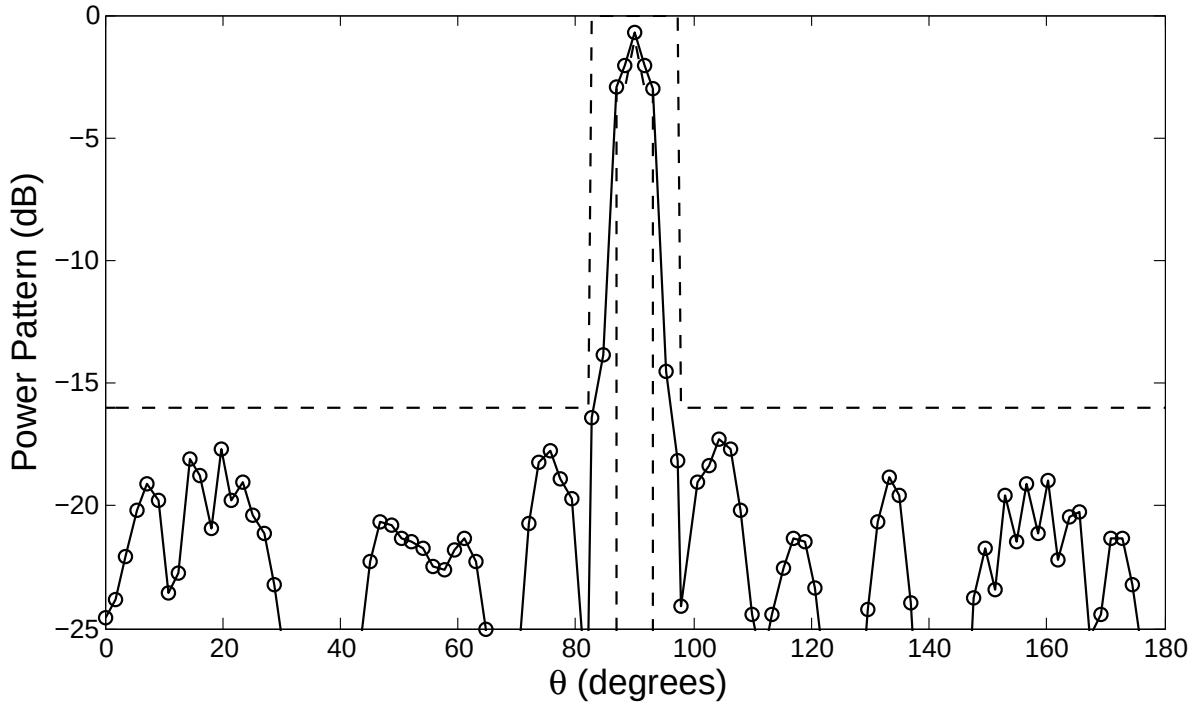

Figure 4.28: Achieved radiation pattern by the final linear antenna array design with the 7th array element being defective. $\boldsymbol{B_U}$ and $\boldsymbol{B_L}$ are denoted by dashed lines.

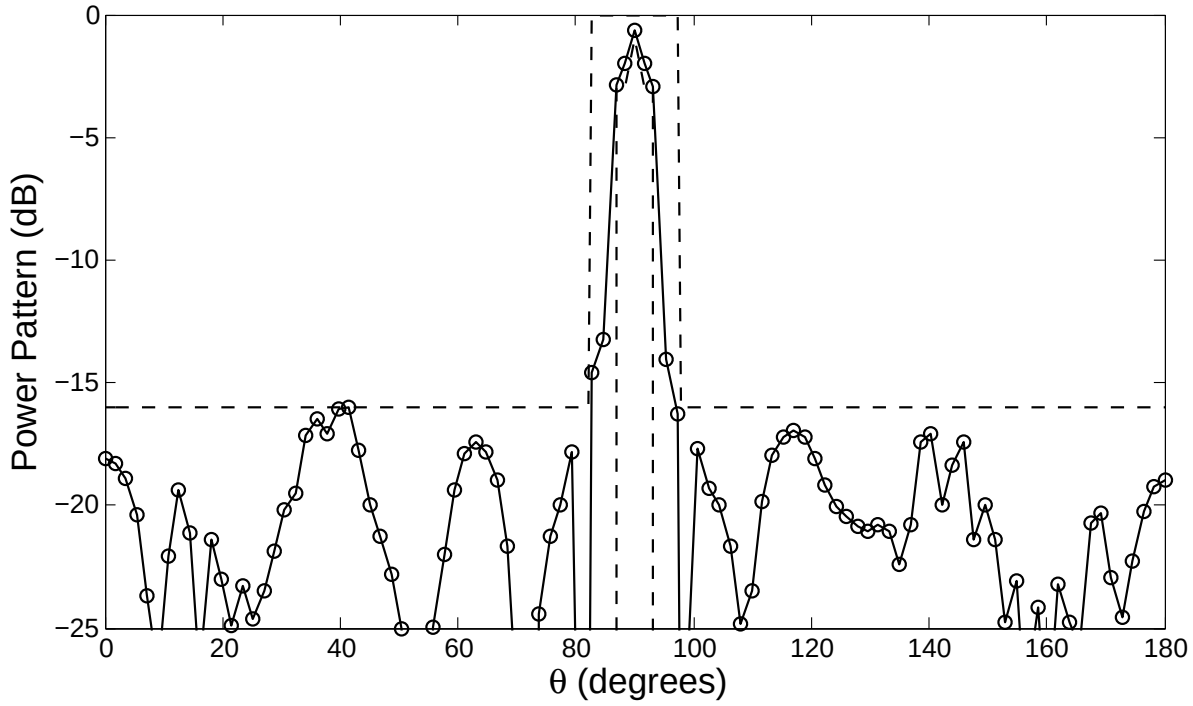

Figure 4.29: Achieved radiation pattern by the final linear antenna array design with the 8th array element being defective. $\boldsymbol{B_U}$ and $\boldsymbol{B_L}$ are denoted by dashed lines.

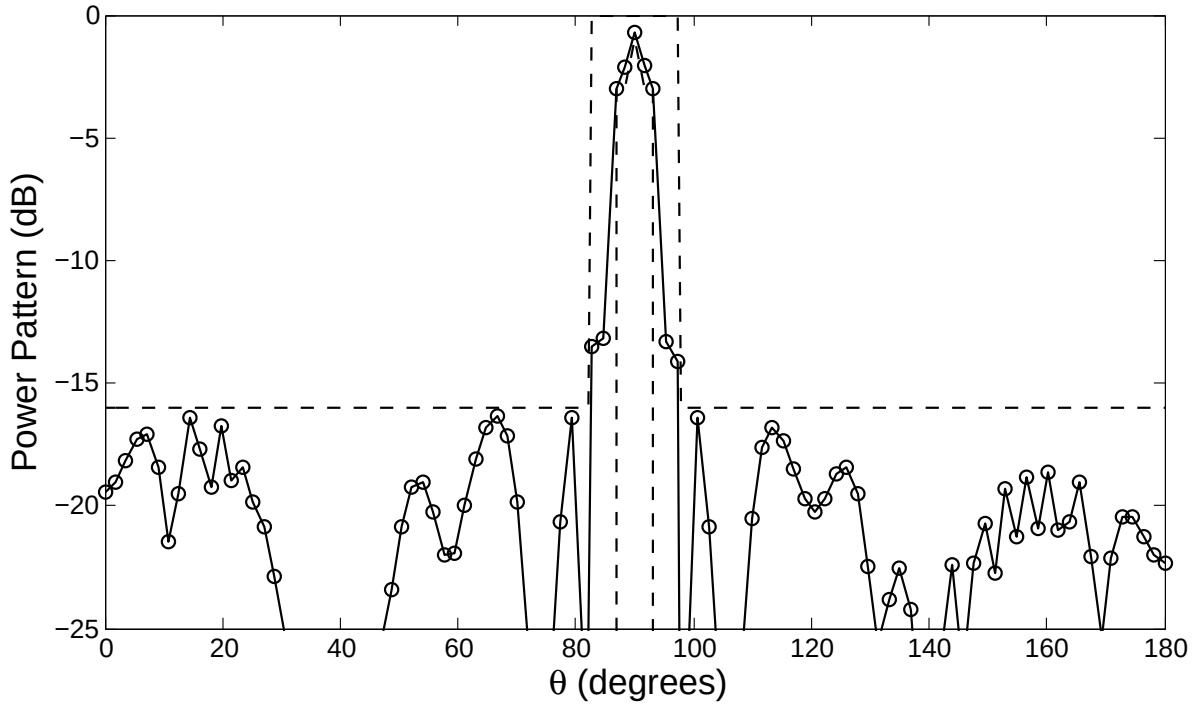

Figure 4.30: Achieved radiation pattern by the final linear antenna array design with the 9th array element being defective. $\boldsymbol{B_U}$ and $\boldsymbol{B_L}$ are denoted by dashed lines.

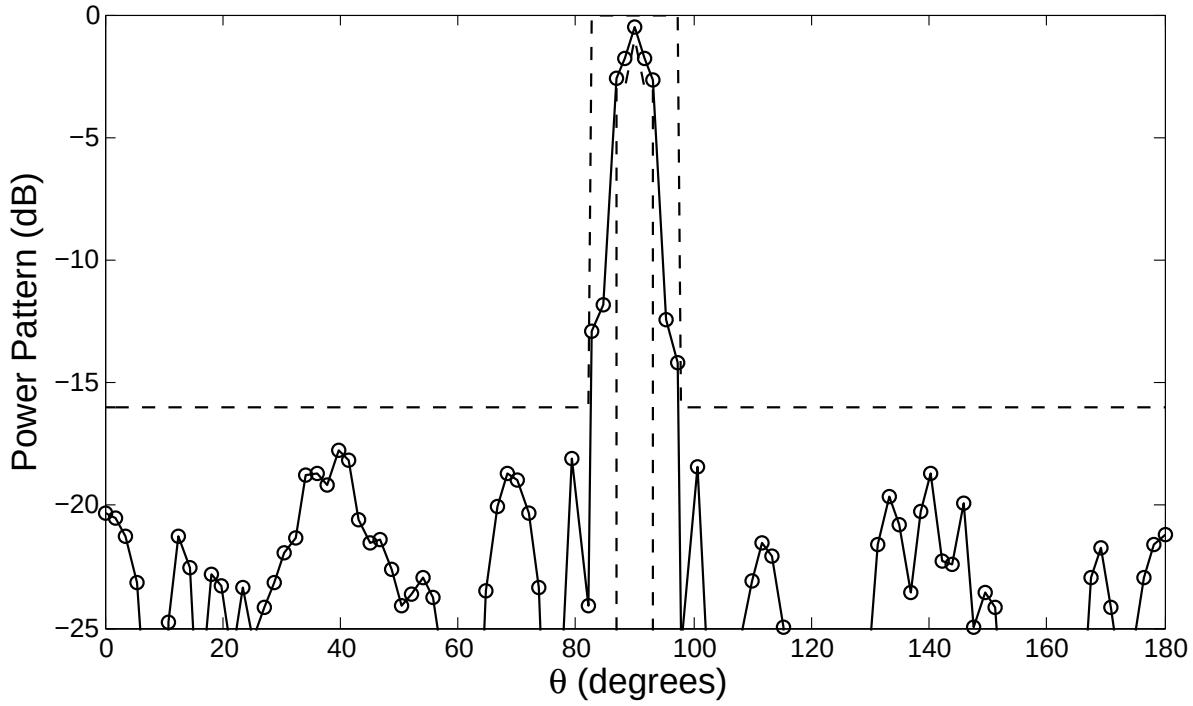

Figure 4.31: Achieved radiation pattern by the final linear antenna array design with the 10th array element being defective. $\boldsymbol{B_U}$ and $\boldsymbol{B_L}$ are denoted by dashed lines.

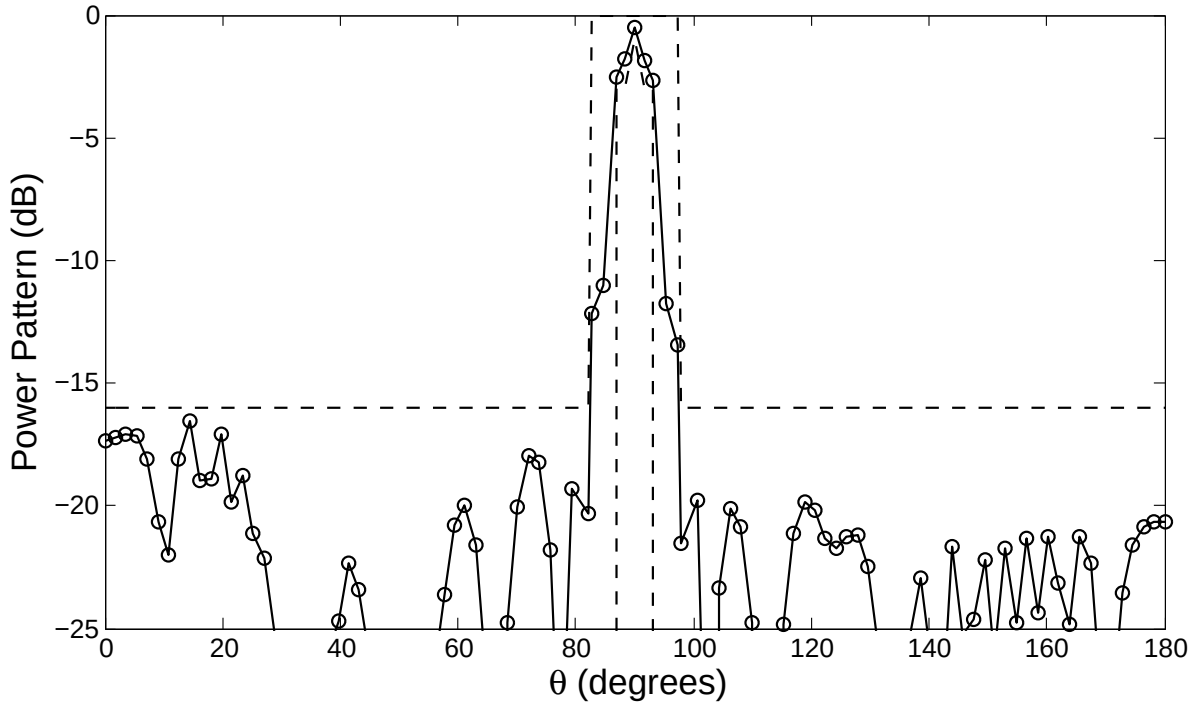

Figure 4.32: Achieved radiation pattern by the final linear antenna array design with the 11th array element being defective. $\boldsymbol{B_U}$ and $\boldsymbol{B_L}$ are denoted by dashed lines.

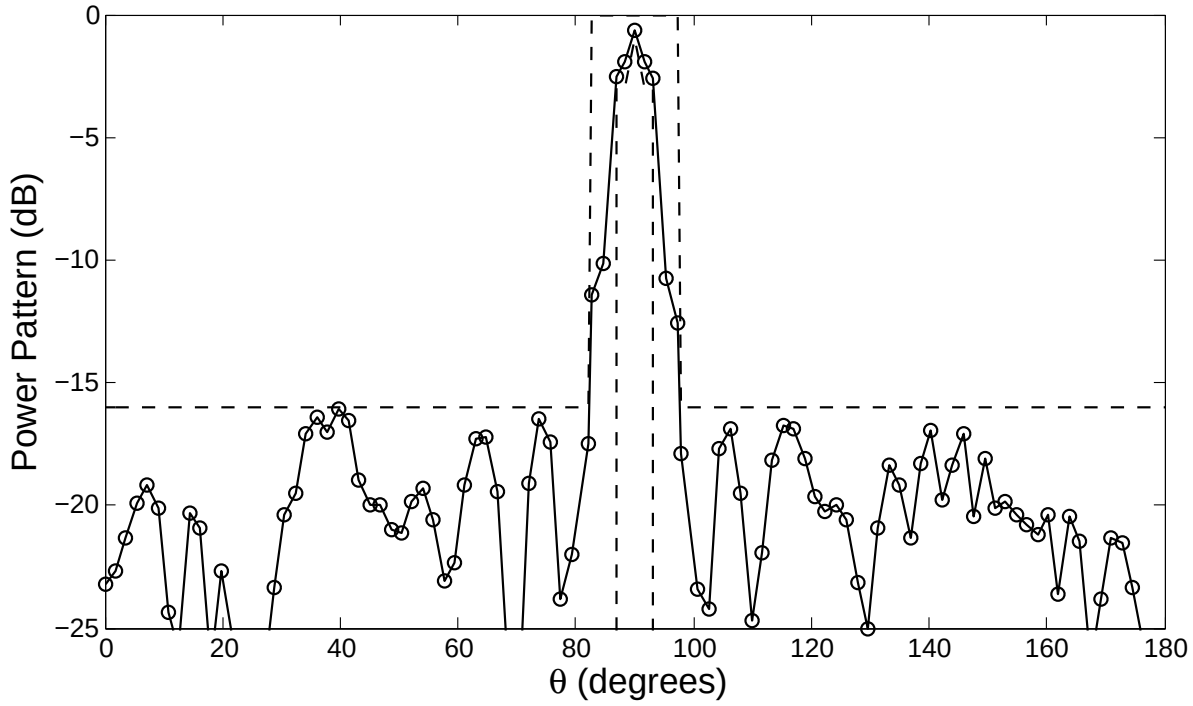

Figure 4.33: Achieved radiation pattern by the final linear antenna array design with the 12th array element being defective. $\boldsymbol{B_U}$ and $\boldsymbol{B_L}$ are denoted by dashed lines.

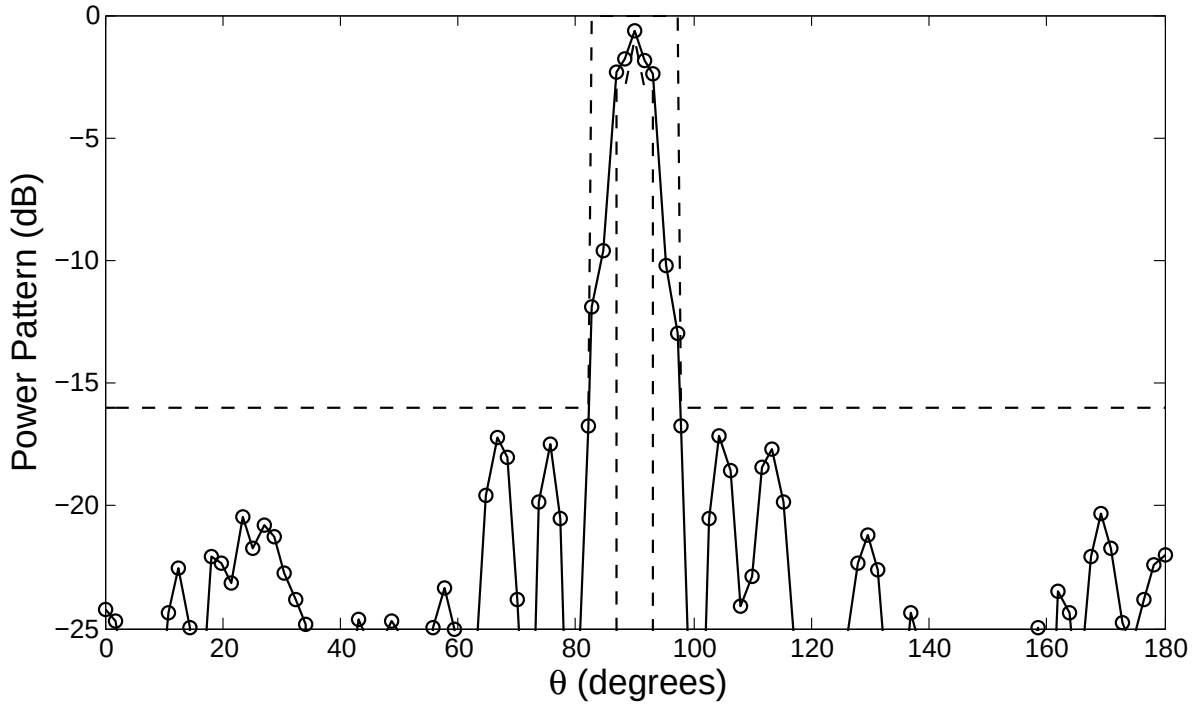

Figure 4.34: Achieved radiation pattern by the final linear antenna array design with the 13th array element being defective. $\boldsymbol{B_U}$ and $\boldsymbol{B_L}$ are denoted by dashed lines.

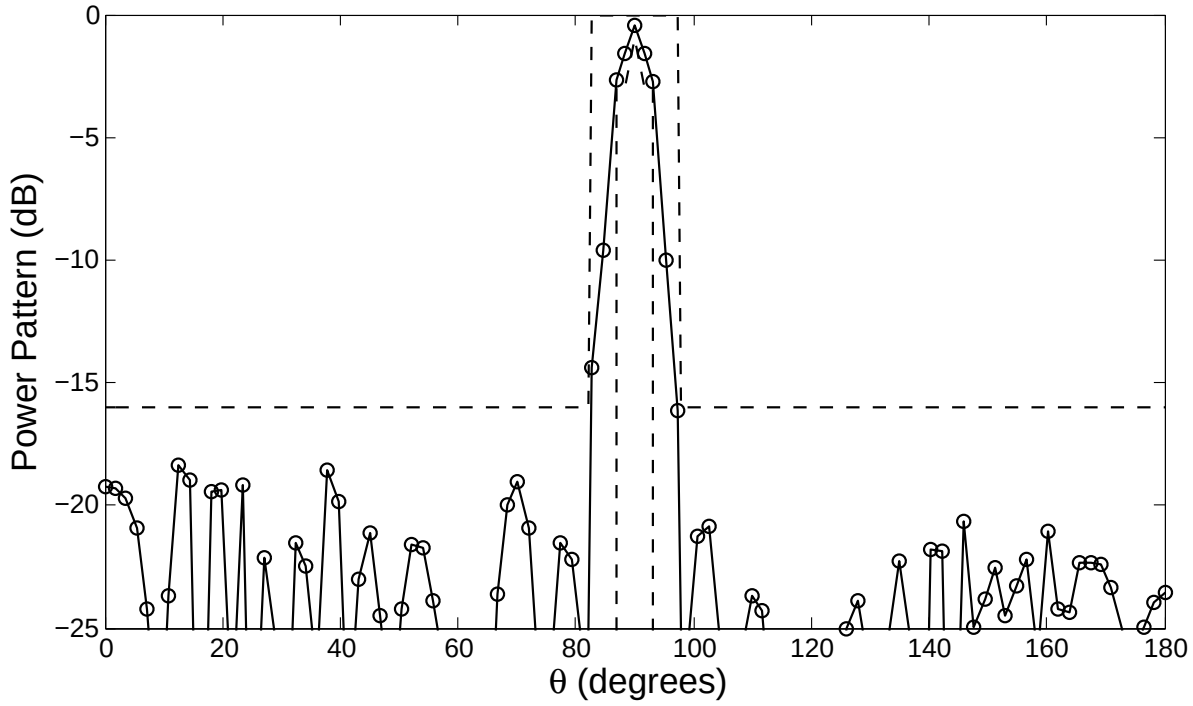

Figure 4.35: Achieved radiation pattern by the final linear antenna array design with the 14th array element being defective. $\boldsymbol{B_U}$ and $\boldsymbol{B_L}$ are denoted by dashed lines.

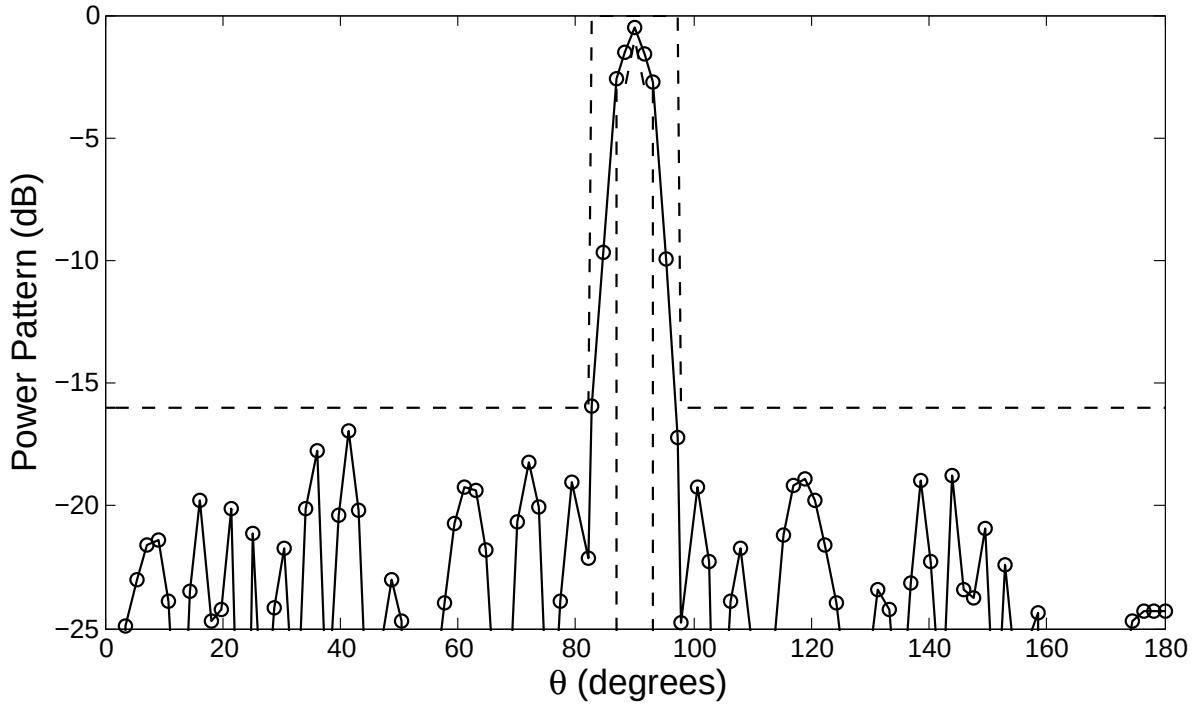

Figure 4.36: Achieved radiation pattern by the final linear antenna array design with the 15th array element being defective. $\boldsymbol{B_U}$ and $\boldsymbol{B_L}$ are denoted by dashed lines.

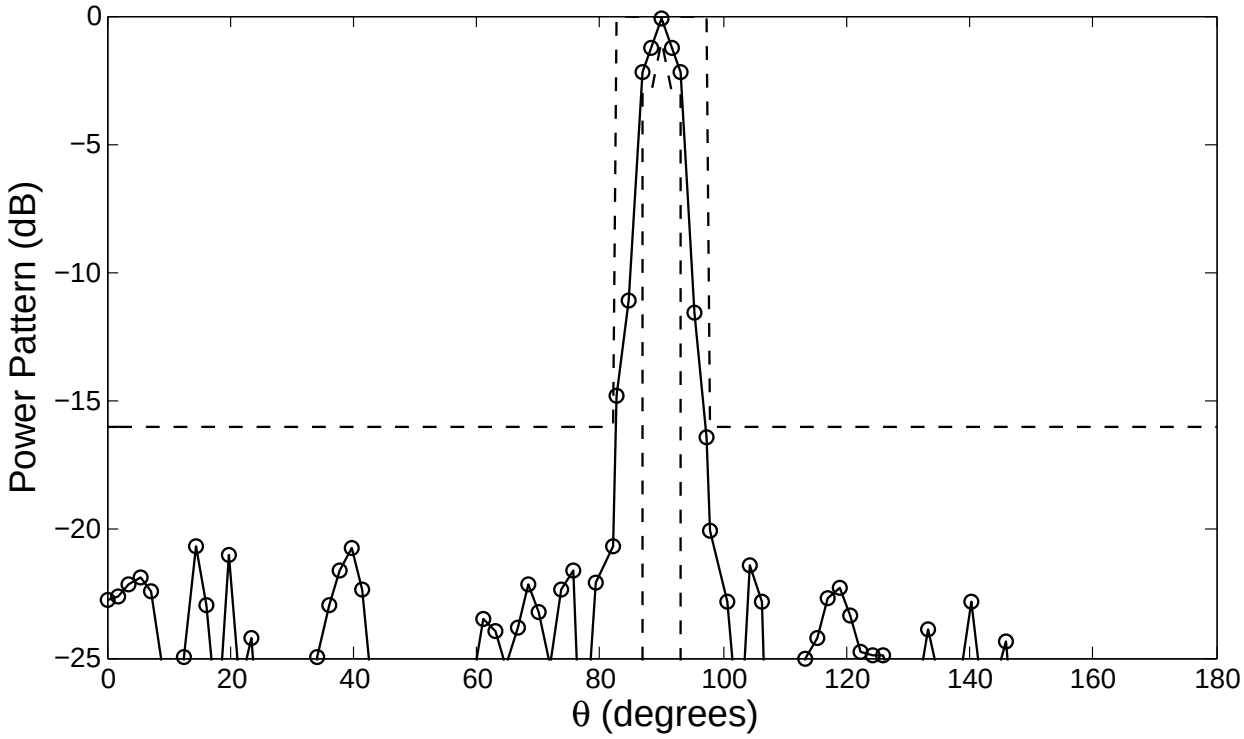

Figure 4.37: Achieved radiation pattern by the final linear antenna array design with the 16th array element being defective. $\boldsymbol{B_U}$ and $\boldsymbol{B_L}$ are denoted by dashed lines.

4.3.10 Planar Array

The Bayesian inference framework for antenna array design has been extended to solve a planar antenna array design problem. In the design example presented here, a planar antenna array with positive and negative real-valued currents is used to realize a desired radiation pattern that has the following design pattern specifications:

$$B_L(\theta_m, \phi_m) = \begin{cases} -3.0 \text{ dB} & \text{for } \theta_m < 10.0^\circ \text{ and } \theta_m > 170.0^\circ \\ -100.0 \text{ dB} & \text{otherwise} \end{cases},$$

and

$$B_U(\theta_m, \phi_m) = \begin{cases} 0.0 \text{ dB} & \text{for } \theta_m < 20.0^\circ \text{ and } \theta_m > 160.0^\circ \\ -30.0 \text{ dB} & \text{otherwise} \end{cases}.$$

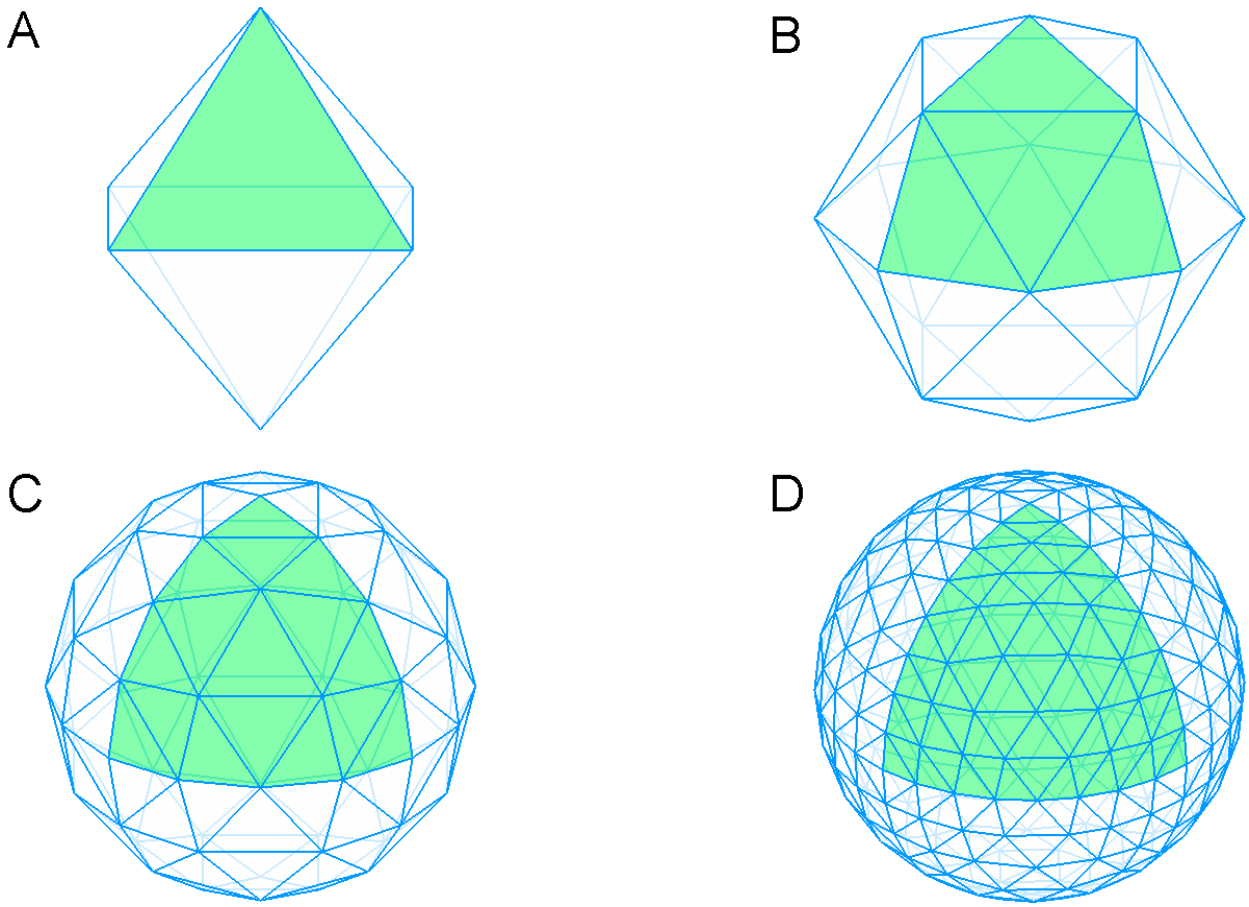

Figure 4.38: Recursive subdivision of an octahedron to obtain a geodesic sphere from which the sampling points for the desired three-dimensional radiation pattern are generated. This image is after [75].

To generate sampling angles for the desired three-dimensional radiation pattern, an octahedral geodesic unit sphere as shown in Figure 4.38D is used. A geodesic sphere can be constructed from recursive subdivision of the triangular faces of a regular tetrahedron, octahedron or icosahedron [74–76]. The process of constructing a geodesic unit sphere using an octahedron is illustrated in Figure 4.38. Figure 4.38B shows the constructed geodesic sphere after the first subdivision process, in which each triangular face is divided into four smaller triangles, and each new vertex is pushed onto the surface of the unit sphere. This subdivision process is repeated recursively to generate a finer octahedral geodesic sphere as shown in Figures 4.38C and 4.38D.

The desired radiation pattern in the current problem is symmetric about $\theta = 90^\circ$ and hence,

only the upper half of an octahedral geodesic unit sphere, which corresponds to $z \geq 0$, is required for generating the sampling angles. For a octahedral geodesic hemisphere, the number of vertices, v, and triangular faces, ϑ, that are produced after r times of recursive subdivision are expressed respectively as

$$v(r) = 2^{r+1}\left(2^r + 1\right) + 1 \quad \text{for} \quad r = 0, 1, 2, 3, \cdots$$

and

$$\vartheta(r) = 2^{2(r+1)} \quad \text{for} \quad r = 0, 1, 2, 3, \cdots.$$

In the current design problem, r is given the value of 4, yielding a total of 545 vertices, all of which represent the sampling points for the desired three-dimensional radiation pattern. For the type of antenna array used in this problem, the parametric model in Eq. (2.4) can be rewritten as

$$AF(\theta, \phi) = \sum_{n=1}^{N} I_n \exp\left[j\frac{2\pi}{\lambda}\left(x_n \cos\phi \sin\theta + y_n \sin\phi \sin\theta\right)\right].$$

The spacing between any two neighboring array elements is not constrained to have a minimum value. For this design problem, the following assignments are made:

$$\begin{aligned} p(N) &= U[1, 50], \\ p(I_n) &= U[-0.5, 0.5], \\ p(x_n/\lambda) &= U[-40.0, 40.0], \\ p(y_n/\lambda) &= U[-40.0, 40.0], \end{aligned}$$

and

$$\sigma_m = \begin{cases} 1/50 \text{ dB} & \text{for} \quad \theta_m < 10.0^\circ \\ 1/10 \text{ dB} & \text{otherwise} \end{cases}.$$

Table 4.24: Estimated posterior probability for the number of array elements for the planar antenna array design problem. In this case, $\langle N \rangle = 42.76$.

N	$p(N\|\mathbf{B}_U, \mathbf{B}_L, \boldsymbol{\sigma})$
41	0.093000
42	0.328333
43	0.357667
44	0.172000
45	0.039667
46	0.008667
47	0.000667

Table 4.25: Real-valued currents and positions of the antenna elements for the final design of the planar antenna array design problem.

n	I_n	x_n/λ	y_n/λ	n	I_n	x_n/λ	y_n/λ
1	0.00691	−24.54321	14.40242	22	−0.05609	17.65650	−25.16116
2	−0.00545	−21.41884	36.07572	23	−0.06760	18.04708	−24.45770
3	−0.00526	−11.12544	25.95846	24	−0.05653	18.33540	−25.84519
4	0.00189	−2.02787	33.75424	25	−0.07014	18.35183	−25.15761
5	−0.00662	−1.29324	16.53823	26	−0.06472	18.82015	−24.44967
6	0.00708	3.12288	−6.07716	27	−0.06812	18.96763	−25.19450
7	−0.00495	6.38431	−15.58806	28	−0.04458	19.00662	−25.90414
8	−0.00512	7.30329	−25.67239	29	−0.03084	19.57438	−33.95100
9	−0.02244	7.73785	−23.82015	30	−0.04612	19.57955	−34.66808
10	−0.00791	8.18518	26.53181	31	−0.03126	19.59271	−35.37544
11	−0.02105	8.40332	−26.59780	32	−0.00853	20.08457	−35.99355
12	−0.03476	8.43995	−23.75220	33	−0.01810	20.22049	−34.44579
13	−0.00690	8.97846	26.22725	34	−0.02295	20.29274	−35.21906
14	−0.01872	9.11191	−26.58519	35	−0.00798	20.92150	−5.19737
15	−0.02919	9.14009	−23.75224	36	−0.00811	26.87732	−25.59971
16	−0.00997	9.85336	−13.98626	37	−0.01066	27.57231	−23.20395
17	−0.00383	9.94509	−16.51306	38	−0.01147	28.15283	−22.93934
18	0.00441	14.39216	34.70999	39	−0.01087	28.42942	−23.52109
19	−0.02093	16.93986	−25.07770	40	−0.00724	29.07019	−13.55400
20	−0.03657	17.30296	−24.47751	41	−0.00602	33.04445	−9.34461
21	−0.03131	17.62038	−25.89460	42	−0.00551	39.99655	−35.83086

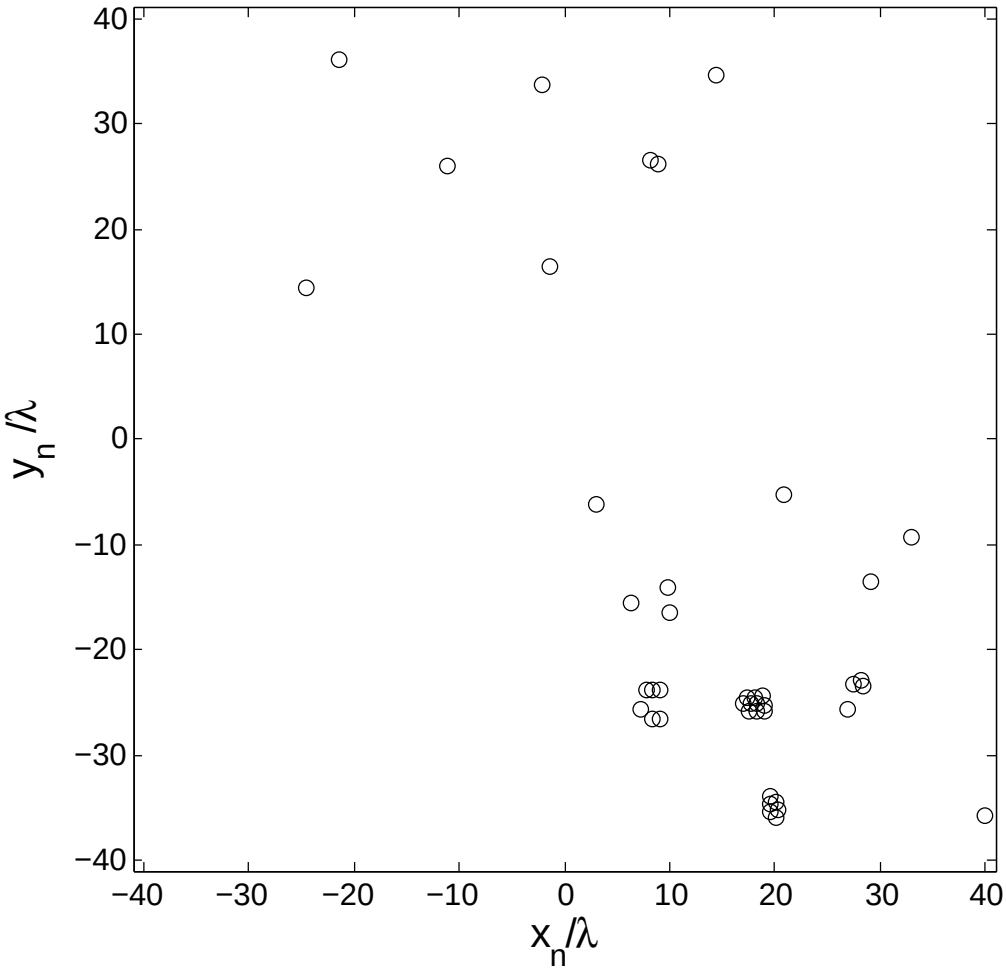

Figure 4.39: Positions of the array elements on the xy-plane.

The obtained results are summarized in Tables 4.24 – 4.25 and Figures 4.39 – 4.40. Table 4.25 indicates that the final design uses a total of 42 array elements. Using the parameter values of the array elements listed in Table 4.23, the achieved three-dimensional radiation pattern is plotted in Figure 4.40. The radiation pattern produced by the final design satisfied the design pattern specifications completely. In addition, even though a minimum spacing is not enforced between any two neighboring array elements, the final planar antenna array design produced by the Bayesian inference framework is physically realizable since all array elements have a Cartesian distance of at least 0.5λ to all neighboring array elements.

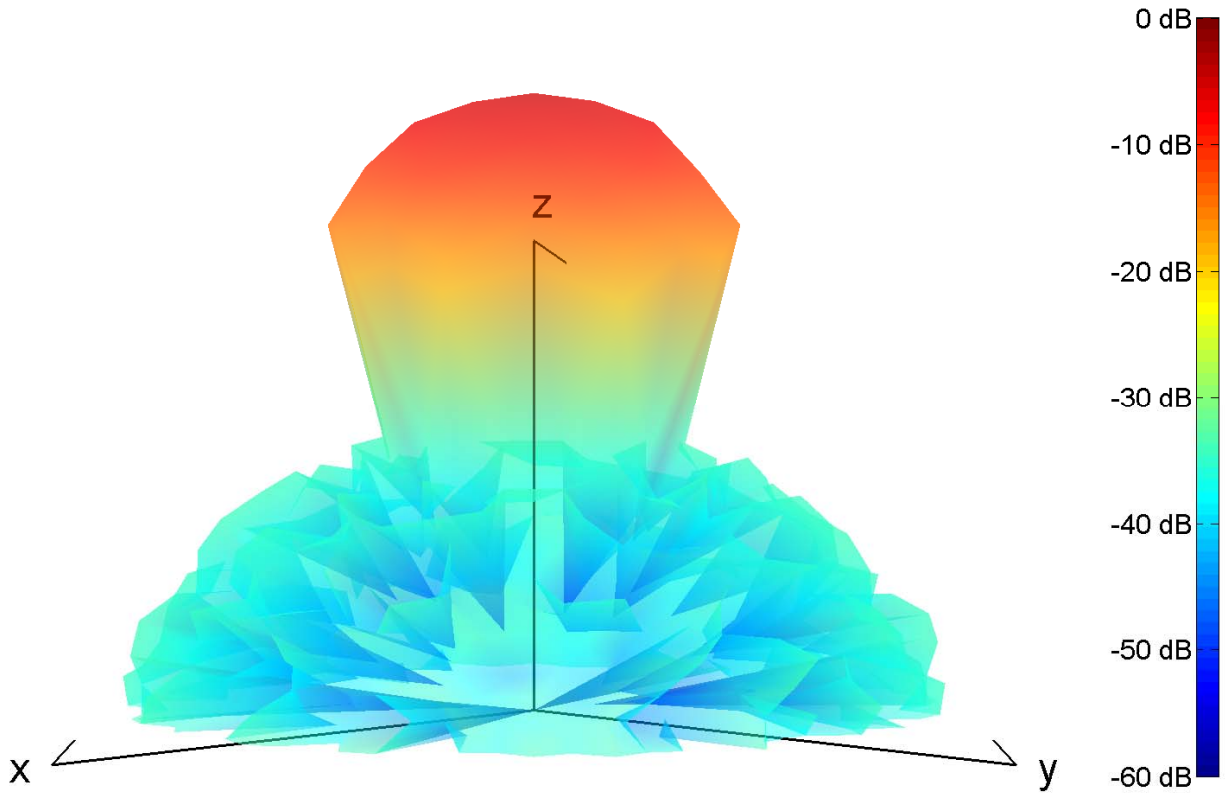

Figure 4.40: Achieved radiation pattern for the planar antenna array design problem.

CHAPTER 5

DESIGN OF LINEAR PHASE FIR FILTER

This chapter presents the application of the Bayesian inference framework for design to solve several linear phase FIR filter design examples. A linear phase FIR filter design problem generally has three main aspects: the desired frequency magnitude response, the type of linear phase FIR filter used and the practical design requirements that are required to be incorporated. All the design examples presented in this chapter use a linear phase FIR filter that has symmetric impulse response and odd filter length to realize various desired frequency magnitude response while satisfying certain prescribed practical design requirements. As illustrated in Figure 2.4, the shape of a desired frequency magnitude response is governed by the passband and stopband edge frequencies, the maximum passband ripple and the minimum stopband attenuation. The specified values for these four filter characteristics are different for the various design examples presented in this chapter. In practice, the filter coefficients of a linear phase FIR filter are limited in dynamic range and accuracy. This practical design requirement is incorporated into two design examples which are presented in Section 5.2.2.

The process of designing a linear phase FIR filter is similar to the design process of an antenna array. The first step towards solving a linear phase FIR filter design problem is to specify the desired frequency magnitude response and the type of linear phase FIR filter to be used. The second step is to obtain the likelihood function via the assignment of either a Laplacian or Gaussian *pdf* to the error between the desired and achieved frequency magnitude response. The third step is to

assign a *pdf* to all design parameters which include the number of filter taps, filter length and filter coefficients. This is followed by the assignment of a value to all σ_m which denote the degree of compliance between the desired and achieved frequency magnitude response. With the likelihood function, $p(\mathbf{B}_U, \mathbf{B}_L|N, \mathbf{X}_N, \boldsymbol{\sigma})$, and the prior *pdf*, $p(N, \mathbf{X}_N)$, in Eq. (2.34) determined, the next step is to obtain a Monte Carlo approximation of the posterior, *pdf*, $p(N, \mathbf{X}_N|\mathbf{B}_U, \mathbf{B}_L, \boldsymbol{\sigma})$, by drawing a reasonable number of samples from it. The design process concludes with the selection of a design candidate from all the drawn posterior samples as the final design.

5.1 Assignments for the Design Parameters and σ_m

The basis for assigning a value to σ_m for the design of antenna array is presented in Section 4.2. For the design of linear phase FIR filter, the same basis applies. For instance, the values assigned to the σ_m in the passband region are smaller than in the stopband region. This is because the passband region is narrower than the stopband region. A systematic procedure for determining the appropriate values for all σ_m has yet to be discovered. In all the design examples presented in this chapter, the assignment of a value to all σ_m is based upon experience, intuition and, in some cases, trial and error.

For a linear phase FIR filter that has continuous filter coefficients, the design parameters N, T_n and c_n, are all assigned a uniform distribution when only the range of a design parameter is known. The filter coefficients, c_n, are all assigned a continuous uniform distribution, $U[c_n^{min}, c_n^{max}]$, where c_n^{min} and c_n^{max} denote the minimum and maximum values of c_n respectively. Since a continuous filter coefficient is generally in the range of $-1.00 \leq c_n \leq 1.00$, the assignments of $c_n^{min} = -1.00$ and $c_n^{max} = 1.00$ are made. The design parameters, N and T_n, are respectively assigned a discrete uniform distribution, $U[N^{min}, N^{max}]$ and $U[T_n^{min}, T_n^{max}]$. The quantities, N^{min} and N^{max} as well as T_n^{min} and T_n^{max}, denote the minimum and maximum values of N and T_n respectively. The positive integers N^{min} and T_n^{min} indicate respectively the minimum number of filter taps and the shortest filter length that are required in a linear phase FIR filter to realize the desired frequency

magnitude response. The positive integers N^{max} and T_n^{max} denote respectively the maximum number of filter taps and the longest filter length that are allowed in a design problem. Both N^{max} and T_n^{max} can be assigned any positive value; however, in practice, their values are generally dictated by the computation and production costs. The computation cost of a digital filter is higher when more multipliers are required due to the increase in the number of filter taps used. The production cost of a digital filter increases as the filter length becomes longer since more filter taps are required to be produced. Therefore, a designer needs to take into consideration the computation and production costs when specifying a value for both N^{max} and T_n^{max}.

For a linear phase FIR filter that has filter coefficients expressed as a sum of signed power-of-two (SPoT) terms, the design parameters, N and T_n, are respectively assigned a discrete uniform distribution, $U[N^{min}, N^{max}]$ and $U[T_n^{min}, T_n^{max}]$. As in the previous case, T_n^{min} and T_n^{max} indicate respectively the minimum and maximum filter lengths that are acceptable in a design problem. The quantity N^{min} denotes the minimum number of SPoT terms that are required in a linear phase FIR filter to realize the desired frequency magnitude response while the quantity N^{max} denotes the maximum number of SPoT terms that are allowed in a design problem. The number of adders and shifters that are required increases with the number of SPoT terms used. Therefore, the computation and production costs have to be taken into account when specifying a value for N^{max}. The samples of the SPoT terms, SPoT$_n$, are generated in a two-step process. The first step is to draw a sample from the continuous distribution, $U[-1, 1]$. This initial step is followed by rounding the sample value to the nearest value of a SPoT term. This sampling method, which renders SPoT terms that have more decimal points less probable, is employed because the practical implementation of a SPoT term that has lower precision requires fewer number of bits. The maximum number of bits that is allowed in a design problem determines the value that is assigned to the maximum integer power, P.

5.2 Design Problems

This section presents the results for several linear phase FIR filter design problems. For the design of a linear phase FIR filter that has continuous filter coefficients, the parametric model in Eq. (2.12) and the Laplacian likelihood in Eq. (2.27) are used. As for the design of a linear phase FIR filter that has filter coefficients expressed as a sum of SPoT terms, the parametric model in Eq. (2.17) and the Gaussian likelihood in Eq. (2.29) are used. In all the following design problems, the desired frequency magnitude response is specified in dB. The number of equally spaced frequency points used is 101 while the number of samples drawn from the posterior distribution is $W = 3000$. Each of the 3000 samples represents a design candidate. For all the design examples presented in this chapter, the final design is selected using a multistep process. The selection process begins by first selecting the design candidates that have zero or minimum error. The next step is to narrow down the selected design candidates to those designs that use the fewest number of filter taps or SPoT terms. Of all the remaining design candidates, the design candidate that has the shortest filter length is chosen as the final design.

5.2.1 Low Pass Filter with Continuous Coefficients

The first linear phase FIR filter design problem to be presented is a low pass filter design problem selected from [42]. This design problem has the following design specifications:

$$\theta_p = 0.4\pi, \quad \theta_s = 0.5\pi, \quad \delta = 0.02, \quad \text{and} \quad \beta = -30dB.$$

For this design problem, the following assignments are made:

$$p(N) = U[1, 30],$$
$$p(c_n) = U[-1.0, 1.0],$$
$$p(T_n) = U[0, 30],$$

Table 5.1: Estimated posterior probability for N for the low pass filter design problem with minimum stopband attenuation of -30 dB.

N	$p(N\|\mathbf{B}_U, \mathbf{B}_L, \boldsymbol{\sigma})$
14	0.155667
15	0.439000
16	0.275667
17	0.099000
18	0.023333
19	0.006000
20	0.001333

Table 5.2: Parameter values for the final design of the low pass filter with minimum stopband attenuation of -30 dB. For values of k not found in the table, $b_k = 0$.

k	b_k
0	-0.453584
1	-0.630978
2	-0.090758
3	0.186878
4	0.082369
5	-0.090434
6	-0.073324
7	0.036079
8	0.058962
9	-0.007865
10	-0.046694
12	0.032349
14	-0.019077
15	-0.014571
16	0.019535

and

$$\sigma_m = \begin{cases} 1/50 \text{ dB} & \text{for } \ 0 \leq \theta_m < 0.5\pi \\ 1/10 \text{ dB} & \text{for } \ 0.5\pi \leq \theta_m \leq \pi \end{cases} .$$

The obtained results are summarized in Table 5.1, Table 5.2 and Figure 5.1. Table 5.2 lists the parameter values of the final design. These values are used to plot the log magnitude response at the 101 predefined frequency points in Figure 5.1. The achieved frequency magnitude response

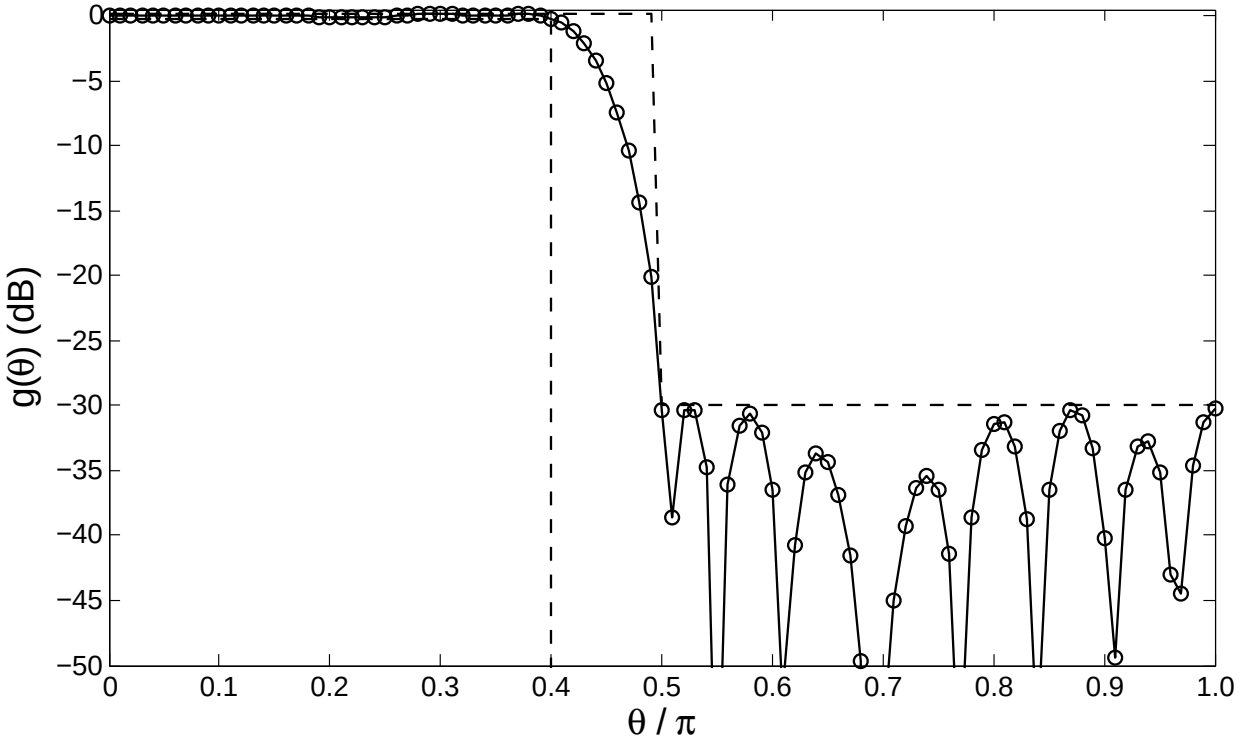

Figure 5.1: Achieved log magnitude response versus frequency for the low pass filter with minimum stopband attenuation of -30 dB.

completely satisfies the design specifications. As indicated in Table 5.2, the filter length and number of filter taps used in the final design are $L = 33$ and $J = 29$ respectively. The filter design produced by the genetic algorithm approach in [42] has filter length $L = 41$ and uses all taps. The results comparison shows that the filter design produced by the Bayesian inference framework has much lower design complexity.

The second design problem involves the design of a low pass filter that has a minimum stopband attenuation of -60 dB. This design problem, which is taken from [77, Ch. 14], consists of the following design specifications:

$$\theta_p = 0.43\pi, \quad \theta_s = 0.63\pi, \quad \delta = 0.025, \quad \text{and} \quad \beta = -60dB.$$

Table 5.3: Estimated posterior probability for N for the low pass filter design problem with minimum stopband attenuation of -60 dB.

N	$p(N\|\mathbf{B}_U, \mathbf{B}_L, \boldsymbol{\sigma})$
9	0.084333
10	0.660000
11	0.210667
12	0.025000
13	0.009333
14	0.010333
15	0.000333

Table 5.4: Parameter values for the final design of the low pass filter with minimum stopband attenuation of -60 dB. For values of k not found in the table, $b_k = 0$.

k	b_k
0	0.499955
1	0.631722
3	-0.197255
5	0.103998
7	-0.061237
9	0.036976
11	-0.026932
12	-0.011939
13	0.002574
15	-0.002248

For this problem, the following assignments are made:

$$p(N) = U[1, 30],$$

$$p(c_n) = U[-1.0, 1.0],$$

$$p(T_n) = U[0, 15],$$

and

$$\sigma_m = \begin{cases} 1/250 \text{ dB} & \text{for } \ 0 \leq \theta_m \leq 0.43\pi \\ 1/12.5 \text{ dB} & \text{for } \ 0.43\pi < \theta_m \leq \pi \end{cases}.$$

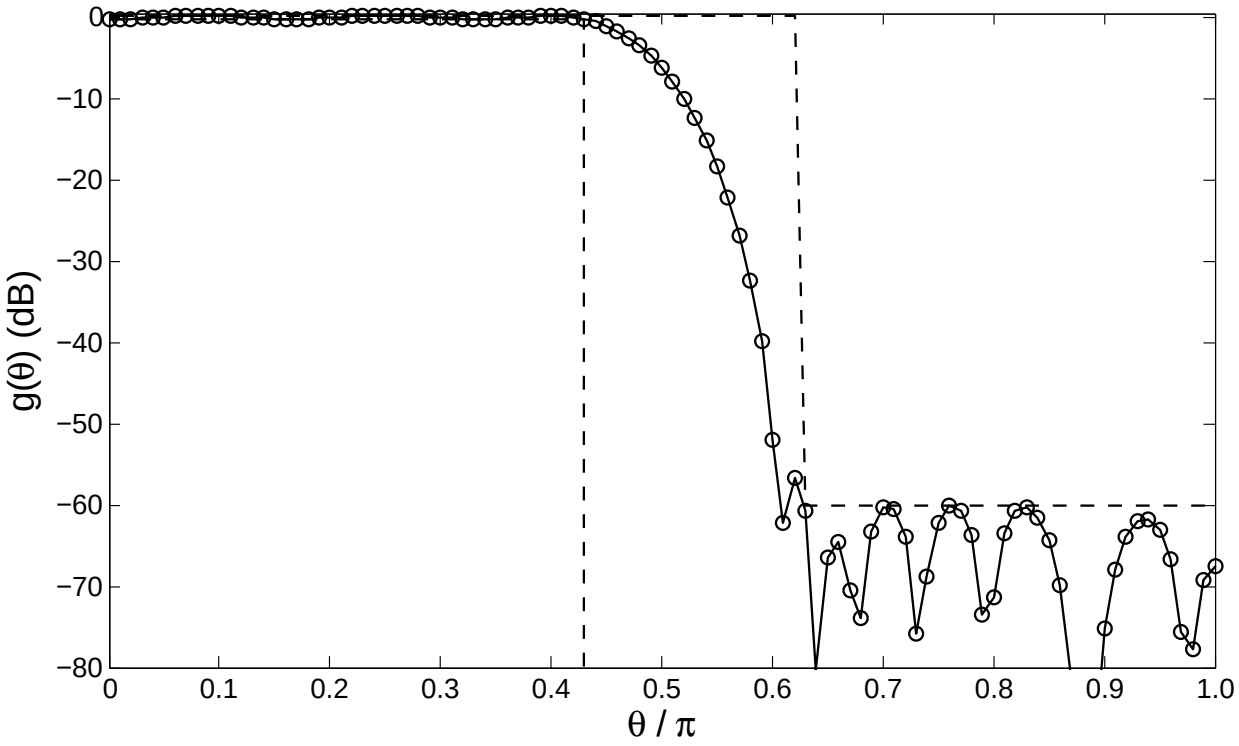

Figure 5.2: Achieved log magnitude response versus frequency for the low pass filter with minimum stopband attenuation of -60 dB.

Table 5.3, Table 5.4 and Figure 5.2 summarize the achieved results. Figure 5.2 illustrates the frequency magnitude response produced by the final design, the parameter values of which are listed in Table 5.4. This plot shows that the realized frequency magnitude response fully satisfies the design specifications. Table 5.4 indicates that the designed filter has a length of $L = 31$ taps, of which 19 taps are used. The filter design presented in [77] has a filter length of $L = 25$ and uses all taps. Although the linear phase FIR filter designed by the inference framework is longer, it uses fewer taps and thus, has lower design complexity. If filters with shorter length are preferred, then $p(T_n)$ should be assigned a shaped probability distribution rather than the uniform distribution used here.

5.2.2 Low Pass Filter using SPoT Terms

This section presents two problems of designing a linear phase FIR filter that has filter coefficients expressed as a sum of SPoT terms. Because of the discrete nature of the filter coefficients, the parametric model in Eq. (2.20) is modified to

$$g(\theta) = 10\log_{10}\left[\frac{|A(\theta)|}{\Omega}\right]^2 \quad \text{for} \quad 0 \leq \theta \leq \pi,$$

where Ω is the average of the maximum and minimum passband values of $A(\theta)$.

The maximum number of SPoT terms that is allowed to represent a filter coefficient is not fixed. Consequently, for the SPoT samples that are drawn to represent a particular filter coefficient, the following situations could arise:

1. Two SPoT terms, 2^{-p_1} and -2^{-p_2}, have the opposite sign and identical power, $p_1 = p_2$, yielding an aggregate value of $2^{-p_1} - 2^{-p_2} = 0$;

2. Two SPoT terms, 2^{-p_1} and 2^{-p_2}, have the same sign and power, $p_1 = p_2$, yielding an aggregate value that can be expressed by one SPoT term, $2^{-p_1} + 2^{-p_2} = 2^{-p_1+1}$;

3. Two SPoT terms, 2^{-p_1} and -2^{-p_2}, have the opposite sign and sequential powers, $p_1 - p_2 = 1$, yielding an aggregate value that can be expressed by one SPoT term, $2^{-p_1} + 2^{-p_2} = 2^{-p_2}$;

4. Two SPoT terms, 2^{-p_1} and -2^{-p_2}, have the same sign and sequential powers, $p_1 - p_2 = 1$, yielding an aggregate value that can be expressed by another combination of two SPoT terms, $2^{-p_1} + 2^{-p_2} = 2^{-p_1+1} - 2^{-p_2}$.

The first three situations must be avoided so that trivial solutions are not produced. The fourth situation, which is detailed in [56], should be prevented to avoid having a combination of three or more SPoT terms that have the same sign and sequential powers. The reason is that this combination can be replaced by another combination that has fewer SPoT terms. As explained in [56], a combination of two SPoT terms that have the same sign and sequential powers can always be

replaced by another combination of two SPoT terms that do not have sequential powers. This notion is always true except when the value of a filter coefficient, b_k, is equal to

$$b_k = \sum_{p_n=0}^{P} 2^{-p_n} \quad \text{or} \quad \sum_{p_n=0}^{P} -2^{-p_n} \quad \text{for} \;\; 0 \leq P \leq \text{Number of Bits}.$$

To take into consideration the above four situations, the likelihood in Eq. (2.29) is required to be modified to

$$p(\mathbf{B}_U, \mathbf{B}_L | N, \mathbf{X}_N, \boldsymbol{\sigma}) \propto \exp\left[-\mathcal{R}^2/2\sigma_{\mathcal{R}}^2 - \sum_{m=1}^{M} Q_m^2/2\sigma_m^2\right], \tag{5.1}$$

where $\mathcal{R}$ denotes the number of times that one of the four situations is encountered, and similar to σ_m, $\sigma_{\mathcal{R}}$ is a quantity that has to be assigned a value.

For demonstration and comparison purposes, two design examples that are picked from [52] are presented here. The first design problem has the following design specifications:

$$\theta_p = 0.3\pi, \quad \theta_s = 0.5\pi, \quad \delta = 0.01, \quad \text{and} \quad \beta = -40dB.$$

For this design problem, the maximum number of bits allowed is specified to be 10, and the following assignments are made:

$$p(N) = U[1, 50],$$
$$p(T_n) = U[0, 20],$$
$$\sigma_{\mathcal{R}} = 1/10,$$

and

$$\sigma_m = \begin{cases} 1/50 \text{ dB} & \text{for} \;\; 0 \leq \theta_m < 0.5\pi \\ 1/2.5 \text{ dB} & \text{for} \;\; 0.5\pi \leq \theta_m \leq \pi \end{cases}.$$

The obtained results are summarized in Table 5.5, Table 5.6 and Figure 5.3. Table 5.6 lists the parameter values of the final design. Using these parameter values, the frequency magnitude response at the 101 predefined frequency points is plotted in Figure 5.3. This plot shows that the

Table 5.5: Estimated posterior probability for the number of SPoT terms for the low pass filter design problem with minimum stopband attenuation of -40 dB. In this case, $\langle N \rangle = 16.39$.

N	$p(N\|\mathbf{B}_U, \mathbf{B}_L, \boldsymbol{\sigma})$
16	0.672000
17	0.268667
18	0.056333
19	0.002333
20	0.000667

Table 5.6: Parameter values for the final design of the low pass filter with minimum stopband attenuation of -40 dB. For this design, $1/\Omega = 0.4010810617953997$.

k	SPoT Terms
0	-2^0
1	$-2^0 - 2^{-1}$
2	$-2^{-1} + 2^{-4}$
3	$2^{-2} + 2^{-5} + 2^{-7}$
4	$2^{-2} + 2^{-4}$
6	$-2^{-3} - 2^{-5} - 2^{-7}$
7	$-2^{-4} - 2^{-7}$
8	2^{-4}
9	2^{-4}
11	-2^{-5}

Table 5.7: Comparison of normalized peak ripples and filter design complexities among different methods for the first design example.

Method	NPR (dB)	L	J
Simulated Annealing [55]	-41.30	27	54
Polynomial-Time Algorithm [54]	-41.35	23	46
Hybrid Genetic Algorithm [52]	-40.19	23	46
Bayesian Inference Framework	-40.15	23	35

achieved frequency magnitude response fully complies with the design specifications. To evaluate the performance of the final design, the normalized peak ripple (NPR), which is defined as the ratio of the peak ripple to the mean value of the passband gain, is computed. The final design produced by the Bayesian inference framework achieves a normalized peak ripple of 40.15 dB which is comparable to the values obtained in [52, 54, 55]. More significantly, the final design has

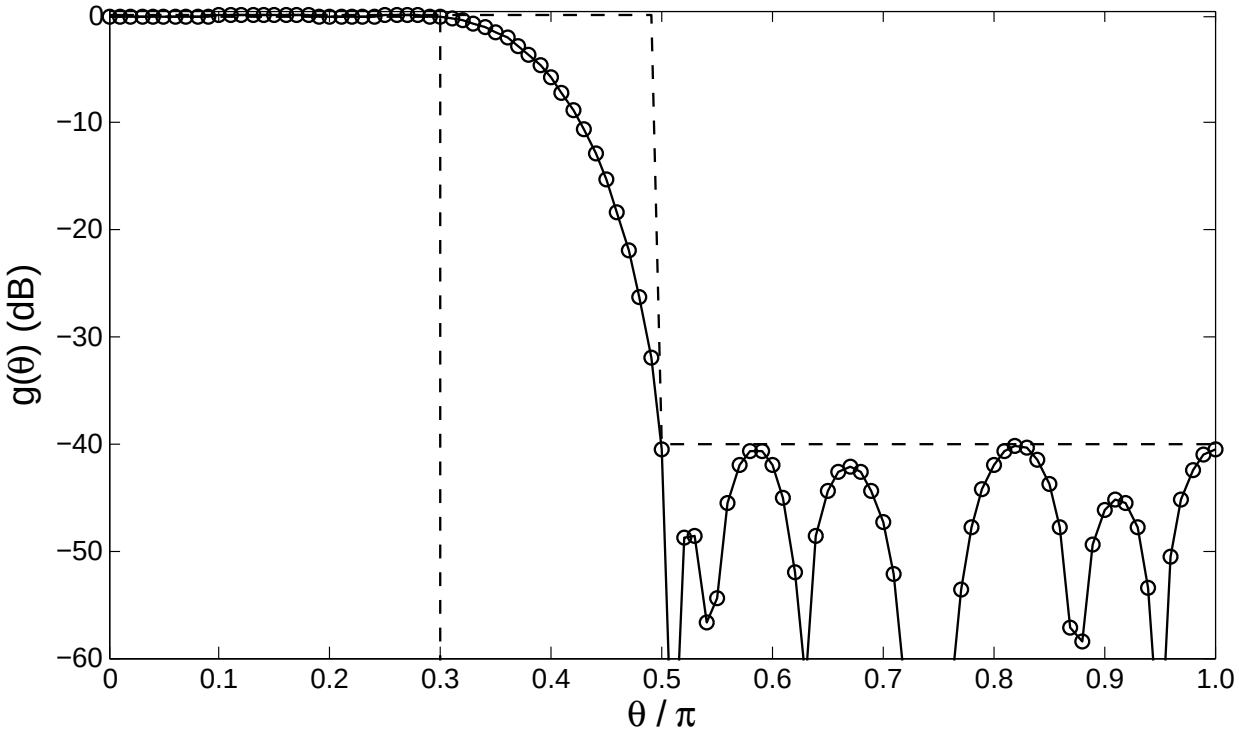

Figure 5.3: Achieved log magnitude response versus frequency for the low pass filter with minimum stopband attenuation of -40 dB.

managed to produce a comparable performance using only a total of $J = 35$ SPoT terms, which corresponds to a 23.9% savings in SPoT terms used.

The second design problem has a desired frequency response that has a narrower transition band and smaller ripple. The design specifications for this problem are as follows:

$$\theta_p = 0.3\pi, \quad \theta_s = 0.44\pi, \quad \beta = -42dB, \quad \text{and} \quad \delta = 10^{\beta/20}.$$

For this design problem, the maximum number of bits that is allowed remains at 10, and the following assignments are made:

$$p(N) = U[1, 50],$$

$$p(T_n) = U[0, 20],$$

$$\sigma_{\mathcal{R}} = 1/10,$$

Table 5.8: Estimated posterior probability for the number of SPoT terms for the low pass filter design problem with minimum stopband attenuation of -42 dB. In this case, $\langle N \rangle = 28.86$.

N	$p(N\|\mathbf{B}_U, \mathbf{B}_L, \boldsymbol{\sigma})$
28	0.195000
29	0.750667
30	0.052333
31	0.001667
32	0.000333

Table 5.9: Parameter values for the final design of the low pass filter with minimum stopband attenuation of -42 dB. For this design, $1/\Omega = 0.3903892405965878$.

k	SPoT Terms
0	$2^0 - 2^{-5} - 2^{-7}$
1	$2^0 + 2^{-1}$
2	$2^{-1} + 2^{-4} + 2^{-8}$
3	$-2^{-2} + 2^{-4} - 2^{-7}$
4	$-2^{-1} + 2^{-3}$
5	$-2^{-3} + 2^{-6}$
6	$2^{-3} + 2^{-5}$
7	$2^{-3} + 2^{-5} + 2^{-7}$
9	$-2^{-3} + 2^{-7}$
10	-2^{-4}
11	2^{-5}
12	2^{-4}
13	2^{-6}
14	-2^{-5}
15	-2^{-5}
17	2^{-6}
19	-2^{-7}

and

$$\sigma_m = \begin{cases} 1/50 \text{ dB} & \text{for } \ 0 \leq \theta_m < 0.44\pi \\ 1/2.5 \text{ dB} & \text{for } \ 0.44\pi \leq \theta_m \leq \pi \end{cases} .$$

For the second design example, the obtained results are summarized in Table 5.8, Table 5.9 and Figure 5.4. Figure 5.4 illustrates the frequency magnitude response produced by the final design, the parameter values of which are listed in Table 5.9. The plot in Figure 5.4 shows that the realized frequency magnitude response fully satisfies the design specifications. The final design here

Table 5.10: Comparison of normalized peak ripples and filter design complexities among different methods for the second design example.

Method	NPR (dB)	L	J
Simulated Annealing [55]	-41.60	39	78
Polynomial-Time Algorithm [54]	-42.31	35	70
Hybrid Genetic Algorithm [52]	-41.67	33	69
Bayesian Inference Framework	-42.00	39	57

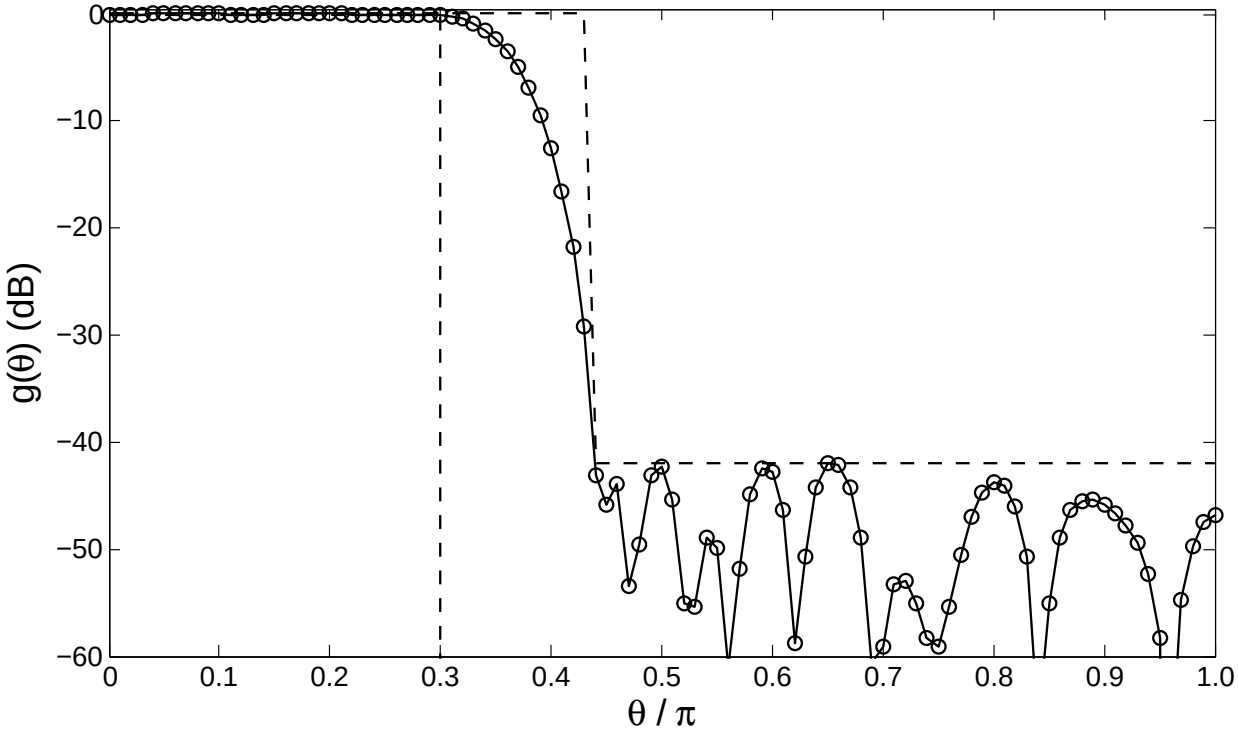

Figure 5.4: Achieved log magnitude response versus frequency for the low pass filter with minimum stopband attenuation of -42 dB.

achieves a normalized peak ripple of -42 dB using a total of $J = 57$ SPoT terms and a filter length of $L = 39$ taps. Although the linear phase FIR filter designed by the Bayesian inference framework has longer filter length, it uses 17.4% fewer SPoT terms as illustrated in Table 5.10. In addition to producing linear phase FIR filters that have lower design complexity, it is also noteworthy to point out that, unlike the methods in [52, 54, 55], linear phase FIR filters that have filter coefficients represented by SPoT terms can be designed by the Bayesian inference framework without having to design a linear phase FIR filter that has continuous filter coefficients in advance.

CHAPTER 6

SUMMARY, CONCLUSION AND SUGGESTION

6.1 Summary

A new approach to solving engineering design problems has been presented in this dissertation. This approach makes use of the observation that an engineering design problem, like an inference problem, is a generalized inverse problem that can be solved using Bayesian inference. In the Bayesian inference framework for design, Bayesian inference tools such as parameter estimation and model selection are adapted and utilized to solve a design problem. The developed Bayesian inference framework has been applied to two design applications, namely antenna arrays and linear phase FIR filters.

Chapter 2 provides an in-depth explanation on the underlying theory of the Bayesian inference framework for design. The explanation began with the discussions on the parametric models, design parameters, requirements and objectives of both design applications. These topics are followed by the description on the Bayesian inference portion of the design process. The solution to a design problem obtained by the Bayesian inference framework is the posterior distribution which is a function of the design parameters. Since the posterior cannot be determined in a closed form, a Monte Carlo method is employed to approximate the posterior by drawing a reasonable number of samples from it. The Bayesian inference portion of the design process concludes with the sampling of the posterior, which produces a number of potential design solutions rather than a single final

design as each posterior sample represents a design candidate. To obtain a final design, a designer has to choose a design candidate from all potential design solutions as the final design based on additional design criteria.

The work presented in this dissertation employs BayeSys to sample the posterior. BayeSys is a Markov chain Monte Carlo algorithm and has a number of important features. These features include the mapping of a multidimensional parameter space into one dimension using a Hilbert space-filling curve, exploration along a Hilbert curve using binary slice sampling, progressive convergence of a sampling process from the prior to the posterior using selective annealing, communication among multiple objects to catalyze each other's sampling progress, and multiple exploration engines that can compensate for each other when one or more engines are thwarted in their sampling progress.

Several design examples in both antenna array and linear phase FIR filter design have been presented in Chapters 4 and 5 respectively. All the presented results verify that the Bayesian inference framework for design, along with BayeSys, has the ability to produce physical systems that have design complexity appropriate to the design specifications and requirements. In antenna array design, several design problems that use different types of antenna arrays such as symmetric linear array with real-valued currents, asymmetric linear array with complex currents, reconfigurable linear array and planar array to realize various desired radiation patterns that include broadside, end-fire, shaped beam, and three-dimensional patterns, have been solved. In addition, various practical design requirements such as a minimum spacing between two adjacent array elements, limitations in the dynamic range and accuracy of the current amplitudes, the ability to generate multiple desired radiation patterns, the ability to maintain a desired radiation pattern over a frequency band, and the ability to maintain a desired radiation pattern when one arbitrary element is inoperable, have all been successfully incorporated into a design problem. In linear phase FIR filter design, several design problems that have different desired frequency responses have been solved. In addition, the practical design requirement of having a filter coefficient expressed as a sum of signed power-of-two (SPoT) terms has also been successfully implemented.

6.2 Conclusion and Suggestion

One of the important steps in using the Bayesian inference framework to solve a design problem is the assignment of an appropriate value to the required degree of compliance between the desired and achieved radiation pattern or frequency response at a designated angle or frequency point. Even though this dissertation has provided some useful guidelines, a systematic procedure for determining the proper values for all σ_m has yet to be discovered. The appropriate assignment for all σ_m depend on the design pattern specifications and practical design requirements of a design problem. A different design problem generally requires different value assignment for all σ_m and thus, it is desirable to have the appropriate σ_m values determined systematically. For this reason, exhaustive investigations on the assignment of a proper value to σ_m are highly recommended for future work.

There are many antenna array and linear phase FIR filter design problems that are interesting to study in the future. In antenna array design, many more radiation patterns in particular power patterns that have multiple main beams at different angles can be studied. Section 4.3.8 presents the design of a narrowband antenna array, and this work can be extended to design wideband antenna arrays which may require more amplitudes and time delays. The work on the design of a linear antenna array that can compensate for the loss of an arbitrary array element can also be extended to solve other similar problems, which include design problems that require compensation for the loss of more than one arbitrary antenna element and allow the use of recovery measures to maintain antenna performance. As for linear phase FIR filter design, the work presented here can be extended to design other types of digital filters such as bandpass or notch filters and infinite impulse response (IIR) filters.

The results presented in this dissertation showcase the abilities, advantages and robustness of the Bayesian inference framework in designing antenna arrays and linear phase FIR filters. With the knowledge that a design problem is an inverse problem, the Bayesian inference framework for

design can be extended to solve design problems in other applications. It would be interesting to study and grasp the application of the Bayesian inference framework for design in other design applications in the future.

BIBLIOGRAPHY

[1] O. M. Alifanov, *Inverse Heat Transfer Problems*, ser. International Series in Heat and Mass Transfer. Springer-Verlag, 1994.

[2] A. Tarantola, *Inverse Problem Theory and Model Parameter Estimation*. Society for Industrial and Applied Mathematics, 2005.

[3] A. Tarantola, "Popper, Bayes and the inverse problem," *Nature Physics*, vol. 2, pp. 492 – 494, August 2006.

[4] Y. Chi, "Calculating posterior probabilities for EM induction landmine detection using MCMC with thermodynamic integration," Ph.D. Dissertation, The University of Mississippi, University, MS, 2005.

[5] P. M. Goggans, C. R. Smith, and C. Y. Chan, "Landmine detection using model selection," in *Detection and Remediation Technologies for Mines and Minelike Targets VI*, A. C. Dubey, J. F. Harvey, J. T. Broach, and V. George, Eds., vol. 4394. SPIE Proceedings, October 2001, pp. 634 – 640.

[6] N. Xiang and P. M. Goggans, "Evaluation of decay times in coupled spaces: Bayesian parameter estimation," *Journal of the Acoustical Society of America*, vol. 110, pp. 1415 – 1424, September 2001.

[7] N. Xiang, P. M. Goggans, T. Jasa, and M. Kleiner, "Evaluation of decay times in coupled spaces: Reliability analysis of Bayeisan decay time estimation," *Journal of the Acoustical Society of America*, vol. 117, no. 6, pp. 3707 – 3715, June 2005.

[8] A. G. Green and D. J. C. MacKay, "Bayesian analysis of linear phased-array radar," in *Maximum Entropy and Bayesian Methods*, G. R. Heidbreder, Ed. Santa Barbara, California: Kluwer Academic Publishers, 1993, pp. 309 – 318.

[9] K. Mosegaard and A. Tarantola, "Monte Carlo sampling of solutions to inverse problems," *Journal of Geophysical Research*, vol. 10, no. B7, pp. 12,431 – 12,447, 1995.

[10] K. Mosegaard and A. Tarantola, "Probabilistic approach to inverse problems," in *International Handbook of Earthquake and Engineering Seismology, Part A*, W. H. Lee, P. Jennings, H. Kanamori, and C. Kisslinger, Eds. Academic Press, 2002, pp. 237 – 265.

[11] P. C. Gregory and T. J. Loredo, "A new method for the detection of a periodic signal of unknown shape and period," *The Astrophysical Journal*, vol. 398, pp. 146 – 168, 1992.

[12] T. J. Loredo and D. F. Chernoff, "Bayesian adaptive exploration," in *Statistical Challenges in Modern Astronomy*, E. D. Feigelson and G. J. Babu, Eds. University Park, Pennsylvania: Springer, 2003, pp. 57 – 70.

[13] J. Kershaw, B. A. Ardekani, and I. Kanno, "Application of Bayesian inference to fMRI data analysis," *IEEE Transactions on Medical Imaging*, vol. 18, no. 12, pp. 1138 – 1153, December 1999.

[14] M. Lee, "Bayesian reconstruction in emission tomography using Gibbs priors," Ph.D. Dissertation, Yale University, 1994.

[15] W.-C. Weng, F. Yang, and A. Z. Elsherbeni, "Linear antenna array synthesis using Taguchi's method: A novel optimization technique in electromagnetics," *IEEE Transactions on Antennas and Propagation*, vol. 55, no. 3, pp. 723 – 730, March 2007.

[16] M. M. Khodier and C. G. Christodoulou, "Linear array geometry synthesis with minimum sidelobe level and null control using particle swarm optimization," *IEEE Transactions on Antennas and Propagation*, vol. 53, pp. 2674 – 2679, August 2005.

[17] N. Jin and Y. Rahmat-Samii, "A novel design methodology for aperiodic arrays using particle swarm optimization," in *2006 National Radio Science Meeting Dig.*, Boulder, CO, Jan 2006, p. 69.

[18] D. Gies and Y. Rahmat-Samii, "Particle swarm optimization for reconfigurable phased-differential array design," *IEEE Transactions on Antennas and Propagation*, vol. 38, no. 3, pp. 168 – 175, August 2003.

[19] N. Jin and Y. Rahmat-Samii, "Advances in particle swarm optimization for antenna designs: Real-number, binary, single-objective and multiobjective implementations," *IEEE Transactions on Antennas and Propagation*, vol. 55, no. 3, pp. 556 – 567, March 2007.

[20] P. J. Bevelacqua and C. A. Balanis, "Minimum sidelobe levels for linear arrays," *IEEE Transactions on Antennas and Propagation*, vol. 55, no. 12, pp. 3442 – 3449, December 2007.

[21] S. M. Mikki and A. A. Kishk, "Quantum particle swarm optimization for electromagnetics," *IEEE Transactions on Antennas and Propagation*, vol. 54, no. 10, pp. 2764 – 2775, October 2006.

[22] S. M. Mikki and A. A. Kishk, *Particle Swarm Optimization: a Physics-based Approach*. Morgan and Claypool, 2008.

[23] D. W. Boeringer, D. H. Werner, and D. W. Machuga, "A simultaneous parameter adaptation scheme for genetic algorithms with application to phased array synthesis," *IEEE Transactions on Antennas and Propagation*, vol. 53, pp. 356 – 371, January 2005.

[24] F. J. Ares-Pena, A. Rodriguez-Gonzalez, E. Villanueva-Lopez, and S. R. Rengarajan, "Genetic algorithms in the design and optimization of antenna array patterns," *IEEE Transactions on Antennas and Propagation*, vol. 47, pp. 506 – 510, March 1999.

[25] D. W. Boeringer and D. H. Werner, "Particle swarm optimization versus genetic algorithm for phased array synthesis," *IEEE Transactions on Antennas and Propagation*, vol. 52, pp. 771 – 779, March 2004.

[26] V. Murino, A. Trucco, and C. S. Regazzoni, "Synthesis of unequally spaced arrays by simulated annealing," *IEEE Transactions on Signal Processing*, vol. 44, no. 1, pp. 119 – 123, January 1996.

[27] D. G. Kurup, M. Himdi, and A. Rydberg, "Synthesis of uniform amplitude unequally spaced antenna arrays using the differential evolution algorithm," *IEEE Transactions on Antennas and Propagation*, vol. 51, no. 9, pp. 2210 – 2217, September 2003.

[28] A. Monorchio, S. Genovesi, S. Bertini, and A. Brizzi, "An efficient interpolation scheme for the synthesis of linear arrays based on Schelkunoff polynomial method," *IEEE Antennas and Wireless Propagation Letters*, vol. 6, pp. 484 – 487, 2007.

[29] Y. Liu, Z. Nie, and Q. H. Liu, "Reducing the number of elements in a linear antenna array by the matrix pencil method," *IEEE Transactions on Antennas and Propagation*, vol. 56, no. 9, pp. 2955 – 2962, September 2008.

[30] B. P. Kumar and G. R. Branner, "Design of unequally spaced arrays for performance improvement," *IEEE Transactions on Antennas and Propagation*, vol. 47, no. 3, pp. 511 – 523, March 1999.

[31] B. P. Kumar and G. R. Branner, "Generalized analytical technique for the synthesis of unequally spaced arrays with linear, planar, cylindrical or spherical geometry," *IEEE Transactions on Antennas and Propagation*, vol. 53, no. 2, pp. 621 – 634, February 2005.

[32] G. K. Mahanti, S. Das, and A. Chakraborty, "Design of phase-differentiated reconfigurable array antennas with minimum dynamic range ratio," *IEEE Antennas and Wireless Propagation Letters*, vol. 5, no. 1, pp. 262 – 264, December 2006.

[33] G. K. Mahanti, A. Chakraborty, and S. Das, "Design of fully digital controlled reconfigurable array antennas with fixed dynamic range ratio," *Journal of Electromagnetic Waves and Applications*, vol. 21, no. 1, pp. 97 – 106, 2007.

[34] G. K. Mahanti, A. Chakraborty, and S. Das, "Phase-only and amplitude-phase synthesis of dual-pattern linear antenna arrays using floating-point genetic algorithms," *Progress In Electromagnetics Research*, vol. 68, pp. 247 – 259, 2007.

[35] K. Guney and M. Onay, "Bees algorithm for design of dual-beam linear antenna arrays with digital attenuators and digital phase shifters," *International Journal of RF and Microwave Computer-Aided Engineering*, vol. 18, no. 4, pp. 337 – 347, July 2008.

[36] B. H. Wang, H. T. Hui, and M. S. Leong, "Optimal wideband beamforming for uniform linear arrays based on frequency domain MISO system identification," *IEEE Transactions on Antennas and Propagation*, vol. 58, no. 8, pp. 2580 – 2587, August 2010.

[37] D. R. Scholnik and J. O. Coleman, "Optimal design of wideband array patterns," in *IEEE International Radar Conference*, Alexandria, VA, May 2000, pp. 172 – 177.

[38] T. Sekiguchi and Y. Karasawa, "Wideband beamspace adaptive array utilizing FIR fan filters for multibeam forming," *IEEE Transactions on Signal Processing*, vol. 48, no. 1, pp. 277 – 284, January 2000.

[39] Y. Yang and H. Stark, "Design of self-healing arrays using vector-space projections," *IEEE Transactions on Antennas and Propagation*, vol. 49, no. 4, pp. 526 – 534, April 2001.

[40] A. V. Oppenheim, R. W. Schafer, and J. R. Buck, *Discrete-Time Signal Processing*, 2nd ed. McGraw-Hill, 1999.

[41] S.-C. Pei and C.-C. Tseng, "Design of equiripple log FIR and IIR filters using multiple exchange algorithm," *Signal Processing*, vol. 59, pp. 291 – 303, 1997.

[42] H.-C. Lu and S.-T. Tzeng, "Design of arbitrary FIR log filters by genetic algorithm approach," *Signal Processing*, vol. 80, pp. 497 – 505, 2000.

[43] J. I. Ababneh and M. H. Bataineh, "Linear phase FIR filter design using particle swarm optimization and genetic algorithms," *Digital Signal Processing*, vol. 18, pp. 657 – 668, July 2008.

[44] J. T. Kim, W. J. Oh, and Y. H. Lee, "Design of nonuniformly spaced linear-phase FIR filters using mixed integer linear programming," *IEEE Transactions on Signal Processing*, vol. 44, pp. 123 – 126, January 1996.

[45] J. Webb and D. M. Jr., "Chebyshev optimization of sparse FIR filters using linear programming with an application to beamforming," *IEEE Transactions on Signal Processing*, vol. 44, pp. 1912 – 1922, August 1996.

[46] D. Mattera, F. Palmieri, and S. Haykin, "Efficient sparse FIR filter design," in *IEEE International Conference on Acoustics, Speech, and Signal Processing*, vol. 2, 2002, pp. 1537 – 1540.

[47] G. Evangelista, "Design of optimum high order finite wordlength digital FIR filters with linear phase," *Signal Processing*, vol. 82, pp. 187 – 194, February 2002.

[48] T. Çiloğlu, "An efficient local search method guided by gradient information for discrete coefficient FIR filter design," *Signal Processing*, vol. 82, pp. 1337 – 1350, October 2002.

[49] W.-Y. Yan and K. L. Teo, "Optimal finite-precision approximation of FIR filters," *Signal Processing*, vol. 82, pp. 1695 – 1705, November 2002.

[50] P. Persson, S. Nordebo, and I. Claesson, "Design of discrete coefficient FIR filters by a fast entropy-directed deterministic annealing algorithm," *IEEE Transactions on Signal Processing*, vol. 53, pp. 1006 – 1014, March 2005.

[51] T. Çiloğlu, "New initialization methods for discrete coefficient FIR filter design with coefficient scaling and the use of scale factor in the design process," *IEEE Transactions on Signal Processing*, vol. 54, pp. 796 – 800, February 2006.

[52] L. Cen, "A hybrid genetic algorithm for the design of FIR filters with SPoT coefficients," *Signal Processing*, vol. 87, pp. 528 – 540, March 2007.

[53] G. J. Dolecek and S. K. MITRA, "Computationally efficient multiplier-free FIR filter design," *Computación y Sistemas*, vol. 10, no. 3, pp. 251 – 267, 2007.

[54] D. Li, Y. C. Lim, Y. Lian, and J. Song, "A polynomial-time algorithm for designing FIR filters with power-of-two coefficients," *IEEE Transactions on Signal Processing*, vol. 50, no. 8, pp. 1935 – 1941, August 2002.

[55] N. Benvenuto, M. Marchesi, and A. Uncini, "Applications of simulated annealing for the design of special digital filters," *IEEE Transactions on Signal Processing*, vol. 40, no. 2, pp. 323 – 332, February 1992.

[56] Y. C. Lim, R. Yang, D. Li, and J. Song, "Signed power-of-two term allocation scheme for the design of digital filters," *IEEE Transactions on Circuits and Systems II: Analog and Digital Signal Processing*, vol. 46, no. 5, pp. 577 – 584, May 1999.

[57] Z. G. Feng and K. L. Teo, "A discrete filled function method for the design of FIR filters with signed-powers-of-two coefficients," *IEEE Transactions on Signal Processing*, vol. 56, no. 1, pp. 134 – 139, January 2008.

[58] C. Y. Chan and P. M. Goggans, "Using Bayesian inference for linear phase log FIR filter design," in *Bayesian Inference and Maximum Entropy Methods in Science and Engineering*, P. M. Goggans and C. Y. Chan, Eds. Oxford, Mississippi: American Insitute of Physics, 2009, pp. 329 – 335.

[59] J. Skilling, *BayeSys and MassInf*, Maximum Entropy Data Consultants Ltd, February 2004, online manual at http://www.inference.phy.cam.ac.uk/bayesys/.

[60] P. Gregory, *Bayesian Logical Data Analysis for the Physical Sciences: A Comparative Approach with Mathematica® Support*. Cambridge University Press, 2005.

[61] D. S. Sivia and J. Skilling, *Data Analysis: A Bayesian Tutorial*, 2nd ed. Oxford University Press, 2006.

[62] D. J. C. MacKay, *Information Theory, Inference, and Learning Algorithms*. Cambridge University Press, 2003.

[63] E. T. Jaynes, *Probability Theory: The Logic of Science*. Cambridge University Press, 2003.

[64] C. P. Robert, *The Bayesian Choice: From Decision-Theoretic Foundations to Computational Implementation*, 2nd ed. New York: Springer-Verlag, 2003.

[65] P. M. Goggans and C. Y. Chan, "Antenna array design as inference," in *Bayesian Inference and Maximum Entropy Methods in Science and Engineering*, M. S. Lauretto, C. A. B. Pereira, and J. M. Stern, Eds. Sao Paulo, Brazil: American Insitute of Physics, 2008, pp. 294 – 300.

[66] D. Hilbert, "Über die stetige Abbildung einer Linie auf ein Flächenstück," *Mathematische Annalen*, vol. 38, pp. 459 – 460, 1891.

[67] P. J. Green, "Reversible jump Markov chain Monte Carlo computation and Bayesian model determination," *Biometrika*, vol. 82, no. 4, pp. 711 – 732, December 1995.

[68] N. Metropolis, A. W. Rosenbluth, M. N. Rosenbluth, A. H. Teller, and E. Teller, "Equations of state calculations by fast computing machine," *Journal of Chemical Physics*, vol. 21, pp. 1087 – 1091, 1953.

[69] W. K. Hastings, "Monte Carlo sampling methods using Markov chains and their applications," *Biometrika*, vol. 57, pp. 97 – 109, 1970.

[70] R. M. Neal, "Slice sampling," *The Annals of Statistics*, vol. 31, no. 3, pp. 705 – 767, 2003.

[71] S. Kirkpatrick, C. D. Gelatt, and M. P. Vecchi, "Optimization by simulated annealing," *Science, New Series*, vol. 220, no. 4598, pp. 671 – 680, May 1983.

[72] P. M. Goggans and Y. Chi, "Using thermodynamic integration to calculate the posterior probability in Bayesian model selection problems," in *Bayesian Inference and Maximum Entropy Methods in Science and Engineering*, G. J. Erickson, Ed. Jackson, Wyoming: American Insitute of Physics, 2004, pp. 59 – 66.

[73] C. A. Balanis, *Antenna Theory: Analysis and Design*, 3rd ed. Wiley Interscience, 2005.

[74] M. J. Wenninger, *Spherical Models*. Dover Publications, 1999.

[75] A. Rodriguez, D. B. Ehlenberger, P. R. Hof, and S. L. Wearne, "Rayburst sampling, an algorithm for automated three-dimensional shape analysis from laser scanning microscopy images," *Nature Protocols*, vol. 1, pp. 2152 – 2161, December 2006.

[76] J. H. Lauchner, R. B. Fuller, J. D. Clinton, M. B. Mabee, R. M. Moeller, R. Flood, and J. Salsburg, "Structural design concepts for future space missions," National Aeronautics and Space Administration, Tech. Rep., November 1968.

[77] C. Rorabaugh, *DSP Primer*. Prentice Hall, 1999.

VITA

Chung Yong Chan was born in Kuala Lumpur, Malaysia on May 31, 1979. His high school work was completed in December 1996 at Chung Hwa Independence High School, Kuala Lumpur. He started his college studies in January 1997. He was enrolled in Taylors College and his major was engineering. In August 1998, he transferred to The University of Mississippi. He was enrolled in the School of Engineering, majoring in electrical engineering. In May 2000, he graduated with a Bachelor of Science in Electrical Engineering degree. Three months later, he began his graduate study at The University of Mississippi by enrolling in the Master of Engineering Science program with emphasis in electrical engineering under the guidance and advice of Dr. Paul M. Goggans. In May 2003, he graduated with a Master of Science in Engineering Science degree. He started his pursuit of a doctorate degree in Engineering Science in August 2006. In 2009, he became the Co-Editor of Bayesian Inference and Maximum Entropy Methods in Science and Engineering: 29th International Workshop, and an Organizing Committee Member of the MaxEnt conference. His research interests include the use of Bayesian inference in engineering design applications such as antenna array and digital filter design, and Bayesian analysis in various inference problems such as landmine detection and sound energy decay analysis in room acoustics.

Permanent Address: Chung Yong Chan

5, Lorong Hujan Satu, O.U.G.,

Jalan Klang Lama,

58200 Kuala Lumpur,

Malaysia.